

Dissertation zur Erlangung des Doktorgrades
der Fakultät für Chemie und Pharmazie
der Ludwig-Maximilians-Universität München

Structural and functional studies on mitotic spindle
orientation in *Saccharomyces cerevisiae*



Daniela Hüls
aus
Mannheim
2011

Erklärung

Diese Dissertation wurde im Sinne von § 13 Abs. 3 bzw. 4 der Promotionsordnung vom 29. Januar 1998 (in der Fassung der sechsten Änderungssatzung vom 16. August 2010) von Herrn Prof. Dr. Klaus Förstemann betreut.

Ehrenwörtliche Versicherung

Diese Dissertation wurde selbständig, ohne unerlaubte Hilfe erarbeitet.

München, den 16.12.2011

.....

Daniela Hüls

Dissertation eingereicht am 16.12.2011

1. Gutachter: Prof. Dr. Klaus Förstemann

2. Gutachter: PD. Dr. Dietmar Martin

Mündliche Prüfung am 06.02.2012

Table of Contents

1	INTRODUCTION	1
1.1	SPINDLE ORIENTATION IN EUKARYOTES	1
1.1.1	<i>Spindle orientation in Saccharomyces cerevisiae</i>	3
1.1.2	<i>Spindle orientation in the Caenorhabditis elegans zygote</i>	5
1.1.3	<i>Spindle orientation in the Drosophila melanogaster neuroectoderm</i>	6
1.1.4	<i>Spindle orientation in mammals</i>	8
1.2	EB1-LIKE FAMILY OF PROTEINS	8
1.2.1	<i>Bim1p</i>	9
1.2.2	<i>human EB1</i>	11
1.3	ROLE OF OTHER PROTEINS INVOLVED IN SPINDLE ORIENTATION	13
1.3.1	<i>Kar9p</i>	13
1.3.2	<i>Adenomatous polyposis coli (APC)</i>	16
1.4	OBJECTIVES	17
2	RESULTS	19
2.1	EXPRESSION, PURIFICATION AND CRYSTALLISATION OF KAR9P	19
2.1.1	<i>Expression and Purification of full-length Kar9p (FL)</i>	19
2.1.2	<i>Crystallisation of Kar9p (FL)</i>	20
2.1.3	<i>Expression and Purification of Kar9p-variants</i>	24
2.1.4	<i>Crystallisation of Kar9p-variants</i>	26
2.1.5	<i>Expression and purification of Kar9p-homologs from other yeast species</i>	28
2.1.6	<i>Co-crystallisation of Kar9p and Bim1p</i>	28
2.2	ROLE OF POSTTRANSLATIONAL MODIFICATIONS OF KAR9P	29
2.2.1	<i>Phosphorylation of Kar9p is not required for the interaction with Bim1p</i>	30
2.2.2	<i>In vivo effects of phosphorylation deficient Kar9p-variants</i>	30
2.2.3	<i>Co-immunoprecipitations of Kar9p from yeast extracts</i>	31
2.2.4	<i>Sumoylation of Kar9p is required for the interaction with Bim1p</i>	32
2.2.5	<i>In vivo effects of sumoylation deficient Kar9p-variants</i>	33
2.3	STRUCTURAL ANALYSES OF BIM1P	35
2.3.1	<i>Expression and Purification of Bim1p (FL)</i>	35
2.3.2	<i>Expression and Purification of Bim1p (C-term)</i>	35
2.3.3	<i>Crystallisation of Bim1p (C-term)</i>	36
2.3.4	<i>Structure determination and refinement of Bim1p (C-term)</i>	36
2.3.5	<i>Crystal structure of Bim1p (C-term)</i>	38
2.3.6	<i>Structural comparison of the cargo-binding domains of Bim1p and human EB1</i>	40

TABLE OF CONTENTS

2.3.7	<i>Analysis of Bim1p (C-term) and (FL) by small-angle-X-ray scattering (SAXS)</i>	41
2.4	<i>IN VITRO AND IN VIVO ANALYSIS OF THE BIM1P-KAR9P INTERACTION</i>	42
2.4.1	<i>The Bim1p-specific loop is not required for the binding to Kar9p</i>	43
2.4.2	<i>Mutational analysis of the Bim1p-Kar9p interaction</i>	43
2.4.3	<i>In vivo effects of the Bim1p-mutations</i>	45
2.4.4	<i>Bim1p has a second binding region for Kar9p</i>	46
2.4.5	<i>In vivo effects of Bim1p lacking the EB1-like motif</i>	47
2.4.6	<i>Aurora B/Ipl1p dependent phosphorylation of Bim1p impairs binding to Kar9p</i> ...	48
3	DISCUSSION	50
3.1	CRYSTALLISATION OF KAR9P	50
3.2	ROLE OF POSTTRANSLATIONAL MODIFICATIONS OF KAR9P	51
3.2.1	<i>Phosphorylation of Kar9p</i>	51
3.2.2	<i>Sumoylation of Kar9p</i>	52
3.3	CRYSTAL STRUCTURE OF BIM1P	54
3.3.1	<i>Comparison of the crystal structure of Bim1p with human EB1</i>	54
3.3.2	<i>The C-terminal domain of Bim1p mediates dimerisation of the protein</i>	55
3.4	KAR9P AND APC SHARE COMMON BINDING FEATURES TO BIM1P AND EB1	56
3.5	ROLE OF THE MIDDLE DOMAIN OF BIM1P IN PROTEIN BINDING	59
3.6	MODEL OF THE CELL-CYCLE DEPENDENT REGULATION OF BIM1P-KAR9P COMPLEX ASSEMBLY AND DISASSEMBLY	61
4	MATERIALS AND METHODS	63
4.1	CONSUMABLES AND CHEMICALS.....	63
4.2	OLIGONUCLEOTIDES	63
4.2.1	<i>Oligonucleotides for biochemical characterization</i>	63
4.2.2	<i>Oligonucleotides for homologous recombination in S. cerevisiae</i>	65
4.3	PLASMIDS.....	65
4.3.1	<i>Plasmids for protein expression in E. coli</i>	65
4.3.2	<i>Plasmids for protein expression in S. cerevisiae</i>	69
4.4	<i>E. COLI STRAINS</i>	70
4.5	<i>S. CEREVISIAE STRAINS</i>	70
4.6	<i>MEDIA FOR E. COLI AND S. CEREVISIAE</i>	71
4.7	ANTIBODIES.....	71
4.8	GENERAL BUFFERS AND SOLUTIONS	72
4.9	MOLECULAR BIOLOGY	72

TABLE OF CONTENTS

4.9.1	<i>Cloning</i>	72
4.9.2	<i>Transformation of E. coli and isolation of plasmid DNA</i>	72
4.9.3	<i>Transformation of S. cerevisiae</i>	73
4.9.4	<i>Isolation of genomic DNA from S. cerevisiae</i>	73
4.9.5	<i>Colony PCR for S. cerevisiae</i>	73
4.10	METHODS FOR PROTEIN ANALYSIS.....	74
4.10.1	<i>Protein separation by SDS-PAGE</i>	74
4.10.2	<i>Protein separation by native PAGE</i>	74
4.10.3	<i>Western blotting</i>	74
4.10.4	<i>Dynamic Light Scattering</i>	75
4.10.5	<i>Small angle X-ray scattering (SAXS)</i>	75
4.10.6	<i>Limited proteolysis</i>	76
4.10.7	<i>Pull-down assays</i>	76
4.11	PROTEIN EXPRESSION AND PURIFICATION.....	76
4.11.1	<i>Recombinant protein expression in E. coli</i>	76
4.11.2	<i>Selenomethionine labeling of proteins</i>	76
4.11.3	<i>Recombinant protein expression in S. cerevisiae</i>	77
4.11.4	<i>Recombinant protein expression in insect cells</i>	77
4.11.5	<i>Purification of recombinant His-tagged Kar9p</i>	78
4.11.6	<i>Purification of recombinant GST-tagged Kar9p</i>	78
4.11.7	<i>Purification of recombinant GST-tagged Bim1p</i>	79
4.11.8	<i>Purification of recombinant MBP-tagged Bim1p</i>	79
4.12	CRYSTALLISATION.....	80
4.12.1	<i>Crystallisation of Kar9p (FL)</i>	80
4.12.2	<i>Crystallisation of Kar9p variants</i>	80
4.12.3	<i>Methylation of Kar9p</i>	81
4.12.4	<i>Co-crystallisation of Bim1p and Kar9p (FL)</i>	81
4.12.5	<i>Crystallisation of Bim1p</i>	81
4.12.6	<i>Heavy atom derivatisation by soaking</i>	82
4.12.7	<i>Structure determination of Bim1p (C-term)</i>	82
4.13	BIOINFORMATICS.....	83
4.13.1	<i>Protein parameters</i>	83
4.13.2	<i>Sequence alignments and structure predictions</i>	83
4.13.3	<i>Structure visualisation and analysis</i>	83

TABLE OF CONTENTS

4.14	YEAST METHODS	84
4.14.1	<i>Preparation of yeast whole-cell extracts</i>	84
4.14.2	<i>Co-immunoprecipitations</i>	84
4.14.3	<i>Benomyl- and temperature-sensitivity</i>	85
5	SUMMARY	86
6	REFERENCES	87
7	APPENDIX	97
7.1	ABBREVIATIONS.....	97
7.2	PROTEINS IDENTIFIED BY CO-IMMUNOPRECIPITATIONS OF KAR9P	98
7.3	SUPPLEMENTAL FIGURES AND TABLES	99
	PUBLICATIONS	101
	ACKNOWLEDGEMENTS	102

1 Introduction

1.1 Spindle orientation in eukaryotes

Correct assembly and orientation of the mitotic spindle is crucial for proper segregation of chromosomes and for determination of cell fate. Errors in chromosome segregation can give rise to aberrant numbers of chromosomes (aneuploidy), which is often correlated with development of cancer. The orientation of the mitotic spindle can furthermore influence distribution of cellular contents to daughter cells and in multicellular organisms positioning of the daughter cell in the tissue. In higher eukaryotes, orientation of the mitotic spindle also dictates the exact position of the cleavage furrow, hence its correct orientation is required to determine whether the cell divides asymmetrically or symmetrically (Figure 1) (Rappaport 1997; Betschinger and Knoblich 2004; Glotzer 2004; Neumuller and Knoblich 2009).

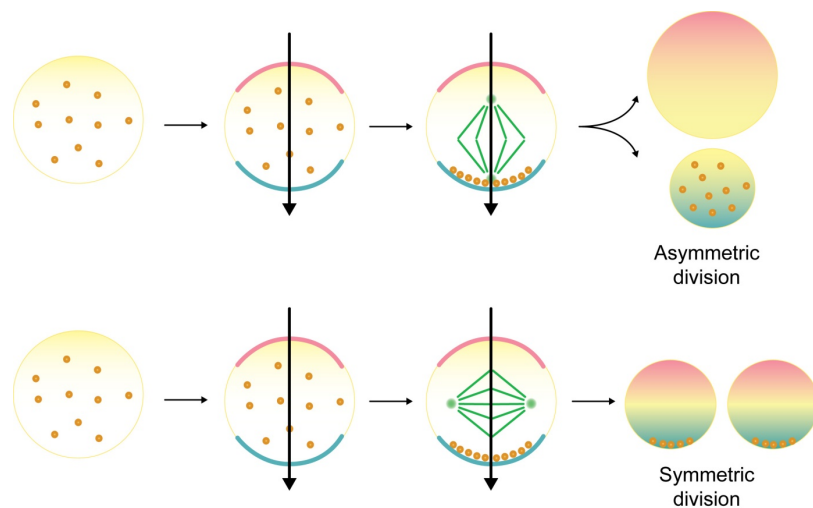


Figure 1 Cartoon representation of asymmetric and symmetric cell divisions. Cell polarity is established through different cell polarity determinants (brown dots, red and blue lines indicate different poles). Arrows indicate cell polarity axes. For asymmetric divisions, the mitotic spindle (green lines and dots) is aligned along the cell polarity axis, ensuring asymmetric distribution of cell fate determinants (brown dots). For symmetric cell divisions the mitotic spindle is oriented perpendicular to the polarity axis, leading to a symmetric distribution of molecules. Illustration taken from <http://www.ifom-ieo-campus.it/research/images/mapelli/fig1.jpg>

Asymmetric cell division is a very common and highly conserved mechanism to generate two daughter cells with different cell fates (Figure 1). This type of cell division is governed by intrinsic and extrinsic signals that influence cell polarity. Alteration of cell polarity may also change the position of the cleavage furrow. This results in an asymmetric distribution of cell content and can additionally affect the size of daughter cells. Three different mechanisms are known to affect cell polarity: 1. asymmetric localisation of cell polarity regulators, which is usually accomplished by reorganisation of the actomyosin network, 2. cell fate determinants localising exclusively to given regions of a polarised cell or 3. regulated orientation of the mitotic spindle in respect to the environment and the cell axis (Palmer, Sullivan et al. 1992; Rhyu and Knoblich 1995). Well studied examples are the one-cell embryo of *C. elegans*,

INTRODUCTION

neurogenesis in *Drosophila*, the budding yeast *S. cerevisiae* and stem cells in mammals (Betschinger and Knoblich 2004; Siller and Doe 2009). All examples will be explained in more detail in the following chapters. Asymmetric cell division also occurs in prokaryotes such as the bacterium *Caulobacter crescentus* (Jenal 2000).

Symmetric cell division, on the other hand, gives rise to daughter cells with identical cell fates (Figure 1). These divisions occur in all proliferating and growing tissues of multicellular organisms, e.g. during development or in injured tissues. In contrast to asymmetric divisions, the spindle is oriented by passive mechanisms at the center of the cell in this process (McCarthy and Goldstein 2006).

Mitotic spindles consist of two spindle poles (centrosomes) and three different types of microtubules. All microtubules are nucleated from their minus end by the gamma-tubulin complex at the spindle poles (Moritz, Braunfeld et al. 2000; Wiese and Zheng 2000). Astral microtubules probe the cytoplasm and cell cortex with their plus-ends and are required for orientation of the spindle along the polarity axis. Inward extending kinetochore microtubules attach to chromosomes to align and segregate them together with interpolar microtubules (Mitchison and Salmon 2001). All microtubules undergo a constant process of growth and shrinkage at their plus-ends through rapid tubulin addition and subtraction, so called "dynamic instability" (Mitchison and Kirschner 1984). Dynamic instability allows astral microtubules to probe the cytoplasm for cortical anchor sites and to exert forces on the spindle (Inoue and Salmon 1995). Although microtubules attach with their plus-ends to cortical sites or kinetochores, dynamic instability is not inhibited and forces are exerted on the mitotic spindle resulting in displacement of the spindle. In addition, forces on the mitotic spindle can be generated by minus-end directed motor proteins, translocating along cortically attached microtubules.

Spindle orientation is one example of important processes that depend on the interaction between actin filaments and microtubules. Actin-based motors interact with proteins (+TIPs) located at free plus-ends of astral microtubules. Translocation of these motors along actin filaments then generates force resulting in displacement of microtubules and the mitotic spindle. This crosstalk between actin-based motors and +TIPs is a well conserved feature in eukaryotes (Lansbergen and Akhmanova 2006).

Spindle orientation is best understood in the budding yeast *S. cerevisiae*, which will be outlined in more detail, with examples from higher eukaryotes, in the following chapters.

1.1.1 Spindle orientation in *Saccharomyces cerevisiae*

Budding yeast divides asymmetrically, with daughter cells smaller at the time of division than mother cells. Given that the yeast bud can divide for several generations, Yamashita and colleagues even proposed that it is a primitive stem cell equivalent (Yamashita and Fuller 2008). Budding yeast undergoes a closed mitosis, without breakdown of the nuclear envelope. Therefore spindle orientation correlates to orientation of the nucleus. Many of the relevant proteins involved in spindle orientation in budding yeast are evolutionarily conserved, making this organism a powerful tool for investigation of the underlying molecular details (Siller and Doe 2009).

The axis of cell polarity is established during G₁-phase of the cell cycle by localisation of Cdc 42p to the cell cortex at the incipient bud site (Figure 2A). In haploids the bud site is adjacent to the previous one, whereas in diploids buds are formed from either end (Bretscher 2003). Cdc 42p is a member of the Rho/Rac like family of Ras-GTPases. It is involved in cell polarisation, control of reorganisation of the actin cytoskeleton, septin recruitment to the future bud site and septin ring assembly. Reorganisation of the actin cytoskeleton at bud emergence results in assembly of two types of F-actin: actin filament bundles (cables) that extend from the incipient bud site into the cell and actin patches at the cortex forming a necklace-type ring around the incipient bud site (Adams and Pringle 1984; Kilmartin and Adams 1984). Both types of F-actin are constantly reorganised during the cell cycle (Bretscher 2003). Septin proteins are subsequently accumulating around the incipient bud site, marking the bud neck (Pruyne and Bretscher 2000).

After establishment of polarity, the mitotic spindle has to be aligned correctly along the so called mother-bud axis to ensure proper chromosome segregation. Spindle orientation in budding yeast is controlled by two partially redundant pathways: the early pathway (Bim1p-Kar9p-Myo2p pathway), aligns the mitotic spindle along the mother-bud axis before anaphase (Miller and Rose 1998; Yin, Pruyne et al. 2000; Liakopoulos, Kusch et al. 2003), whereas the late pathway (dynein-dynactin pathway) elongates the spindle through the bud neck during anaphase (Lee, Tirnauer et al. 2000; Grava, Schaerer et al. 2006) (Figure 2B). Each pathway can rescue defects in the other one. However, a knock-out of components in both pathways impairs nuclear segregation and results in lethality (Carminati and Stearns 1997; Miller and Rose 1998).

Astral microtubules and microtubules required for the formation of the mitotic spindle emanate from spindle pole bodies (SPBs), the yeast equivalent of centrosomes. SPBs are cylindrical multilaminar organelles embedded in the nuclear envelope (Byers, Shriver et al. 1978; O'Toole, Winey et al. 1999). Duplication of the SPB occurs during G₁-phase of the cell cycle (Figure 2A). The new and the old SPB are subsequently separated to form the mitotic spindle (Jaspersen and Winey 2004). The old SPB is destined for the daughter cell

INTRODUCTION

and consequently oriented towards the bud neck, whereas the new SPB stays in the mother cell (Pereira, Tanaka et al. 2001). SPB asymmetry is established by three different steps: 1. In S-phase Clb5p associated kinase inhibits microtubule nucleation from the new SPB until a bipolar spindle is formed (Segal, Clarke et al. 2000). 2. Localisation of the protein Kar9p from the early spindle orientation pathway is restricted to the old SPB (Liakopoulos, Kusch et al. 2003; Maekawa, Usui et al. 2003). 3. Dynein involved in the spindle elongation pathway localises to the old SPB during metaphase (Grava, Schaerer et al. 2006).

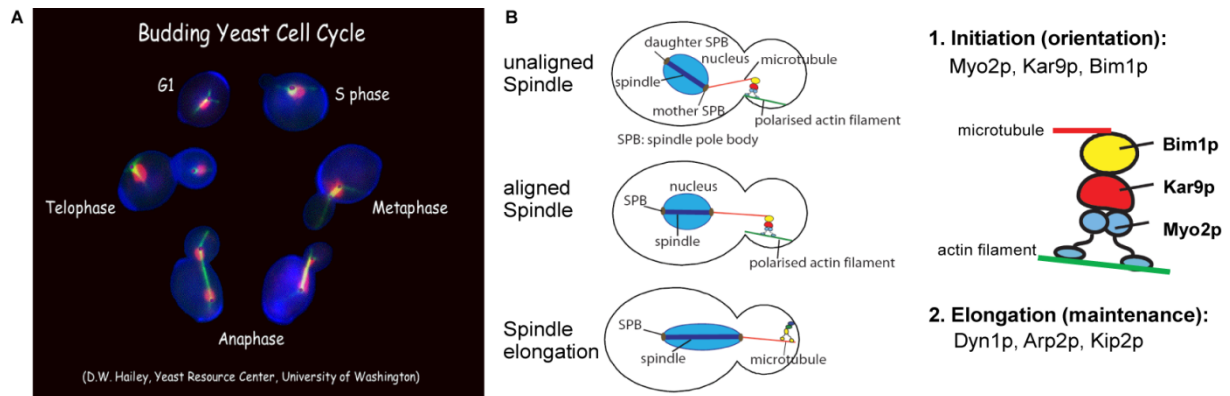


Figure 2 Mitotic spindle orientation in *S. cerevisiae* (A) Cell cycle in budding yeast. Image was taken from D.W. Haley, Yeast Resource Center, University of Washington. Microtubules are labelled in green and DNA in red. (B) Cartoon representation of the two pathways involved in spindle orientation and elongation in budding yeast.

The early and the late pathway of spindle orientation

The early pathway of spindle orientation promotes capture of astral microtubules emanating from the old SPB at the bud cortex before anaphase. These microtubules are then guided into the nascent bud via association of microtubule plus-ends with actin cables at the bud neck and bud tip resulting in an orientation of the mitotic spindle along the mother-bud axis (Moore and Cooper 2010; Merlini and Piatti 2011). This process involves the EB1-family member Bim1p, the adapter Kar9p (related to adenomatous polyposis coli (APC)) and the type-V myosin Myo2p (Figure 2B). Myo2p generates the force required for spindle orientation via translocation along actin filaments. The research presented here investigates the role of the proteins Bim1p and Kar9p in this pathway. These proteins will be introduced in more detail in following chapters (see 1.2.1 and 1.3.1).

After the mitotic spindle is aligned along the mother-bud axis, astral microtubules are captured at the bud neck and bud tip by the actin- and formin-binding protein Bud6p (Segal, Bloom et al. 2000). Bud6p localises to those regions in a septin-dependent manner (Luedeke, Frei et al. 2005). While attached to the cortex, these microtubules undergo shortening, resulting in final orientation of the mitotic spindle (Adames and Cooper 2000; Kusch, Meyer et al. 2002; Huisman, Bales et al. 2004).

INTRODUCTION

During anaphase, the nuclear envelope is elongated and the old SPB translocated through the bud neck by the late pathway. This pathway requires the minus-end directed dynein-dynactin complex, a large multi-subunit complex conserved in all eukaryotes (Eshel, Urrestarazu et al. 1993; Carminati and Stearns 1997). The dynein-dynactin complex is transported to microtubule plus-ends at the bud neck and bud tip by several associated proteins, where it is cortically anchored and activated. The activated dynein-dynactin complex then generates force with its minus-end directed motor activity, resulting in microtubule sliding along the cell cortex, thereby pulling the old SPB toward the bud cortex (Adames and Cooper 2000).

Budding yeast has evolved at least two control mechanisms to ensure proper orientation of the mitotic spindle (Caydasi, Ibrahim et al. 2010). First of all, the redundancy of both pathways involved in spindle orientation ensures that upon failure of one pathway the other pathway can still rescue correct orientation of the mitotic spindle. Besides this redundancy, yeasts have developed the so called spindle position checkpoint (SPOC), which prevents cells exiting from mitosis with misaligned spindles. The SPOC delays exit from mitosis by inhibiting the mitotic exit network (MEN). Further details are beyond the scope of this introduction, but several reviews can guide the interested reader (Schuyler and Pellman 2001; Piatti, Venturetti et al. 2006; Fraschini, Venturetti et al. 2008; Caydasi, Ibrahim et al. 2010; Merlini and Piatti 2011).

1.1.2 Spindle orientation in the *Caenorhabditis elegans* zygote

The *C. elegans* zygote is one of the best understood model systems for generating asymmetric cell sizes. The zygote divides into a larger anterior AB cell and a smaller posterior P1 cell (Cowan and Hyman 2004; Neumuller and Knoblich 2009). This first mitotic division relies on reorganisation of the cortical actin cytoskeleton (Moore and Cooper 2010). After fertilisation, the cortex of the zygote is covered with a meshwork of actin filaments (Figure 3A). Symmetry is broken by a cue associated with the position of the sperm pronucleus (paternal nucleus) within the egg (Pearson and Bloom 2004; Munro and Bowerman 2009). Subsequently, the actomyosin network retracts away from the sperm cue to the anterior half of the cell cortex, thereby subdividing the cortex into an anterior and a posterior domain (Figure 3A) (Cowan and Hyman 2004; Munro and Bowerman 2009; Moore and Cooper 2010). Polarisation of the cell is further established by enrichment of evolutionary conserved polarity determinants (Par proteins) within the anterior and posterior domain. A complex formed by Par-3, Par-6 and the atypical protein kinase C (aPKC-3) retracts together with the actomyosin network towards the anterior domain, whereas Par-2 and Par-1 become enriched at the posterior domain upon depletion of the other proteins (Figure 3A) (Gonczy 2008). The asymmetric distribution of the Par proteins results in a

differential localisation of cell fate determinants. Asymmetry of Par proteins furthermore guides the orientation of the spindle along the anterior-posterior axis by controlling microtubule-cortex interactions (Kusch, Liakopoulos et al. 2003). Subsequent displacement of the spindle towards the posterior pole ensures correct segregation of cell fate determinants and occurrence of unequally sized daughter cells (Figure 3A). Pulling forces to orient and position the spindle are exerted by attachment of astral microtubule plus-ends to cortically anchored dynein-dynactin complexes (Siller and Doe 2009). Posteriorly directed forces are higher than anteriorly directed forces, resulting in spindle displacement toward the posterior pole (Gusnowski and Srayko 2011). In contrast to budding yeast, force for spindle orientation is generated by dynein motor activity, whereas force for spindle positioning is generated by microtubule depolymerisation at the plus-ends and the dynein-dynactin complex simply acting as a cortical anchor (Siller and Doe 2009).

1.1.3 Spindle orientation in the *Drosophila melanogaster* neuroectoderm

Spindle orientation during asymmetric cell division

Drosophila neuroblasts are a well-established model system for studying the molecular mechanisms of tissue-renewing and asymmetric stem cell division. Asymmetric cell division is one of the primary mechanisms of neural stem cells (neuroblasts) to generate neuronal diversity (Kim and Hirth 2009). The mono-layered neuroectoderm of *Drosophila* embryos contains pre-neuroblasts that delaminate from the monolayer to undergo asymmetric divisions along the apical-basal axis (Figure 3B) (Bienz 2001). Each asymmetric division gives rise to a larger apical neuroblast that retains its stem cell characteristics and a smaller basal ganglion mother cell (GMC) (Gonczy 2008; Kim and Hirth 2009). The smaller ganglion mother cell inherits cell-fate determinants that enable the cell to undergo a terminal division to produce two post-mitotic neurons/glia cells (Kim and Hirth 2009). Apical-basal polarity is established before the pre-neuroblast delaminates from the polarised epithelium. The delaminating neuroblast inherits the highly conserved Par-complex proteins Bazooka (Baz/Par-3), Par-6 and aPKC, (see chapter 1.1.2) from the neuroectoderm (Kim and Hirth 2009; Siller and Doe 2009). The Par-complex then binds through Baz to several adapter proteins that interact with the heterotrimeric G protein subunit, Gai (Egger, Chell et al. 2008). Gai itself binds to the microtubule-associated adapter Mud, which either directly anchors microtubules at the cortex or possibly recruits the dynein-dynactin complex to the apical cortex. Analogue to *S. cerevisiae* and *C. elegans*, pulling forces are exerted to align the spindle along the apical-basal axis (Siller and Doe 2009).

Similar to *S. cerevisiae*, a second, eventually redundant spindle orientation pathway involving the kinesin Khc73 exists in *Drosophila* neuroblasts (Kim and Hirth 2009; Siller and

Doe 2009). The latter is primarily active during metaphase, whereas the Par/Mud-pathway is active prior to metaphase (Yu, Kuo et al. 2006).

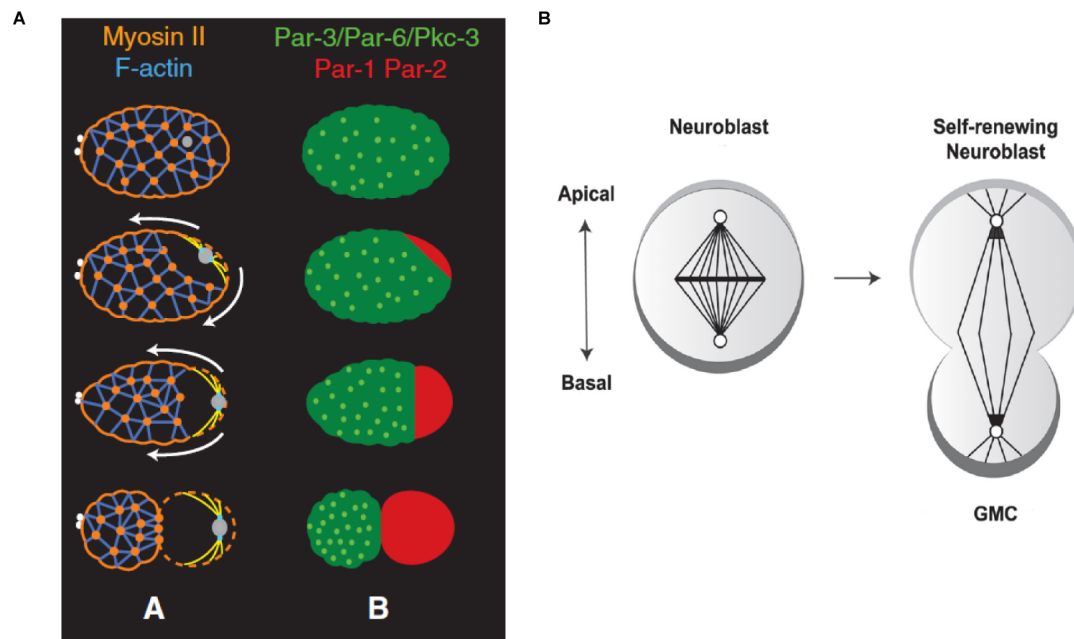


Figure 3 Asymmetric cell divisions in higher eukaryotes. (A) Molecular mechanism involved in cell-polarity determination in the *C. elegans* zygote. A: Initial asymmetry is established by reorganisation of the actin-cytoskeleton. grey: paternal nucleus, blue/orange: F-actin/Myosin II. B: Differential localisation of Par-proteins in concert with the reorganisation of the actin-cytoskeleton further establishes cell polarity. green: Par-3, Par-6, PKC-3, red: Par-1, Par-2. Picture taken from (Toyoshima and Nishida 2007). (B) Asymmetric cell divisions in *Drosophila* neuroblasts. The mitotic spindle is oriented along the apical-basal axis. Apical-basal polarity is established by differential localisation of cell-fate determinants (light and dark grey). Neuroblasts divide into self-renewing neuroblasts and ganglion mother cells (GMC), which can undergo differentiation. Picture taken from (Munro and Bowerman 2009).

Spindle orientation during symmetric cell divisions

Epithelial cells in the neuroectoderm can also undergo symmetric cell divisions along the planar axis (Bienz 2001). The cue for symmetric cell divisions is provided by adherens junctions, which mediate adhesion between epithelial cells (Bienz 2001). This cue depends on a homologue of the tumour suppressor adenomatous polyposis coli (APC) namely E-APC (dAPC2) and the microtubule-end binding protein 1 (dEB1) (Lu, Roegiers et al. 2001). APC has been proposed to be a functional homologue of Kar9p in budding yeast whereas dEB1 is a homologue of Bim1p, suggesting a similar role in spindle orientation. E-APC associates with adherens junctions and is required for planar spindle orientation together with dEB1 (Bienz 2001). Since E-APC is missing its C-terminal domain mediating EB1-binding and does not bind dEB1 (Lu, Roegiers et al. 2001), it remains elusive how both proteins contribute to spindle orientation. One possible link is the other *Drosophila* APC-homologue (dAPC) that contains the EB1-binding region, but it is not known if dAPC is involved in this process (Bienz 2001). APC is furthermore important for the alignment of the spindle in male germline stem cells (mGSCs) in *Drosophila*, possibly by linking adherens junctions with microtubules (Toyoshima and Nishida 2007).

1.1.4 Spindle orientation in mammals

Similar to *Drosophila* neuroblasts, mammalian stem cells undergo asymmetric or symmetric divisions, depending on the orientation of the mitotic spindle along the planar or apical-basal axis (Pease and Tirnauer 2011). Establishment of cell-polarity depends on the formation of cell-cell junctions and cell-extracellular matrix (ECM) interactions (Pease and Tirnauer 2011). Spindle orientation is also dependent on the evolutionary conserved Par-proteins and the dynein-dynactin complex, as already described for *C. elegans* and *Drosophila* (see chapter 1.1.2 and 1.1.3). Cortical attachment sites for astral microtubules are provided by adherens junctions (Siller and Doe 2009; Pease and Tirnauer 2011). In HEK293 cells and HeLa cells, positioning of the mitotic spindle in the geometrical center of the cell requires APC and/or EB1 (Toyoshima and Nishida 2007). A knock-down of APC in HEK293 cells by RNAi results in spindle misorientation due to destabilisation of astral microtubules. APC has been shown to stabilise microtubules through its binding to microtubules and EB1 (Pease and Tirnauer 2011). Additionally, APC plays a role in cell polarisation, suggesting that mutations of APC could cause spindle misorientation by altering cortical cues. (Etienne-Manneville, Manneville et al. 2005). This effect may be mediated by interaction of APC with components of the actin cytoskeleton or with the adherens-junctions associated protein β -catenin (Nathke 2005).

Taken together, these results show the importance of APC in controlling spindle orientation through effects on astral microtubule stabilisation and cell cortex polarisation in mammalian cells (Pease and Tirnauer 2011). Whether its role is similar to Kar9p remains unknown. Another interesting question is whether the Par/dynein pathway and the APC/EB1 pathway in *Drosophila* and mammals function independently in spindle orientation or exhibit a similar redundancy as the Kar9p/Bim1p and dynein-dynactin dependent pathways in *S. cerevisiae*.

1.2 EB1-like family of proteins

Members of this highly conserved family are so called +-TIP proteins, which associate with and selectively track the growing plus-ends of microtubules (Lansbergen and Akhmanova 2006; Wolyniak, Blake-Hodek et al. 2006; Morrison 2007; Akhmanova and Steinmetz 2011). All members of the EB1-like family are characterised by an N-terminal CH- (calponin-homology) domain, a flexible linker region (middle domain), and a C-terminal dimerisation/cargo-binding domain, the so called EB1-like motif (Figure 4A,C) (Bu and Su 2003). The structures of the CH-domain and the EB1-like motif have been solved individually. (Honnappa, John et al. 2005; Slep, Rogers et al. 2005; Slep and Vale 2007; Honnappa, Gouveia et al. 2009) (Figure 4B).

The highly conserved CH-domain mediates binding to microtubules (Hayashi and Ikura 2003; Slep and Vale 2007) and is responsible for the autonomous microtubule plus-tip tracking

activity (Bieling, Laan et al. 2007). The C-terminal domain of EB1 comprises a coiled-coil mediating the dimerisation of these proteins (Honnappa, John et al. 2005; Slep, Rogers et al. 2005; De Groot, Jelesarov et al. 2010) and binding to cargo (Honnappa, Gouveia et al. 2009). Heterodimerisation of the CH-domain is furthermore a prerequisite *in vivo* for microtubule binding and plus-end localisation (Slep and Vale 2007; Zimniak, Stengl et al. 2009; De Groot, Jelesarov et al. 2010).

Common features of EB1-like proteins are the promotion of microtubule polymerisation and the association of microtubules with kinetochores, the cell cortex or the actin cytoskeleton (Akhmanova and Hoogenraad 2005; Akhmanova and Steinmetz 2008). *Drosophila* EB1 and budding yeast Bim1p increase catastrophe frequencies of microtubules whereas fission yeast Mal3p and vertebrate EB1 decrease catastrophe frequencies (Lansbergen and Akhmanova 2006). *In vivo* experiments indicate that Bim1p and EB1 localise exclusively to the plus-ends of microtubules (Tirnauer, O'Toole et al. 1999; Mimori-Kiyosue, Shiina et al. 2000), whereas Mal3p has additional functions. Electron microscopy (EM) together with metal-shadowing revealed that Mal3p interacts with the microtubule lattice seam. Further results strongly suggest that Mal3p is stabilising microtubules by “clamping” the lattice seam (Sandblad, Busch et al. 2006). If this is also true for Bim1p or EB1 remains to be shown.

1.2.1 Bim1p

BIM1 (binding to microtubules) has been first identified in a yeast-two hybrid screen using the entire coding sequence of *TUB1* (encoding α -tubulin) as bait (Schwartz, Richards et al. 1997). Deletion mutants of *BIM1* are viable, but have a strong bilateral karyogamy defect. Additionally, deletion of *BIM1* results in hypersensitivity to the microtubule destabilising drug *Benomyl*, aberrant spindle behaviour, nuclear positioning defects and growth defects at extremely high ($\geq 37^\circ\text{C}$) or low ($\leq 14^\circ\text{C}$) temperatures (Schwartz, Richards et al. 1997). Synthetic lethality is observed with mutations of *tub1*, spindle assembly checkpoint genes and genes encoding kinetochore components (Mayer, Pot et al. 2004). Overexpression of *BIM1* results in lethality and cell-cycle arrest in wild-type cells (Schwartz, Richards et al. 1997). Localisation experiments with Bim1p show that it colocalises with intranuclear and extranuclear microtubules in wild-type cells, presumably by binding sites on α -tubulin (Schwartz, Richards et al. 1997). Tirnauer and colleagues have shown that Bim1p localises to dots at the distal ends of microtubules and regulates microtubule dynamics in a cell-cycle dependent manner (Tirnauer, O'Toole et al. 1999). The authors furthermore showed that a deletion of *BIM1* affects the length and dynamics of microtubules during G_1 phase, indicating a role of Bim1p in promoting dynamic instability of microtubules (Tirnauer, O'Toole et al. 1999).

INTRODUCTION

Sequence alignments confirm that Bim1p belongs to the highly conserved family of EB1-like proteins. Bim1p is well conserved, with 33-36 % identity and 56-61% similarity of the protein sequence to its human, mouse, *Drosophila* and *S. pombe* homologues (Schwartz, Richards et al. 1997) (Figure 30).

For Bim1p structural information is only available for the N-terminal CH-domain (Slep and Vale 2007), whereas for the C-terminal EB1-like motif of Bim1p only the homologous crystal structure from human EB1 has been published so far (Honnappa, John et al. 2005; Slep, Rogers et al. 2005) (Figure 4A-C). Since both proteins share about 35% sequence identity, structure predictions are of limited reliability (Rost 1999).

Structural analyses of the tubulin-binding CH-domains together with biochemical analyses have revealed common properties of those domains (Slep and Vale 2007). Superimposition of the crystal structures of Bim1p with human EB1 shows a high structural conservation within this class of proteins, suggesting that this might be also true for the EB1-like motif (Slep and Vale 2007). Additional experiments demonstrated that the homodimerised CH-domain together with the middle domain of Bim1p potently promotes microtubule binding and polymerisation, which agrees with the results of Tirnauer and colleagues showing that Bim1p affects microtubule dynamics (Tirnauer, O'Toole et al. 1999; Slep and Vale 2007; Zimniak, Stengl et al. 2009) (Figure 4C).

Role of Bim1p in the early spindle orientation pathway

Together with Kar9p, Bim1p is essential for the early spindle orientation pathway in budding yeast. An interaction between both proteins was first observed in a yeast-two hybrid screen using full-length Kar9p as bait (Korinek, Copeland et al. 2000; Miller, Cheng et al. 2000). A double knock-out of *BIM1* and *KAR9* is viable, indicating that only the early spindle elongation pathway is affected. In contrast, double knock-outs of *BIM1* or *KAR9* with genes of the late pathway are lethal (Miller, Cheng et al. 2000).

Co-immunoprecipitation experiments with either protein confirmed their interaction *in vivo* (Korinek, Copeland et al. 2000; Lee, Tirnauer et al. 2000; Miller, Cheng et al. 2000). A direct interaction between Bim1p and Kar9p was also observed *in vitro* using *in vitro* synthesised radiolabelled Kar9p and Bim1p expressed in *E. coli* (Korinek, Copeland et al. 2000). Furthermore, co-immunoprecipitation experiments with Bim1p and Kar9p co-expressed *in vitro* in rabbit reticulocyte lysate confirmed strong interaction between both proteins (Lee, Tirnauer et al. 2000). Moreover, Bim1p and Kar9p co-fractionated in velocity sedimentation and size-exclusion experiments (Lee, Tirnauer et al. 2000). The size of the complex was estimated to be 250 kDa based on the Stokes radii and Svedberg values, suggesting that several molecules of each protein are present in the complex or that additional factors contribute to the complex (Lee, Tirnauer et al. 2000).

INTRODUCTION

Upon deletion of *BIM1*, localisation of Kar9p to the bud tip or the SPB was not altered, whereas localisation of Kar9p along cytoplasmic microtubules was affected (Miller, Cheng et al. 2000). These data suggest that Bim1p plays a direct role in the interaction of cytoplasmic microtubules with the cortical dot of Kar9p. *In vitro* experiments showed that Bim1p efficiently promotes recruitment of Kar9p onto microtubules, whereas Kar9p alone does not bind microtubules efficiently (Lee, Tirnauer et al. 2000).

A minimal binding region in Bim1p for Kar9p has been mapped by yeast-two hybrid experiments. This region encompasses 89 residues (187-254) and comprises the EB1-like motif (Miller, Cheng et al. 2000). The high conservation of this region strongly suggests that the mode of cargo-binding is similar in all EB1-family members. However, further delineation of this region with specific mutations is required to determine the residues involved in binding to Kar9p.

In addition to its role in spindle orientation, Bim1p localises to the nucleus and is important for the structural stability of the anaphase spindle (Gardner, Haase et al. 2008). Bim1p supports a stable interpolar microtubule (ipMT) overlap in the spindle midzone by promoting polymerization of ipMTs during anaphase, which is required for proper spindle elongation (Khmelniskii and Schiebel 2008). Bim1p is furthermore required for efficient sister chromatid cohesion (Mayer, Pot et al. 2004). Taken together, these results indicate that Bim1p plays several roles at different locations. However, most of the molecular details and the regulation of Bim1p activity remain undetermined.

One possible regulation mechanism of Bim1p activity might be through phosphorylation by Aurora B/Ipl1p. Bim1p associates directly with the Ipl1p kinase and becomes phosphorylated at six serine residues in the flexible middle domain (Zimniak, Stengl et al. 2009). Phosphorylation of Bim1p occurs in mid to late anaphase and reduces binding of Bim1p to microtubules. Also human EB1 interacts with Aurora-B kinase (Sun, Gao et al. 2008), suggesting conservation of this posttranslational modification.

1.2.2 human EB1

The sequence of human EB1 is to 35 % identical with its yeast ortholog Bim1p (Schwartz, Richards et al. 1997). EB1 was initially identified as a protein that interacts with the C-terminal part of the adenomatous polyposis coli (APC) tumour suppressor protein (Su, Burrell et al. 1995). The C-terminal domain of EB1 is important for interaction with APC, the dynactin component p150^{glued} and spectraplakins (Bu and Su 2003; Slep, Rogers et al. 2005). EB1 targets APC to microtubules and a stable interaction between EB1 and APC is required for microtubule capturing and stabilisation (Nakamura, Zhou et al. 2001; Wen, Eng et al. 2004). In humans, the C-terminal EB1-like motif is sufficient to bind to a peptide of the APC protein (Honnappa, John et al. 2005; Slep, Rogers et al. 2005). Likewise

in yeast the EB1-like domain of Bim1p is sufficient to bind to Kar9p (Miller, Cheng et al. 2000). The APC-EB1 interaction is likely to be critical for cancer progression of many malignant human colon tumours. The majority of APC mutations in those tumours lack the EB1-binding site, suggesting that the abrogation of the APC-EB1 interaction may contribute to cancer progression (Powell, Zilz et al. 1992; Su, Burrell et al. 1995; Tirnauer and Bierer 2000).

Crystal structures of human EB1

Crystal structures of the CH domain from yeast and human (Hayashi and Ikura 2003; Slep and Vale 2007) and of the EB1-like motif from human EB1 (Honnappa, John et al. 2005; Slep, Rogers et al. 2005) have been determined (Figure 4B). The structure of the CH-domain is very similar to the one in Bim1p and all features of this domain have been already described in chapter 1.2.1.

The crystal structure of the C-terminal EB1-like motif reveals a dimeric structure formed by a coiled-coil that folds back to form a four-helix bundle (Slep, Rogers et al. 2005). Each monomer consists of a long smoothly curved helix, which is followed by a hairpin-like loop and a short second helix at the C-terminus (Honnappa, John et al. 2005) (Figure 4B). The four-helix bundle contains many highly conserved residues forming a hydrophobic core (Honnappa, John et al. 2005; Slep, Rogers et al. 2005). The large hydrophobic surface buried in this bundle is also expected to contribute to the stability of the EB1-dimer (Honnappa, John et al. 2005). Of particular significance is a highly conserved “FYF”-motif flanked by several acidic residues (Slep, Rogers et al. 2005). This region is a putative cargo-binding site.

To identify residues in EB1 that bind cargo, surface plasmon resonance experiments using a fragment of the mammalian spectraplakine MACF (Slep, Rogers et al. 2005) and ITC experiments using an APC-derived C-terminal peptide (Honnappa, John et al. 2005) were performed. MACF and APC both bind to EB1 with a similar binding motif, suggesting that their binding modes are similar (Slep, Rogers et al. 2005). Mutational analysis of the highly conserved region in EB1 revealed a cluster of residues along the long helix with particular importance of the highly conserved “FYF”-motif (Slep, Rogers et al. 2005). These results have been confirmed by co-crystallisation of the EB1-like motif with MACF and by NMR analysis of the EB1-like motif with a peptide of APC (Honnappa, Gouveia et al. 2009).

The high degree of conservation of the binding regions in either EB1 or APC/MACF argues for a similar mode of cargo binding. The functional homologue of APC in yeast (Kar9p) does not have a repeat motif as APC or MACF, but shares limited sequence homology to the EB1-binding-mediating domain in APC (Bienz 2001). It will be therefore interesting to compare the

molecular basis of the APC-EB1 and the Kar9p-Bim1p interaction to determine if similar or unique features govern these interactions (Slep, Rogers et al. 2005).

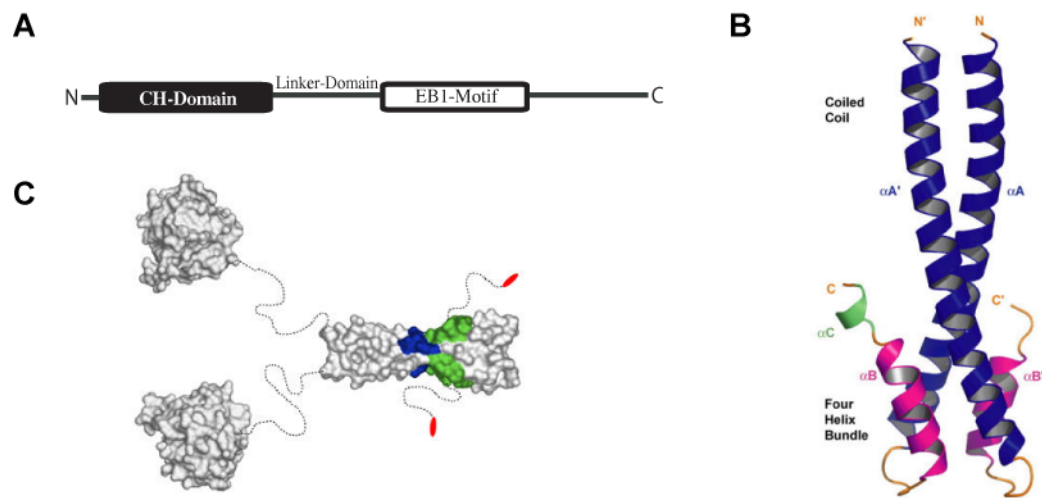


Figure 4 EB1-like family of proteins (A) Domain composition of EB1-like proteins. All proteins have an N-terminal CH-domain followed by an unstructured linker domain and a C-terminal dimerisation/cargo-binding domain (EB1-motif). (B) Crystal structure of the C-terminal domain of human EB1. Image was taken from (Slep, Rogers et al. 2005). PDB-ID: 1YIB. (C) Structural organisation of EB1-like proteins. Crystal structures of the N-terminal CH-domain and the C-terminal EB1-like motif are depicted as surface representations. Dashed lines indicate flexible linker regions. The binding site for APC is indicated in blue and green. Picture taken from (Slep, Rogers et al. 2005)

1.3 Role of other proteins involved in spindle orientation

1.3.1 Kar9p

The *KAR9* gene was originally identified as a bilateral karyogamy mutant (Kurihara, Beh et al. 1994). There have been many functional studies reported in yeast (Miller and Rose 1998) but there is not much information available about the protein itself. The protein has an overall size of 644 amino acids and a molecular weight of 74 kDa. It consists of an N-terminal acidic domain, a coiled-coil region in the middle and a proline-rich and basic domain at the C-terminus (Figure 6A). Within different yeast species this protein is highly conserved and there is the previously mentioned functional homolog APC in higher eukaryotes. Kar9p and APC have sequence homologies at their C-termini, which mediates the binding to Bim1p in yeast and respectively to EB1 in higher eukaryotes (Bienz 2001).

Kar9p initially localises together with Bim1p to the spindle pole body (SPB) independently of astral microtubules (Liakopoulos, Kusch et al. 2003; Maekawa and Schiebel 2004). Interestingly the homologues EB1 and APC also localise to centrosomes, the equivalent of SPBs (Louie, Bahmanyar et al. 2004). In contrast to Bim1p, Kar9p localises exclusively to the mother SPB destined for the daughter cell. (Liakopoulos, Kusch et al. 2003; Maekawa, Usui et al. 2003; Maekawa and Schiebel 2004; Miller, D'Silva et al. 2006). This step is critical for proper spindle orientation and tightly regulated, ensuring deployment of Kar9p to astral

INTRODUCTION

microtubules adjacent to the bud (Liakopoulos, Kusch et al. 2003; Maekawa, Usui et al. 2003; Maekawa and Schiebel 2004; Miller, D'Silva et al. 2006). Kar9p localises to the SPB in G₁ phase of the cell-cycle and moves to the plus-end during S phase and metaphase (Maekawa, Usui et al. 2003). This translocation is enhanced by the kinesin related Kip2p and requires the plus-end tracking proteins Bik1p (CLIP-170), Stu2p (XMAP215) and Bim1p (Moore and Cooper 2010). Interestingly, the Kar9p-homolog APC also moves to the end of microtubules in a kinesin-dependent manner (Bloom 2000; Mimori-Kiyosue, Shiina et al. 2000). Located at the plus-ends of dynamically growing microtubules, Kar9p can encounter cortical Myo2p. Through interaction with the globular tail (cargo binding) domain of Myo2p, the Kar9p-decorated microtubules are then guided along actin filaments into the bud (Beach, Thibodeaux et al. 2000; Yin, Pruyne et al. 2000; Hwang, Kusch et al. 2003). A fusion protein of Myo2p and Bim1p is sufficient to orient the spindle in the cell, supporting the role of Kar9p as adapter protein (Hwang, Kusch et al. 2003). The Myo2p-Kar9p dependent transport of microtubules along actin filaments furthermore enhances the efficiency of microtubule capture at the cortex. As previously mentioned (chapter 1.1.1), microtubules are captured at the cortex by the formin-binding protein Bud6p. This protein is also required to maintain Kar9p at the bud cortex (Beach, Thibodeaux et al. 2000; Huisman, Bales et al. 2004).

Posttranslational modifications of Kar9p

Kar9p is subjected to three different types of posttranslational modifications: phosphorylation, sumoylation, and ubiquitination. Phosphorylation of Kar9p is required for asymmetric localisation of Kar9p to the mother SPB (Liakopoulos, Kusch et al. 2003; Maekawa, Usui et al. 2003; Maekawa and Schiebel 2004; Miller, D'Silva et al. 2006; Moore and Miller 2007). Asymmetric localisation of Kar9p is regulated by the yeast Cdk1 Cdc28p in a Clb5p/Clb4p (B-type cyclins) dependent manner (Liakopoulos, Kusch et al. 2003; Maekawa, Usui et al. 2003; Maekawa and Schiebel 2004; Moore and Miller 2007). Two Cdc28p-dependent phosphorylation sites have been identified in Kar9p, at serines 197 and 496 (Liakopoulos, Kusch et al. 2003; Maekawa, Usui et al. 2003; Maekawa and Schiebel 2004; Miller, D'Silva et al. 2006; Moore and Miller 2007). Serine 496 lies within the homologous region to APC. Since APC is also phosphorylated (Trzepacz, Lowy et al. 1997), modification of this residue is thought to represent a conserved mechanism for regulated association with microtubules and microtubule organising centres (Liakopoulos, Kusch et al. 2003; Honnappa, John et al. 2005; Moore and Miller 2007). Mutations that disrupt Cdc28p or Clb5p/Clb4p activity as well as mutations of the phosphorylation sites in Kar9p result in localisation of Kar9p to both SPBs (Liakopoulos, Kusch et al. 2003; Maekawa and Schiebel 2004; Moore and Miller 2007; Moore and Cooper 2010). This possibly results in an orientation of microtubules from both SPBs towards the bud (Liakopoulos, Kusch et al. 2003;

INTRODUCTION

Moore, D'Silva et al. 2006; Moore and Cooper 2010). Phosphorylation of serine 197 is critical for the essential function of Kar9p revealed by the absence of dynein, whereas phosphorylation of serine 496 is not (Moore and Miller 2007). Phosphomimetic mutations of Kar9p rescue asymmetric localisation of Kar9p to the mother SPB when Cdc28p or Clb5p are mutated. Phosphorylation of serine 496 is of particular importance for its localisation to the mother SPB, whereas phosphorylation of serine 197 attenuates the interaction of Kar9p with Stu2p (Moore and Miller 2007). Taken together these results indicate that phosphorylation by Cdc28p allows Kar9p to recognise an intrinsic asymmetry between the SPBs (Moore and Miller 2007; Moore and Cooper 2010). However, molecular details remain unclear.

Two recent studies identified four lysine residues in Kar9p that are sumoylated (Leisner, Kammerer et al. 2008) and one leucine residue that alters sumoylation of Kar9p (Meednu, Hoops et al. 2008). In both studies, mutations of those residues impair localisation of Kar9p to one SPB, but the overall findings differ from each other in both studies.

Meednu and colleagues identified L304 which upon mutation to proline disrupts the interaction with proteins in the sumoylation pathway in yeast-two hybrid screens. The interaction to other Kar9p binding proteins such as Bim1p, Stu2p, Bik1p and Myo2p was not disrupted (Meednu, Hoops et al. 2008). L304 is in close vicinity to a SUMO consensus site (Ψ K x D/E, K301), suggesting a regulatory role of L304 in sumoylation of K301 (Hay 2005; Meednu, Hoops et al. 2008). They furthermore show that Kar9p is sumoylated *in vitro* on at least two residues by proteins of the sumoylation machinery (Meednu, Hoops et al. 2008). Sumoylation of proteins can also be influenced by phosphorylation. Consistently a phosphomimetic mutant (A196E S197E) does not interact with the sumoylation machinery anymore in yeast-two hybrid screens (Meednu, Hoops et al. 2008). Although these results suggest a regulatory role of phosphorylation for sumoylation of Kar9p, the molecular details and the *in vivo* relevance remain unclear.

In the other study, Leisner and colleagues identified four lysine residues in Kar9p that are sumoylated (K301, K333, K381, and K529) *in vivo* (Leisner, Kammerer et al. 2008). A yeast strain expressing a Kar9p version that has mutated all four sumoylation sites fails to accumulate Kar9p asymmetrically on the mother-directed spindle pole body and emanating astral microtubules (Leisner, Kammerer et al. 2008). They could furthermore show that sumoylation and phosphorylation regulate Kar9p asymmetry independently (Leisner, Kammerer et al. 2008). Since sumoylation is hardly detectable in G₁ phase but well-established during metaphase, this modification was proposed to have a positive effect on the function of Kar9p during mitosis (Leisner, Kammerer et al. 2008). Meednu and colleagues furthermore detected in a yeast-two hybrid screen that sumoylation might control multimerisation of Kar9p (Meednu, Hoops et al. 2008). But it might also control the

accessibility of Kar9p to other regulators, or the interaction with microtubule or SPB associated proteins such as Bim1p, Bik1p, Stu2p. Further *in vitro* binding assays will be required to study the role of sumoylation of Kar9p (Leisner, Kammerer et al. 2008).

In contrast to sumoylation, the ubiquitination of Kar9p requires phosphorylation of Kar9p by Cdc28p (Kammerer, Stevermann et al. 2010). Upon ubiquitination Kar9p is degraded by the proteasome. Both processes depend on an intact cleavage apparatus (septins and formins) and the transport of Kar9p to the bud neck by Myo2p. Mutations that prevent Kar9p ubiquitination enhance the interaction of astral microtubules with the cortex at the cleavage plane (Hotz and Barral 2010). Ubiquitination of Kar9p is especially important after the metaphase-anaphase transition to maintain the correct orientation of the mitotic spindle. Kammerer and colleagues proposed that ubiquitination affects the binding of Kar9p to Myo2p and reduces the interaction between astral microtubules and the bud neck (Kammerer, Stevermann et al. 2010).

1.3.2 Adenomatous polyposis coli (APC)

APC is the functional homolog of yeast Kar9p in higher eukaryotes. It is much larger in size than Kar9p and involved in many different processes (Bienz 2001; Nathke 2004) (Figure 5A,B). In humans, mutations in APC or loss of APC are responsible for development of familial adenomatous polyposis (FAP) and resulting colorectal cancer (Half, Bercovich et al. 2009). Loss of the C-terminal part of APC that mediates binding to EB1 is also correlated with tumorigenesis (Powell, Zilz et al. 1992; Su, Burrell et al. 1995; Tirnauer and Bierer 2000). APC is a multifunctional protein that is involved in degradation of β -catenin and plays a role in cell migration, cell adhesion and mitosis by regulating cytoskeletal proteins (Figure 5A). It can bind to actin and microtubules itself but also interacts with EB1 for its tethering to microtubules (Nathke 2004). APC has a size of 312 kDa and consists of multiple domains mediating its different functions (Aoki and Taketo 2007). During mitosis, APC localises to kinetochores, spindles and centrosomes, suggesting a role in kinetochore function and chromosome segregation through direct or indirect interaction with microtubules (Aoki and Taketo 2007; Cheng and Mao 2011).

Although the sequence similarity between Kar9p and APC is very limited (Figure 5B) (Bienz 2001), both proteins have common binding partners and functions (Nathke 2004). Both bind to EB1/Bim1p and the mode of this interaction seems to be similar. However, the molecular details are still unknown. Furthermore, Kar9p and APC both localise to centrosomes/SPBs and microtubule tips and might be both involved in sustaining asymmetric cell divisions (Liakopoulos, Kusch et al. 2003; Yamashita, Jones et al. 2003; Nathke 2004).

In *Drosophila* one form of APC might play a role in cortical attachment. Loss of such specific cortical attachment sites might result in defective spindle anchoring (Nathke 2004). Similar to

this function of APC, Kar9p also mediates the anchoring of microtubules at the bud neck and cortex (Huisman, Bales et al. 2004).

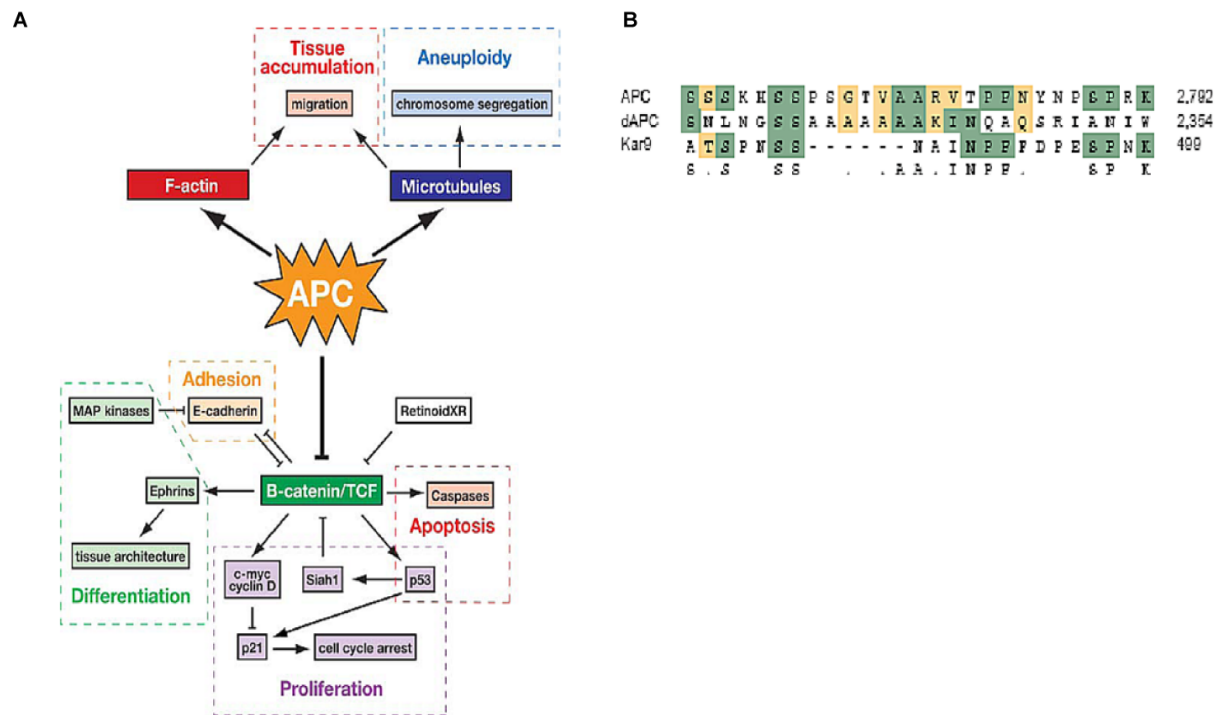


Figure 5 Functions of adenomatous polyposis coli (APC) (A) Representation of the different functions of APC. APC binds directly or indirectly to F-actin and microtubules but also plays an important role in β -catenin signalling. Image taken from (Huisman, Bales et al. 2004). (B) Sequence alignment of human and *Drosophila* APC with the functional yeast homologue Kar9p. The region mediating the binding to EB1 in APC and the EB1 homologue Bim1p in yeast are conserved, suggesting a common binding mechanism. Picture taken from (Nathke 2004).

1.4 Objectives

Mitotic spindle orientation is a well conserved mechanism that is important for proper chromosome segregation and determination of cell fate. In humans, impaired spindle orientation is often correlated with development of cancer. Identifying the molecular mechanisms regulating mitotic spindle orientation will likely contribute to our understanding of these disorders. Most proteins involved in spindle orientation are conserved from yeast to human, making yeast an adequate, but also comparably easier model system to investigate the underlying molecular details.

This research presented here aims to understand the assembly of the mitotic spindle orientation complex in *Saccharomyces cerevisiae*, formed by Bim1p, Kar9p and Myo2p. Although yeast-two hybrid screens helped to identify domains that mediate interactions with their respective binding partners, the underlying molecular details remain sketchy (Miller, Cheng et al. 2000).

In this study a multidisciplinary approach using biochemical and structural experiments as well as functional studies in living cells was employed. Such a multidisciplinary approach

INTRODUCTION

established a more detailed understanding of the Bim1p-Kar9p interaction. It furthermore helped to relate structural information with functionality by cross-validating mechanistic insights from different experimental approaches.

The first part of the work focused on determination of the three-dimensional structure of Kar9p and posttranslational modifications of Kar9p required for interaction with Bim1p. In the second part, the interaction between Bim1p and Kar9p and its regulation by posttranslational modifications was studied in more detail to elucidate the molecular principles underlying spindle orientation in yeast.

2 Results

2.1 Expression, purification and crystallisation of Kar9p

2.1.1 Expression and Purification of full-length Kar9p (FL)

Full-length Kar9p (FL) is comprised of 644 amino acids and has a molecular weight of 74.2 kDa. Secondary structure and domain predictions (Miller, Cheng et al. 2000) suggest that the protein consists of three domains. Recent studies have shown that the protein is posttranslationally modified by phosphorylation (Maekawa and Schiebel 2004; Moore, D'Silva et al. 2006; Moore and Miller 2007) and sumoylation (Leisner, Kammerer et al. 2008; Meednu, Hoops et al. 2008) (Figure 6A). I cloned the full-length *KAR9* gene from yeast genomic DNA into different *E.coli* and insect cell expression vectors (see chapter 4.11.1 and 4.11.4). Protein expression was accomplished as a GST- or His-tagged version in *E.coli* (BL21 and Rosetta) as well as in insect cells and in yeast.

Purification of the protein was performed as described in chapter (4.11.5 and 4.11.6). Kar9p (FL) with a GST-tag was found to degrade rapidly, whereas the His-tagged protein did not degrade after addition of 10 mM arginine and 10 mM glutamic acid to the buffer during the first purification step. Ultimate purity achieved was $\geq 95\%$, as shown in Figure 6B. Expression in yeast cells under the endogenous *KAR9* promoter did not yield satisfactory amounts of protein, a likely cause being low expression levels in yeast (656 molecules/cell). Purification of Kar9p (FL) from both insect and *E.coli* cells achieved similar and higher yields. With the protein from insect cells not as well behaving as the one extracted from *E.coli*, for all crystallisation experiments purified Kar9p (FL) from *E. coli* was used. Crystallisation experiments were always done in the presence of the His-Tag as the usual removal of the His-tag with TEV-protease also degraded the protein. Kar9p (FL) expressed in minimal medium containing Selenomethionine could also be purified as soluble protein.

Dynamic-light scattering analysis showed that Kar9p (FL) has a hydrodynamic radius of ~ 7.5 nm and that it aggregates at concentrations ≥ 4 mg/ml. This aggregation could be reversed by diluting the protein solution to concentrations below 4 mg/ml. Small-angle X-ray scattering analysis (SAXS) (see chapter 4.10.5) revealed that Kar9p has a radius of gyration of 5.15 nm and a molecular weight of 180 kDa, which corresponds to a trimer or tetramer. Initial bead models were calculated from the SAXS data using the *Gasborp* and *Gasbori* software (Svergun, Petoukhov et al. 2001). Despite the apparent good quality of input data, resulting bead models were variable and not sufficient for further structural characterisation of this protein.

RESULTS

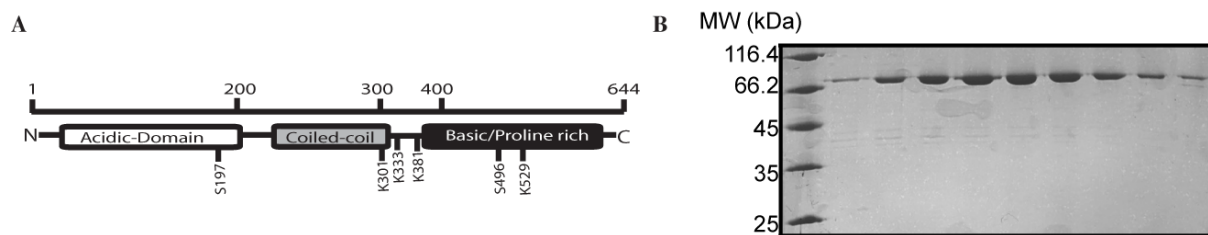


Figure 6 Domain organisation and purification of Kar9p (FL) (A) Kar9p (FL) consists of three domains: an acidic domain at the N-terminus, followed by a coiled-coil region in the middle domain and a basic (proline-rich) domain at the C-terminus. The protein is posttranslationally modified at four lysine residues (sumoylation: K301, K333, K381, K529) and two serine residues (phosphorylation: S197, S497). (B) Example of a purification of Kar9p (FL) from *E.coli* after size-exclusion chromatography. The protein is stable and can be purified to high purity ($\geq 95\%$).

2.1.2 Crystallisation of Kar9p (FL)

Recombinant Kar9p (FL) was concentrated in size-exclusion chromatography (SEC) buffer to concentrations up to 6 mg/ml. Initial crystallisation screens were performed with different concentrations of protein solution (1-6 mg/ml) at RT and 4°C. Crystals of Kar9p (FL) appeared after 1-2 days in three conditions ([A] 0.1 M Hepes pH 7.5 + 25 % (w/v) PEG 2000 MME; [B] 0.2 M trisodium citrate + 20 % (w/v) PEG 3350; [C] 0.2 M tripotassium citrate + 20 % (w/v) PEG 3350) (Figure 7A). After refinement, crystals of Kar9p (FL) were grown at 21°C by hanging-drop vapor-diffusion using a 1:1 mixture of protein (1-6 mg/ml) and crystallisation solution containing 0.1M Hepes pH 8.0, 21 % PEG 2000 MME, 125 mM serine or 0.1 M potassium citrate, 20 % PEG 3350, 125 mM serine. Needle-like crystals with cracked ends appeared within 1-2 days and had a size of 20 - 50 μm x 100 - 400 μm (Figure 7B). The cracked ends were present in all crystals and are likely to be caused by fast crystal growth. Formation of ice crystals while freezing the crystals was prevented by adding a number of cryo-protectants (glycerol, ethylene glycol, PEG 400) in different concentrations and for a variety of incubation periods. Diffraction data of crystals were collected at various beam lines at the ESRF in Grenoble and crystals showed diffraction up to 7 Å resolution. The diffraction patterns displayed mostly well-defined spots (Figure 7E) and datasets could be processed with *XDS* or *Mosflm*. Processing of the datasets showed that the crystals belong to space group P3 with unit-cell parameters of 200x200x250 Å and approximately 16 molecules per asymmetric unit.

One crystal grown in 0.1M Hepes pH 7.5, 29 % PEG 2000 MME, 125 mM serine with 20 % glycerol as cryo-protectant showed diffraction up to 3 Å resolution. The dataset, however, was incomplete, as only 180° were recorded and some angles showed smeared spots that could not be used for processing of the dataset. The presence of several ice-rings in the diffraction pattern caused additional problems, and prevented processing of resolutions better than 3.4 Å (Figure 7F). Processing of the dataset with *XDS* showed that this crystal consists of the space group P2 and has a smaller unit cell with a size of 46x76x120 Å. This form of crystal however, could not be reproduced again (see below).

RESULTS

To prevent the appearance of cracked ends and to improve the X-ray diffraction properties of the crystals, different growth conditions were tested to slow down the speed of crystal formation. In a first attempt at this, the reservoir solution was covered with oil as a barrier to slow down vapour diffusion between the reservoir solution and the drop (Chayen 1997). For this purpose, silicone oil and paraffin oil were used in different ratios (50:50, 65:35) and different volumes (200 μ l - 500 μ l) to cover the reservoir solution. Paraffin oil alone allows only for very little vapour diffusion, whereas silicone oil alone allows for vapour diffusion almost comparable to crystallisation without oil. Thus, using different mixtures and volumes of these oils, the rate of vapour diffusion was controlled. Despite several trials, also at 4°C, this attempt did not slow down crystal growth. None of the crystals thus generated displayed better X-ray diffraction properties.

Organic solvents are frequently used in crystallisation to alter the sample-sample as well as the sample-solvent interactions. They can stabilise the protein but also act as precipitants, as they can cause denaturation of the protein by displacing water molecules on the protein surface (Anand, Pal et al. 2002). Addition of 4-6 % isopropanol or MPD to the crystallisation solution was tried, but did not improve the properties of the crystals.

Glycerol is another component that has been successfully used in the crystallisation of proteins with flexible domains. It has been shown to stabilise unstructured parts of proteins (Sousa 1995). It is also thought to interfere with nucleation. Therefore addition of glycerol to the crystallisation solution may result in fewer but bigger crystals. Accordingly, low concentrations of glycerol (2-10%) were added to the purified Kar9p (FL) and the crystallisation solution, but did not help to improve the quality of the crystals.

Crystals grown at 4°C in the conditions described above appeared after 3-4 days and were again needle shaped, but thicker than the crystals grown at 21°C and without cracked ends (Figure 7C). Despite the slower growth and the better morphology, however, these crystals only showed X-ray diffraction up to 10 Å.

Elsewhere, it has been shown that the addition of proteases to proteins (*in situ* proteolysis) that have already formed crystals can improve the X-ray diffraction properties of the crystals (Dong, Xu et al. 2007; Wernimont and Edwards 2009). Addition of trace amounts of proteases to the crystallisation trials mostly results in the digestion of flexible parts of the protein. Usually 20-40 residues of the N- or C-termini as well as affinity tags (His-tag etc.) are removed. Addition of proteases can also result in the removal of internal flexible loops or even of entire domains. Flexible regions may interfere with the crystal packing and therefore hinder the formation of a well-ordered crystal lattice with good X-ray diffraction properties.

Trypsin and Endoproteinase Glu-C were consequently added to the protein solution in different ratios (w/w, 1:1000, 1:500, 1:200) prior to setting up crystal screens. Trypsin cleaves at the C-terminal part of basic residues, whereas Glu-C cleaves at the C-terminal part of

RESULTS

glutamic acid residues and with a much slower rate at aspartic acid residues. Although Kar9p (FL) can be digested with these proteases into smaller fragments, this did not improve the quality of the crystals.

A technique termed “seeding” can be used to control the growth rates of crystals or to change the crystal morphology (Bergfors 2003). It allows crystals to grow in a metastable zone where the protein and the reagent concentration are not sufficient for spontaneous nucleation, but allow seed crystals to grow bigger. Two different techniques have been tried, namely streak seeding and Seed beads. Both methods were utilized with tools from Hampton Research (Seed beads and Seeding Tool, Aliso Viejo, USA). For the Seed beads method one crystal was transferred from a plate into an Eppendorf tube containing the crystallisation solution and one Seed bead, and broken up into small crystal fragments by vigorous vortexing. Serial dilutions of this solution were prepared (10^{-1} – 10^{-5} , in crystallisation solution) and added to fresh crystallisation setups. Streak seeding uses an animal whisker to break loose small crystal fragments from existing crystals and transfer those seeds into a new drop. It can also be used to stir old drops with precipitate since this can equally induce nucleation and crystal growth. Seeds were prepared as described with the Seed beads and transferred to crystallisation setups with a cat whisker. Despite several trials, none of both methods improved the diffraction quality of the Kar9p (FL)-crystals.

Another attempt to improve the crystals was made by methylating Kar9p *in vitro*. It has been shown that methylation of lysine residues can help to improve the formation of a crystal lattice by changing the surface properties of the protein and by immobilizing these flexible side chains (Kim, Quartey et al. 2008).

A protocol how lysine residues of purified Kar9p were methylated is described in chapter 4.12.3. The methylated protein was concentrated to 6 mg/ml and initial crystallisation screens were set up with protein concentrations of 2, 4 and, 6 mg/ml. Crystals appeared after 2-3 days in various conditions in the initial screens. The shapes of the crystals were either thin needles or thin plates, which were often intergrown (Figure 7D). The needles lacked the cracked ends found in crystals of unmethylated Kar9p (FL). Refinement initiated crystal growth in 0.1 M ammonium acetate, 0.1 M Bis-Tris pH 6.5 and 16 % PEG 3350. Subsequently, different additives (amino acids, sugars) were tested in a ratio of 1:20 (v/v), resulting in the formation of both crystal forms, depending on the additive. Cryo-protection was achieved with different concentrations of ethylene glycol or sucrose. None of the crystals tested at the synchrotron diffracted X-rays.

Kar9p was also expressed and purified as Selenomethionine labelled protein. Crystals appeared in the same conditions as the unlabelled protein but either showed no or only weak X-ray diffraction (≥ 10 Å). Soaking of the native crystals with different heavy atom solutions

RESULTS

was also tried, (see chapter 4.12.6), but did not improve the diffraction properties of the crystals.

In addition to all the attempts described, crystals of Kar9p (FL) were tested at room temperature using the MiTeGen MicroRT system (MiTeGen, LLC, Ithaca USA). Measurements at room temperature were used to determine whether the cause of poor X-ray diffraction properties is due to poorly ordered crystals, crystal damage caused by cryoprotectant soaks, or crystal damage caused by the flash cooling in liquid nitrogen. Crystals were mounted on a MicroMount, which was subsequently covered with a polymer capillary tubing filled with some mother liquid at the tip to prevent the crystal drying out. When tested at the synchrotron, all crystals showed the same X-ray diffraction properties as the ones frozen in liquid nitrogen. Hence the poor diffraction properties were not due to suboptimal cryo-protection or issues with the freezing of the crystals, but rather due to crystal packing.

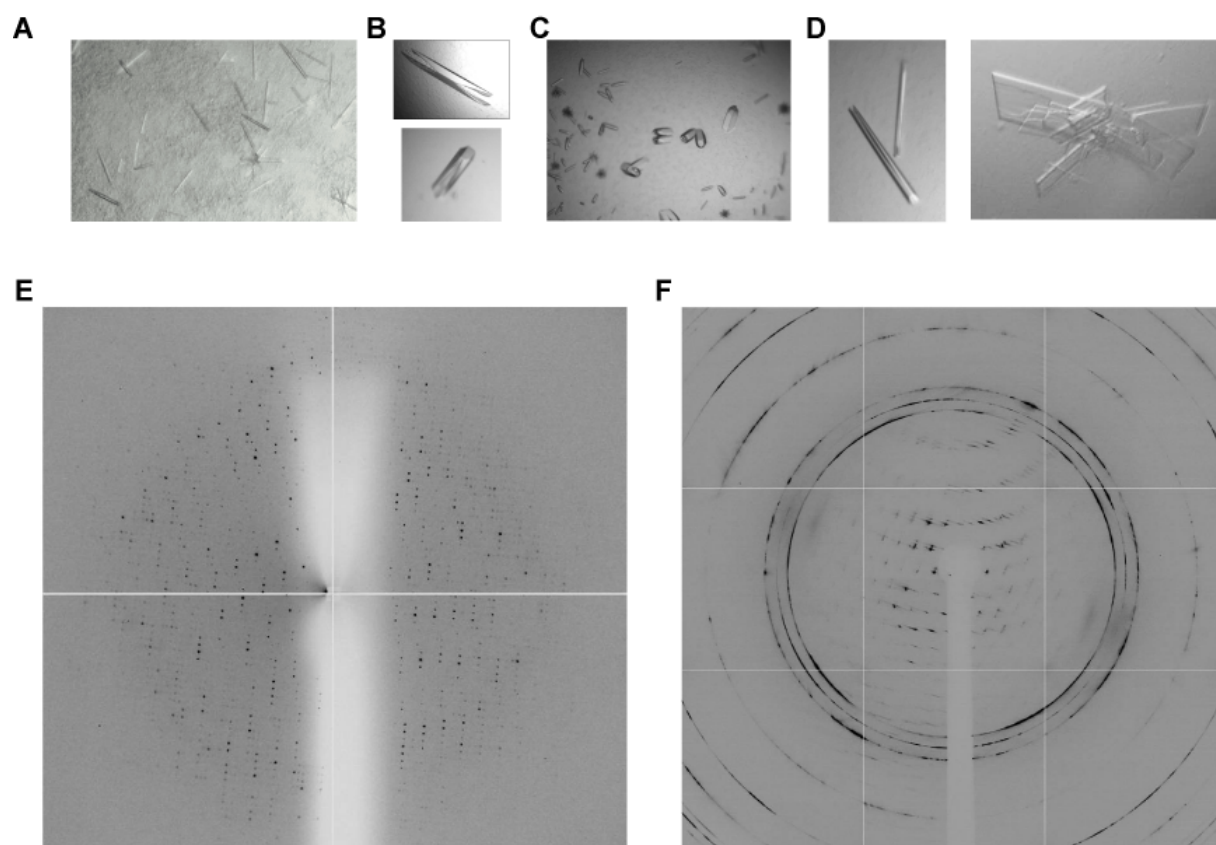


Figure 7 Crystallisation of Kar9p (FL) (A) Crystals of Kar9p (FL) in the initial crystallisation screens and (B) crystals of Kar9p (FL) in the refinement screens. The crystals were needle shaped and had always cracked ends. (C) Crystals of Kar9p (FL) at 4°C lacked cracked ends (D) Crystals of methylated Kar9p (FL) were either needle shaped or plate-like, which were often intergrown (E) Diffraction pattern of a crystal of Kar9p (FL). Crystals diffracted up to 7 Å with many well-defined spots. (F) Diffraction pattern of one crystal of Kar9p (FL) showing diffraction up to 3 Å. Some angles of the data set contained many well-defined spots (as in (E)), whereas some diffraction patterns at certain angles contained many smeared spots (F). All frames of the dataset contained ice-rings, which made processing of the dataset above 3.4 Å impossible.

2.1.3 Expression and Purification of Kar9p-variants

As purification and crystallisation of Kar9p (FL) did not yield good enough results to solve the crystalline structure of Kar9p, several strategies were pursued to identify shorter fragments of Kar9p, to be used for crystallisation and interaction studies with Bim1p. Differences of only a few residues at the C- or N-termini of proteins can have dramatic effects on the solubility of the protein and protein crystallisation. Expressing many variants of the protein can therefore increase success rates.

First, limited proteolysis of Kar9p (FL) with different site-specific proteases was performed as described in chapter 4.10.6. Four of the resulting protease-resistant protein fragments were subjected to Edman-sequencing. Due to sample heterogeneity no sequence could be unambiguously assigned to Kar9p (FL) and thus not be used to design new constructs. Therefore, shorter fragments of Kar9p were designed based on secondary structure predictions (Jpred, (Cole, Barber et al. 2008)) and on a three-dimensional structure prediction calculated by the *HHPred Server* (Soding, Biegert et al. 2005). The structure prediction from *HHPred Server* suggests that the N-terminal half of the protein consists mostly of α -helices, whereas the C-terminal part of the protein is supposedly completely devoid of structure (Figure 8A). Secondary structure predictions propose mostly α -helices in the N-terminus, but also some α -helices together with large unstructured parts in the C-terminal half of the protein. Several new fragments of *KAR9* were cloned in vectors with either a GST- or a His-tag and tested for protein expression and purification in *E.coli*. Because the C-terminal part of Kar9p interacted with Bim1p in yeast-two hybrid screens (Miller, Cheng et al. 2000; Moore and Miller 2007), this portion of the protein was also considered in expression tests. An overview of the fragments tested and their behavior during purification and crystallisation is shown in Table 1.

It was then first observed that variants of Kar9p lacking only some amino acids at the N-terminus or the C-terminus had the same expression and purification characteristics as full-length Kar9p.

Deletion of the structured N-terminal part leads to rapidly degrading proteins that were hard to express and purify, both in the presence of a GST- or a His-Tag. Because the putative coiled-coil region of Kar9p is missing in these fragments, a GST-tag was tested. GST-tags can dimerise and stabilise the proteins. However, in light of the unsatisfactory outcome of these expression and purification tests, the purification of the fragments was not pursued further.

Deletion of the unstructured N-terminal part on the other hand resulted in highly expressible proteins. Depending on the length of the deletion, however, some proteins degraded during purification. Only one fragment consisting of the amino acids 1-398 remained sufficiently soluble and could be purified either with a GST- or a His-tag. All other fragments could only

RESULTS

be expressed and purified in the presence of a His-tag. A purification of Kar9p (1-398) with either tag is shown in Figure 8B.

Construct	Tag	Expression	Purification	Initial crystals	Refined crystals
Kar9p (FL)	His	+	+	+	7Å (one with 3Å)
Kar9p (FL)	GST	+/-	-	-	-
Kar9p (5-644)	His	+	+	-	-
Kar9p (7-644)	His	+	+	-	-
Kar9p (10-644)	His	+	+	+	7Å (as crystals from Kar9p (FL))
Kar9p (12-644)	His	+	+	+	7Å (as crystals from Kar9p (FL))
Kar9p (1-640)	His	+	+	Not tested	
Kar9p (5-640)	His	+	+	Not tested	
Kar9p (7-640)	His	+	+	Not tested	
Kar9p (10-640)	His	+	+	Not tested	
Kar9p (12-640)	His	+	+	Not tested	
Kar9p (1-637)	His	+	+	Not tested	
Kar9p (5-637)	His	+	+	Not tested	
Kar9p (7-637)	His	+	+	Not tested	
Kar9p (10-637)	His	+	+	Not tested	
Kar9p (12-637)	His	+	+	Not tested	
Kar9p (1-635)	His	+	+	Not tested	
Kar9p (5-635)	His	+	+	Not tested	
Kar9p (7-635)	His	+	+	Not tested	
Kar9p (10-635)	His	+	+	Not tested	
Kar9p (12-635)	His	+	+	Not tested	
Kar9p (1-608)	His	+	+	Not tested	
Kar9p (12-608)	His	+	+	Not tested	
Kar9p (1-478)	His	++	++	No crystals	
Kar9p (1-517)	His	++	++	No crystals	
Kar9p (245-644)	His	+/-	-	Not tested	
Kar9p (245-644)	GST	+/-	-	Not tested	
Kar9p (250-644)	His	+/-	-	Not tested	
Kar9p (250-644)	GST	+/-	-	Not tested	
Kar9p (298-644)	His	+/-	-	Not tested	
Kar9p (298-644)	GST	+/-	-	Not tested	
Kar9p (307-644)	His	+/-	-	Not tested	
Kar9p (307-644)	GST	+/-	-	Not tested	
Kar9p (1-451)	His	++	+/-	Not tested	
Kar9p (1-451)	GST	+/-	-	Not tested	
Kar9p (1-429)	His	++	+/-	Not tested	
Kar9p (1-429)	GST	+/-	-	Not tested	
Kar9p (1-408)	His	++	++	Crystalline precipitate	
Kar9p (1-404)	His	++	++	Crystalline precipitate	
Kar9p (1-401)	His	++	++	Crystalline precipitate	
Kar9p (10-401)	His	++	++	Not tested	
Kar9p (12-401)	His	++	++	Not tested	
Kar9p (1-398)	His	++	++	+	7Å, additional spots at 4-5Å
Kar9p (1-398)	GST	++	++	+	Not tested
Kar9p (10-398)	His	++	++	Not tested	
Kar9p (12-398)	His	++	++	Not tested	
Kar9p (1-395)	His	++	++	Crystalline precipitate	
Kar9p (10-395)	His	++	++	Not tested	
Kar9p (12-395)	His	++	++	Not tested	
Kar9p (1-373)	GST	+/-	-	Not tested	
Kar9p (1-355)	GST	+/-	-	Not tested	
Kar9p (1-338)	GST	+/-	-	Not tested	
Kar9p (1-307)	His	+	+	Not tested	
Kar9p (1-307)	GST	+/-	-	Not tested	
ACR023W1 (1-769)	His	+/-	-	Not tested	
ACR023W1 (1-769)	GST	+/-	-	Not tested	
CAGL0A01155g (1-609)	His	+/-	-	Not tested	
CAGL0A01155g (1-609)	GST	+/-	-	Not tested	

Table 1 Overview of Kar9p variants tested for expression, purification and crystallisation ++: high level of expression/high amount of purified protein; +: good level of expression/amount of protein enough for purification; +/-: very low protein expression/protein rapidly degrading

RESULTS

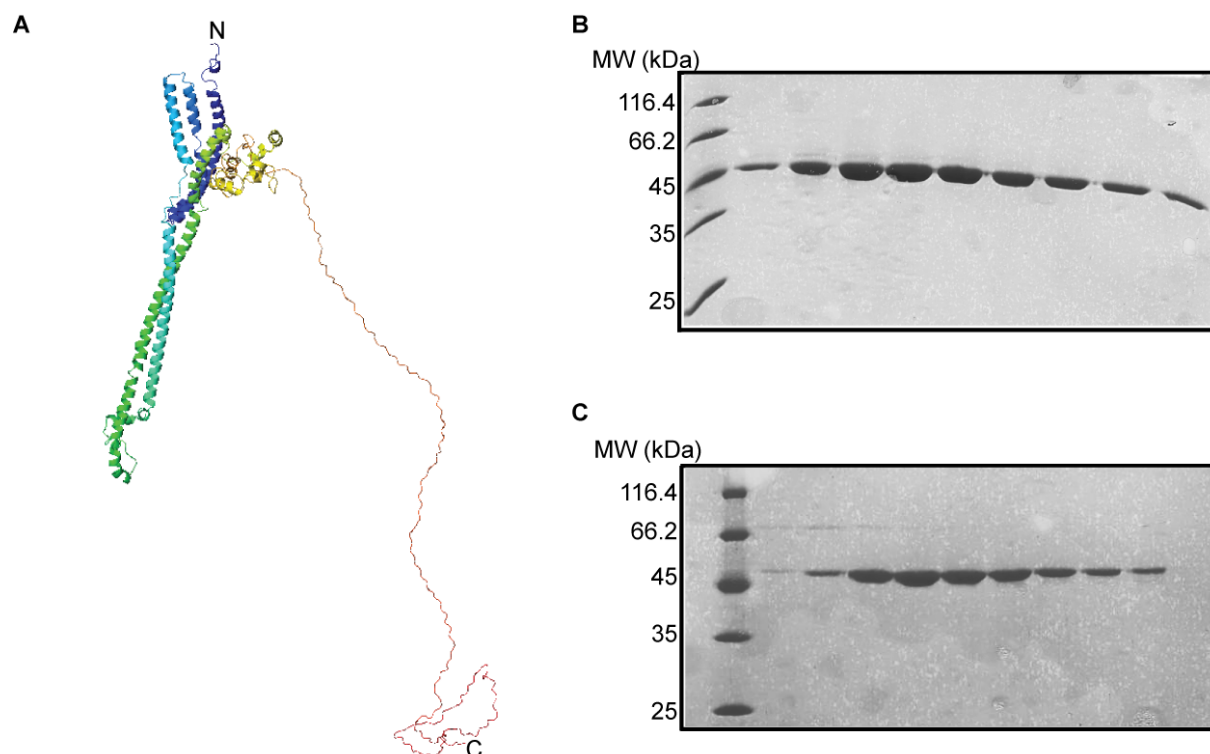


Figure 8 Structure prediction of Kar9p (FL) and purification of Kar9p (1-398) (A) Structure prediction of Kar9p (FL) from *HHPred-Server*. The N-terminal part of the protein is predicted to be structured, whereas the C-terminal part may be unstructured. (B) and (C) Purification of Kar9p (1-398) with a His-tag (B) or a GST-tag (C). Both proteins are shown after cleavage of the GST-tag with the PreScission protease and size-exclusion chromatography.

A fragment consisting of amino acids 1-517 was also successfully purified and subsequently used for limited proteolysis with Endoproteinase Glu-C (see chapter 4.10.6). Two shorter fragments could be identified by Edman-sequencing, one starting at the N-terminal His-tag and the other one starting at amino acid 8 of Kar9p. Molecular weight determination by mass spectrometry, however, did not give interpretable results. The molecular weight of these fragments was instead estimated from SDS-PAGE. It suggests that both fragments comprise the structured N-terminal part predicted by *HHPred server* (residues ~1 - 400). From this experiment, it can be concluded that the N-terminal part of Kar9p is likely to fold into a globular domain. In contrast, the C-terminal domain can be digested by proteases and thus might be flexible and partially unfolded. These interpretations are consistent with structure predictions.

2.1.4 Crystallisation of Kar9p-variants

As the crystallisation of Kar9p (FL) did not yield high quality diffracting crystals, different shorter Kar9p variants were crystallised as described for Kar9p (FL). Most of these Kar9p variants did not form crystals in the initial screens (Table 1). Only Kar9p-fragments lacking a few amino acids at the very N-terminus (1-12) or lacking large parts of the C-terminus (1-398; 1-401) formed crystals in the initial screens. Crystals lacking parts of the N-terminus grew in

RESULTS

similar conditions as Kar9p (FL) and did not show any improvement in X-ray diffraction. Those crystals also had the same shape as crystals of Kar9p (FL).

Crystals grown from Kar9p (1-398) were needle shaped but did not have cracked ends like crystals from Kar9p (FL). These crystals were grown at concentrations of 0.5-1 mg/ml with a crystallisation solution containing 50 mM MES pH 6.0; 5 % PEG400, 0.5 M ammonium sulfate and either 0.1 M urea, 2.5 mM Glutathione or 1 % MPD as additive. Crystals appeared after 2-3 days. Crystals of this fragment showed diffraction up to 7 Å resolution with some additional smeared spots around 4-5 Å resolution (Figure 9A-C). Processing of the datasets with *XDS* or *Mosflm* was not possible, since some spots of the diffraction patterns were too smeared and could therefore not be correctly integrated by the programs. Different cryo-protectants (MPD; ethylene glycol, PEG 400, glycerol, sucrose, glucose) and incubation times with cryo-protectants as well as longer exposure times to the X-rays at the synchrotron did not improve the diffraction properties of these crystals. Additionally, X-ray diffraction properties of the crystals were tested at room temperature using the MiTeGen MicroRT system (MiTeGen, LLC, Ithaca USA), but were worse. To improve the properties of the crystals, several slightly larger or smaller fragments were purified and screened for crystallisation, but only crystalline precipitation was obtained in the initial screens. Considering that the morphology and X-ray diffraction properties of the crystals of Kar9p (1-398) did not change or improve in comparison to crystals of Kar9p (FL), fragments identified by limited proteolysis (Kar9p (10-398) and (7-398)) have not been tested for crystallisation.

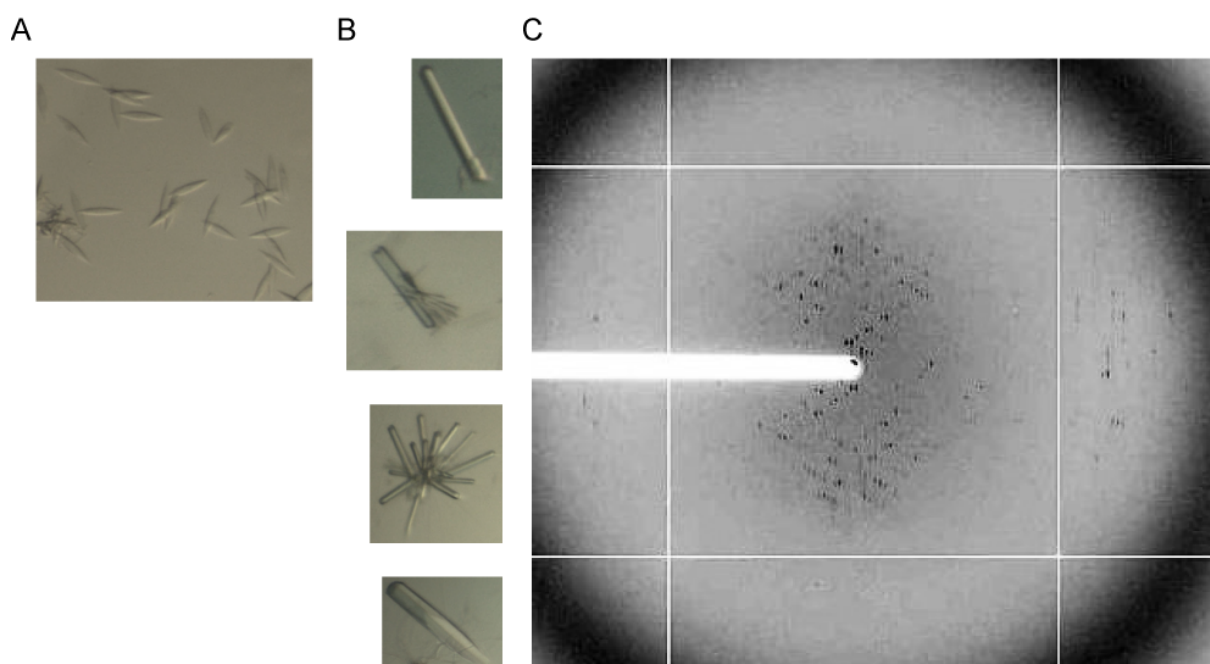


Figure 9 Crystallisation of Kar9p (1-398) (A) Crystals in the initial screens. (B) Crystals after refinement. (C) Diffraction pattern of the crystals at the synchrotron. Crystals diffract up to 7 Å with some additional spots around 4-5 Å (weak smeared spots on the left and right side in the middle).

2.1.5 Expression and purification of Kar9p-homologs from other yeast species

To increase the likelihood of successful crystallisation of Kar9p, databases were searched to identify homologous proteins from other yeast species. Homologues of Kar9p from *Ashbya gossypii* (ACR023W1) and *Candida glabrata* (CAGL0A1155g) were identified as possible candidates. The proteins have a sequence identity of 34%/35% and a sequence similarity of 52%/56% compared to Kar9p. ACR023W1 is comprised of 769 amino acids and thus 125 amino acids longer than Kar9p (FL) whereas CAGL0A1155g is comprised only of 609 amino acids and therefore 35 residues shorter than Kar9p (FL) (Figure10). Both genes were cloned as full-length constructs and expressed in *E.coli* as His- or GST-tagged fusion proteins. However, both proteins degraded during purification regardless of the tag used, this approach was not pursued further.

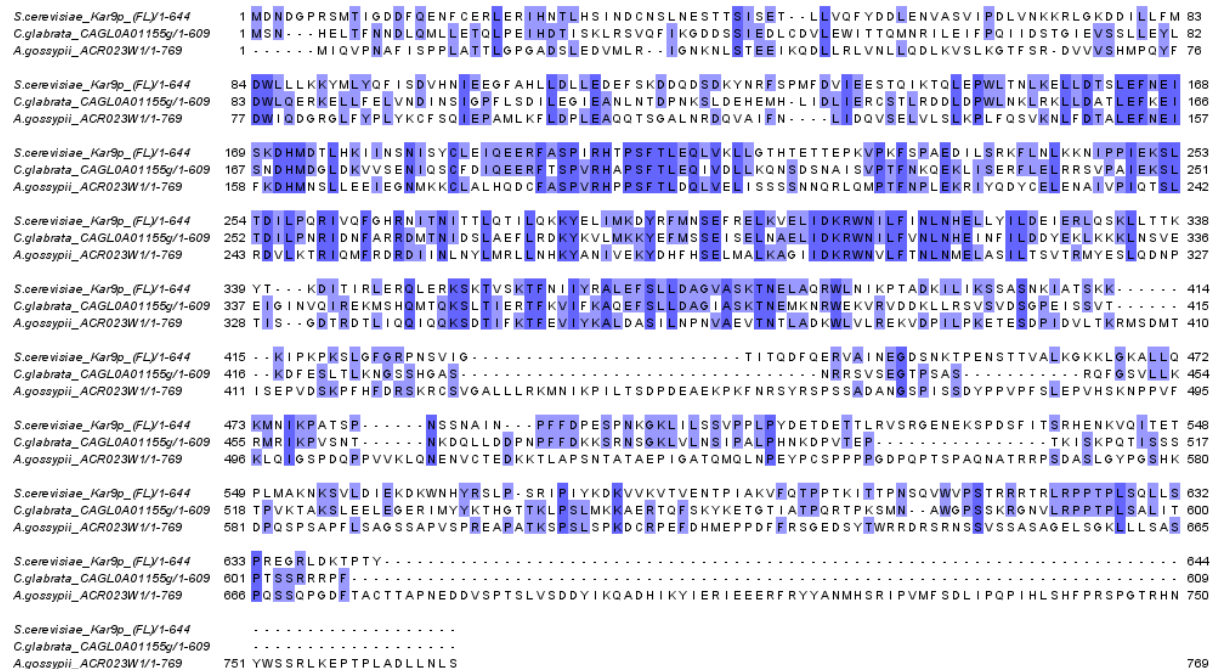


Figure 10 Sequence alignment of Kar9p (FL) and homologous proteins from other yeast species Colour code: dark blue: identical residues, light blue: medium conservation, white: no conservation

2.1.6 Co-crystallisation of Kar9p and Bim1p

Another commonly used procedure to improve X-ray diffraction properties of crystals is to crystallise proteins in the presence of an interaction partner. An interaction partner can stabilise the other protein, for instance when the protein binds to unstructured regions or when the interaction partner induces folding of unstructured parts. Since Bim1p has been suggested to bind to the unstructured part in the C-terminus of Kar9p, it was chosen as candidate for co-crystallisation (see also 2.1.3). Two different variants of Bim1p were chosen for co-crystallisation trials: Bim1p (FL) and the C-terminal dimerisation domain of Bim1p (182-282, C-term), which has been suggested to bind to Kar9p (Miller, Cheng et al. 2000). Proteins were purified separately and mixed in different molar ratios prior to

RESULTS

crystallisation trials (see chapter 4.12.4). Crystals appeared under several crystallisation conditions only with Bim1p (C-term) and Kar9p (FL). Dependent on the conditions the crystals were either needle-shaped like crystals from Kar9p (FL) or plate-like. Both crystal forms could be reproduced in refinement screens. Cryo-protection was achieved with different concentrations of glycerol or ethylene glycol and the crystals were tested for diffraction at various beamlines at the ESRF in Grenoble. Needle-shaped crystals only weakly diffracted X-rays up to 8 Å, whereas the plate-like crystals showed diffraction up to 2.5 Å, albeit with some anisotropy. Processing of the datasets recorded from the plate-like crystals showed that they belong to space group P222 with a unit cell size of 27x43x99 Å. This unit cell size is too small to fit in both proteins, therefore molecular replacement with the known human EB1 structures (PDB IDs 1wu9, 1YIB, 1YIG) was performed and a solution was obtained with the *MOLREP* software (Vagin and Teplyakov 2010). As the refinement statistics of this solution were not sufficient and could not be further refined, the structure of Bim1p (C-term) could not be solved by this approach. With both proteins not co-crystallising, no additional attempts to co-crystallise Bim1p and Kar9p were performed. Subsequent experiments showed that the proteins when purified from *E.coli* do not interact with each other and thus offered an explanation for the failed crystallisation trials. Therefore, with no success in producing diffraction-quality crystals despite serious efforts, the aim of the research was revised to focus more prominently on the interaction between Kar9p and Bim1p.

2.2 Role of posttranslational modifications of Kar9p

Parallel to the co-crystallisation experiments with Bim1p (C-term) and Kar9p (FL) I tested the potential of a direct interaction between Bim1p and Kar9p purified from *E.coli* without posttranslational modifications. Pull-down experiments with either GST-tagged Bim1p (C-term) or Bim1p (FL) and His-tagged Kar9p (FL) were carried out. No direct interaction between these proteins could be observed. Moreover, no interaction was observed when both proteins were loaded together onto a size-exclusion chromatography column. Both proteins eluted at their respective elution volume.

This poses the question whether posttranslational modifications of Kar9p are required for the interaction with Bim1p. Earlier studies have shown that Kar9p is posttranslationally modified by sumoylation and phosphorylation (Liakopoulos, Kusch et al. 2003; Maekawa, Usui et al. 2003; Maekawa and Schiebel 2004; Moore, D'Silva et al. 2006; Moore and Miller 2007; Leisner, Kammerer et al. 2008; Meednu, Hoops et al. 2008). Since the unmodified proteins from bacteria do not interact, these modifications might be required for the interaction of Bim1p and Kar9p. To test this hypothesis, pull-down experiments with recombinant Bim1p (FL) or Bim1p (C-term) and extracts from Myc-Kar9p expressing yeast cells were

RESULTS

performed. With both proteins Kar9p could be clearly detected in subsequent western blots with an α -myc antibody (Figure 19). This indicates that posttranslational modifications of Kar9p or a yet unknown additional binding partner are required for the interaction of Kar9p and Bim1p. For further analysis of the role of posttranslational modifications, several yeast strains harbouring mutant versions of Kar9p were generated and tested in pull-down experiments.

2.2.1 Phosphorylation of Kar9p is not required for the interaction with Bim1p

Kar9p is phosphorylated at two serines (197 and 496) by the Clb4p/Cdc28p kinase (Figure 11A) (see chapter 1.3.1). To test whether these posttranslational modifications play a role in formation of complexes with Bim1p, yeast strains that harbour single point mutations in either Kar9p phosphorylation site, preventing their modification were generated. Another yeast strain harbouring the corresponding double mutant was generated. In pull-down experiments with recombinant Bim1p all of the Myc-Kar9p (S197A)/(S496A) or (S197A+S496A) expressing strains showed a wild type like binding to Bim1p (Figure 11B). It can therefore be concluded that the formation of complexes between Bim1p and Kar9p is not regulated by Clb4p/Cdc28p-dependent phosphorylation at serine 197 or serine 496.

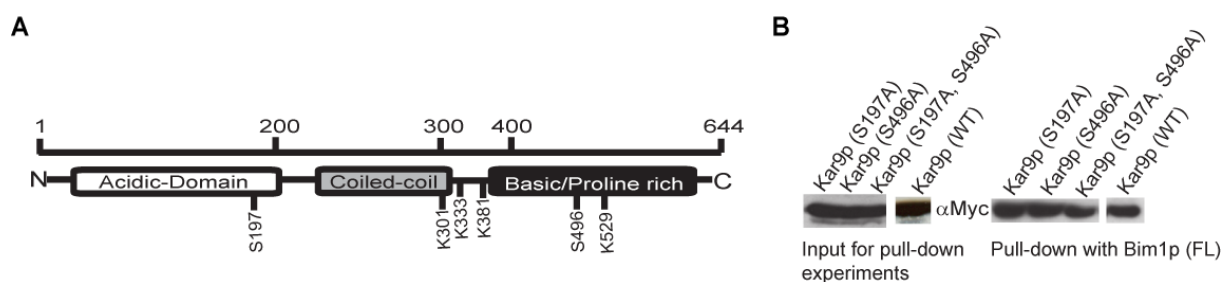


Figure 11 Role of phosphorylation of Kar9p on complex formation with Bim1p (A) Domain composition of Kar9p (FL), showing the two modification sites S197 and S496. (B) Western blot of pull-down experiments with yeast strains harbouring point mutations in Kar9p. None of the mutants showed an effect on complex formation between Bim1p and Kar9p.

2.2.2 In vivo effects of phosphorylation deficient Kar9p-variants

Another not yet answered question was whether mutations of phosphorylation sites in Kar9p do have an effect in vivo, when the yeast strains are challenged by different temperatures or exposed to *Benomyl*. The Myo2p-Kar9p-Bim1p dependent spindle orientation pathway is partially redundant with the dynein-dependent spindle elongation pathway (Miller and Rose 1998). Therefore, the effect of mutations on spindle orientation in either pathway is better observed when cells are challenged. *Benomyl* is a microtubule-destabilising antimitotic fungicide, which is often used to analyse mutants causing defects in mitosis (Quinlan, Pogson et al. 1980; Stearns, Hoyt et al. 1990). When the cells were exposed to different temperatures and *Benomyl* concentrations (see chapter 4.14.3), weak effects were observed with the double mutant. This mutation showed better growth on *Benomyl*-plates and at 37°C

RESULTS

compared to the wild-type (Figure 12). With Kar9p overexpressed under the *GAL1*-promoter, expression of the wild-type protein already leads to increased sensitivity towards *Benomyl* and reduced growth at 37°C. The reduced sensitivity therefore likely means that the protein is less active. Yeast strains harbouring the single point mutation S197A are also less sensitive to *Benomyl* than wild-type yeast strains. An overview of the effects is given in Table 2.

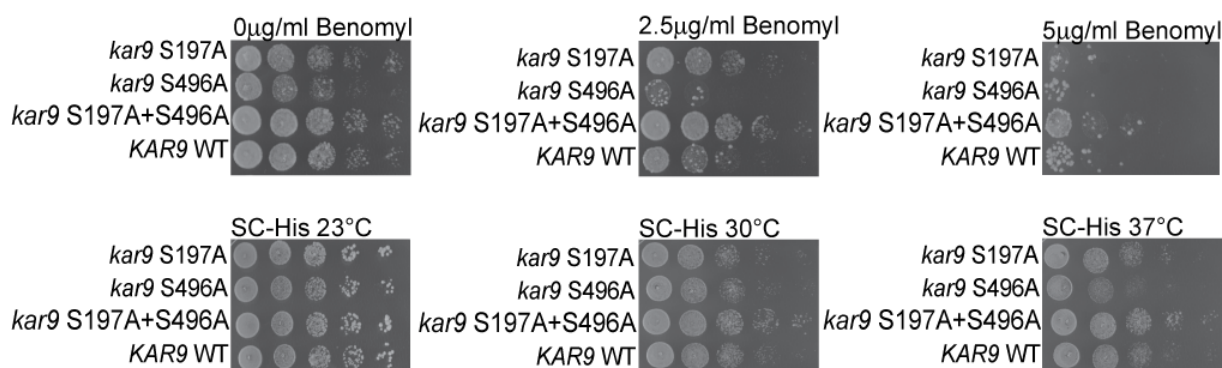


Figure 12 *In vivo* effects of phosphorylation deficient Kar9p mutations Growth test at different temperatures and *Benomyl* concentrations.

	Effect in pull-down	Benomyl supersensitivity	Temperature sensitivity
Kar9p (WT)	normal binding	Highly sensitive at 2.5 µg and 5 µg	Slightly sensitive at 30°C and 37°C
Kar9p (S197A)	normal binding	Highly sensitive at 2.5 µg and 5 µg	as WT
Kar9p (S496A)	normal binding	Highly sensitive at 2.5 µg and 5 µg	more sensitive at 30°C and 37°C as compared to WT
Kar9p (S197A + S496A)	normal binding	less sensitive at 2.5 µg and 5 µg as compared to WT	less sensitive at 30°C and 37°C as compared to WT

Table 2 Overview of the effects of mutations of the phosphorylation sites in Kar9p

2.2.3 Co-immunoprecipitations of Kar9p from yeast extracts

Co-immunoprecipitation (co-IP) experiments with myc-tagged Kar9p were performed as described in 4.14.2. These experiments were to identify possible new interaction partners of Kar9p. In addition, to these co-IPs with wild-type Kar9p, co-IPs with all three yeast strains harbouring mutations in the phosphorylation sites of Kar9p were carried out. Since these mutations did not have an effect on the binding to Bim1p it was of interest to establish a potential effect on other proteins co-immunoprecipitating with Kar9p. After co-IP, the samples were analysed by SDS-PAGE, followed by silver staining and analysis of desired bands by mass-spectrometry.

The overall complex composition was similar in all four strains tested (WT, S197A, S496A, S197A+S496A). All known complex components could be identified by mass-spectrometry (Bim1p, Myo2p), but also other associated proteins were co-immunoprecipitated. The amount of peptide sequences in relation to protein sequences is much higher for Myo2p than

RESULTS

for Bim1p. The abundance of Bim1p was very low, suggesting that the association of Kar9p with Myo2p is comparably stronger than with Bim1p under the given conditions.

Actin and Tpm1/2p were identified in all co-IPs. Both proteins are likely to be co-immunoprecipitated via their interaction with Myo2p. The tropomyosins Tpm1p and Tpm2p bind to and stabilise actin cables and filaments. Therefore, it is likely, that these proteins were immunoprecipitated via their association with actin.

Another protein present in all co-IPs is Nap1p. This protein interacts with mitotic cyclin Clb2p. It is furthermore required for the regulation of microtubule dynamics during mitosis and controls bud morphogenesis. Another role of the protein is the transport of H2A and H2B histones to the nucleus. Why this protein is present in all co-IPs remains unknown and further experiments are required to elucidate whether the interaction with Kar9p is direct or indirect. Clb2p is known to interact with Cdc28p, which might suggest an association with Kar9p via Cdc28p. Chapter 7.2 gives a detailed overview of the proteins identified by mass-spectrometry.

2.2.4 Sumoylation of Kar9p is required for the interaction with Bim1p

Kar9p is sumoylated at amino acids K301, K333, K381, and K529 (Leisner et al., 2008) (see chapter 1.3.1). To test the effect of sumoylation of Kar9p on the interaction with Bim1p, different yeast strains harbouring point mutations in the sumoylation sites of Kar9p were generated (Figure 11A). As for the phosphorylation mutants, these proteins had to be expressed under the *GAL1*-promoter to allow for their detection in western blots. Pull-down experiments were performed as described in chapter 4.10.7 and myc-tagged Kar9p was detected by western blot.

Mutation of individual sumoylation sites into residues that are not sumoylated had different effects on the binding to Bim1p. Whereas strong defects were observed with Kar9p (K333E) and Kar9p (K381R), the Bim1p interaction was only slightly impaired with Kar9p (K333R) and almost no effect was observed with Kar9p (K301R) and Kar9p (K529R). Mutation of multiple sumoylation sites resulted in an additive decrease in binding. The double (2R: K301R + K381R) and triple (3R: 2R + K529) mutants showed only mild defects, while an almost complete loss of binding to Bim1p (FL) was observed when all four sumoylation sites (4R: 3R + K333R) are mutated (Figure 13)

It was therefore concluded that all sumoylation sites seem to have an effect on binding to Bim1p (FL), with an important role for K381. An overview of the effects of the different mutations in pull-down experiments and *in vivo* is given in Table 3.

RESULTS

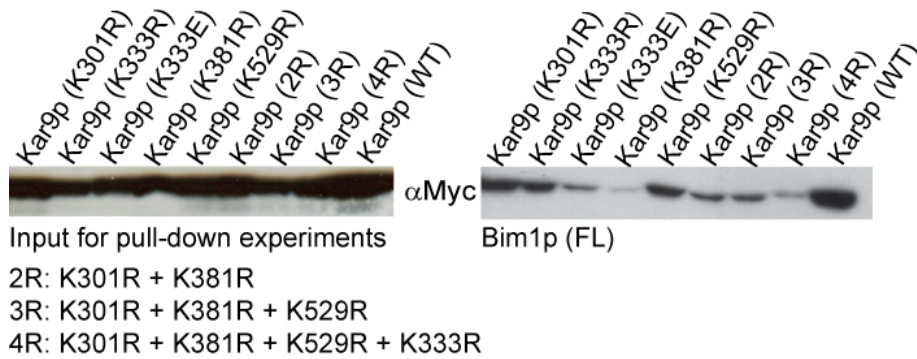


Figure 13 Effect of sumoylation of Kar9p on the interaction with Bim1p. Pull-down experiments with different yeast strains harbouring mutations in the sumoylation sites of Kar9p. Mutations of all for residues (4R) and of K381 led to an almost complete loss of binding, whereas the other mutations showed only mild effects.

2.2.5 In vivo effects of sumoylation deficient Kar9p-variants

To study the effect of mutating individual or several Kar9p-sumoylation sites *in vivo*, growth defects were analysed by temperature- and *Benomyl*-sensitivity test as already described for the phosphorylation mutants (see chapter 2.2.2).

Since the overexpression of Kar9p (WT) already leads to growth defects at 37°C and with low concentrations of *Benomyl*, it was assumed that mutant proteins showing a weaker phenotype are less active. As a matter of fact, the mutation Kar9p (K333E), which showed the strongest effect in the pull-down experiments was less sensitive to *Benomyl*, whereas the mutations Kar9p (K301R) and Kar9p (K529R), which showed almost no effects in the pull-down experiments displayed the same strong phenotype in response to *Benomyl* as the wild-type. The same was true for the double, triple and quadruple mutations of Kar9p. Whilst the double mutant showed only mild defects in the pull-down experiments upon *Benomyl* treatment, it showed the same growth phenotype as the wild-type protein. On the other hand the triple and quadruple mutants showed minor growth defects, which is fully consistent with the *in vitro* results (Figure 13 and Figure 14).

It was consequently assumed that a more complex mechanism exists *in vivo*. The inconsistent pull-down and *in vivo* results point to this. However, the overall outcome of the experiments suggests that sumoylation plays an important role in Bim1p binding and that the effect is additive. These findings also explain why recombinant Kar9p from *E.coli* does not interact with Bim1p.

RESULTS

	Effect in pull-down	Benomyl-supersensitivity	Temperature sensitivity
Kar9p (WT)	normal binding	highly sensitive at 2.5 μ g and 5 μ g	slightly sensitive at 30°C and 37°C
Kar9p (K301R)	slightly reduced binding	highly sensitive at 2.5 μ g and 5 μ g	slightly sensitive at 30°C and 37°C
Kar9p (K333R)	slightly reduced binding	less sensitive at 2.5 μ g and 5 μ g than compared to WT	slightly sensitive at 30°C and 37°C
Kar9p (K333E)	strongly reduced binding	no sensitivity at 2.5 μ g and less sensitivity at 5 μ g	slightly sensitive at 30°C and 37°C
Kar9p (K381R)	strongly reduced binding	highly sensitive at 2.5 μ g and 5 μ g	slightly sensitive at 30°C and 37°C
Kar9p (K529R)	slightly reduced binding	highly sensitive at 2.5 μ g and 5 μ g	slightly sensitive at 30°C and 37°C
Kar9p (2R)	reduced binding	more sensitive at 2.5 μ g and 5 μ g than compared to WT	slightly sensitive at 30°C and 37°C
Kar9p (3R)	reduced binding	less sensitive at 2.5 μ g and 5 μ g than compared to WT	slightly sensitive at 30°C and 37°C
Kar9p (4R)	strongly reduced binding	less sensitive at 2.5 μ g and 5 μ g than compared to WT	slightly sensitive at 30°C and 37°C

Table 3 Overview of the effects of mutations of sumoylation sites in Kar9p

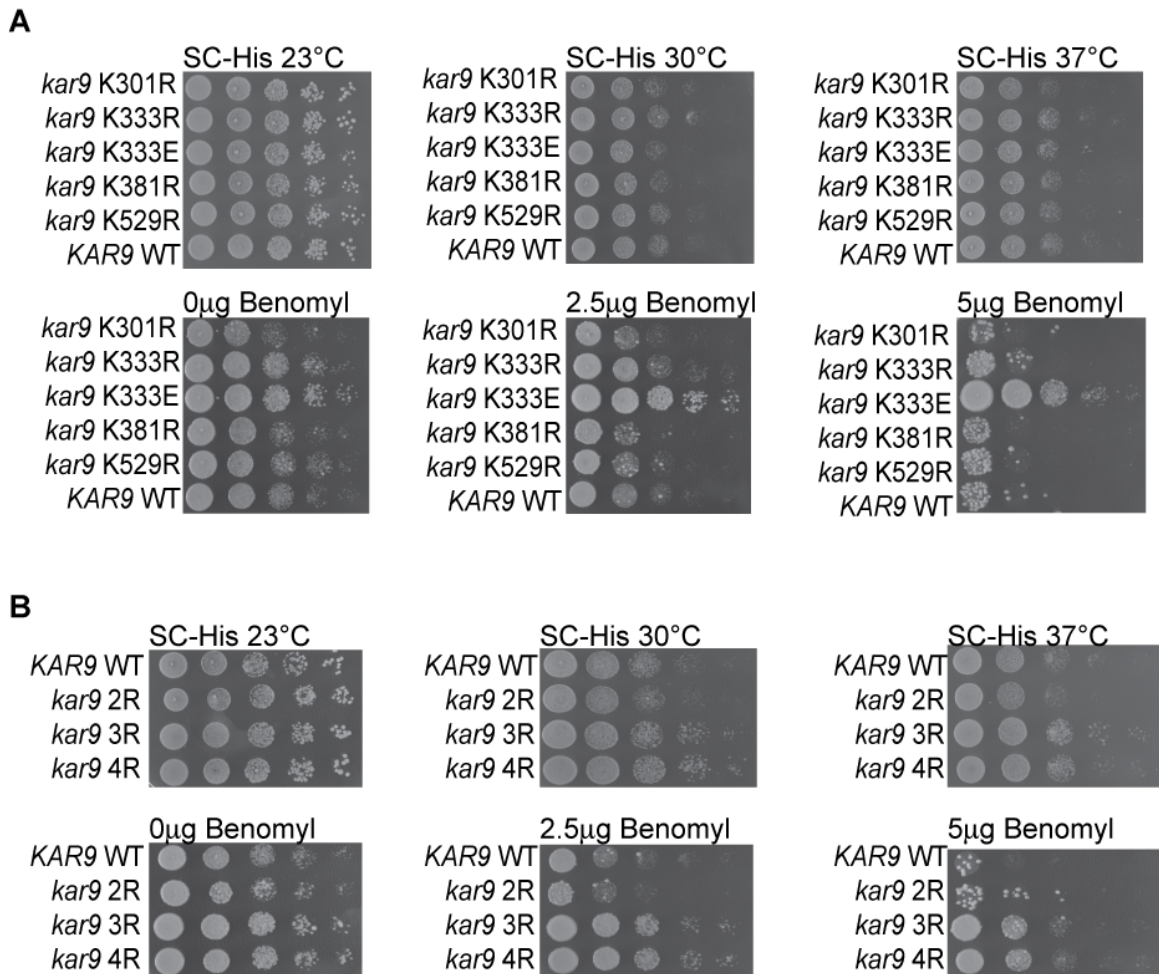


Figure 14 In vivo effects of sumoylation deficient Kar9p-variants (A) Temperature and *Benomyl* sensitivity of single mutations of Kar9p. **(B)** Temperature and *Benomyl* sensitivity of double, triple and quadruple mutations of Kar9p. 2R: K301R + K381R; 3R: 2R + K529R; 4R: 3R + K333R

2.3 Structural analyses of Bim1p

Bim1p belongs to the family of EB1-like proteins. Members of this family are highly conserved in all eukaryotes and share an overall sequence identity of ~ 35%. A sequence alignment in Figure 30 shows the high conservation of this class of proteins. The protein consists of two domains: an N-terminal CH-domain, which mediates the binding to microtubules; and a C-terminal EB1-like domain, which mediates the binding to different cargoes (Figure 15A). The crystal structure of the CH-domain has been solved (Slep and Vale 2007), whereas structural information of the EB1-like domain is only available on the human homolog (Honnappa, John et al. 2005; Slep, Rogers et al. 2005). No structural information is available for this cargo-binding domain of Bim1p. Furthermore, Bim1p contains a sequence insertion of 24 residues (Figure 20, red box) (amino acids 240 to 263), for which structure predictions fail. Since this domain also mediates the binding to Kar9p a crystal structure would be of high interest.

2.3.1 Expression and Purification of Bim1p (FL)

Full-length Bim1p (FL) is comprised of 344 amino acids and has a molecular weight of 38.4 kDa. I have cloned the full-length gene from yeast genomic DNA into different *E.coli* expression vectors (see chapter 4.9.1). Protein expression was achieved as a GST- or MBP-tagged version in *E.coli* (BL21) and purification was performed as described in chapter 4.11.7 and 4.11.8. The GST-tagged protein was used after cleavage and removal of the GST-tag with the PreScission protease for crystallisation trials and SAXS experiments, whereas the MBP-tagged protein was used for pull-down experiments. The result of a purification of Bim1p (FL) with a GST-tag is shown in Figure 15B.

2.3.2 Expression and Purification of Bim1p (C-term)

In crystallisation trials with Bim1p (FL) only amorphous precipitate was observed. To find a soluble fragment of the C-terminal cargo-binding domain that binds to Kar9p, several fragments were cloned and expressed in *E.coli* as GST-tagged proteins (see chapter 4.11.1). The shortest fragment comprising amino acids 182-282 (see Figure 15A) could be expressed and purified (see chapter 4.11.7) in high amounts. This fragment was used for co-crystallisation trials with Kar9p, as well as for crystallisation trials alone and SAXS-experiments. The MBP-tagged protein was purified as described in chapter 4.11.8 and used for pull-down experiments.

2.3.3 Crystallisation of Bim1p (C-term)

In order to establish whether Bim1p (C-term) adopts a similar fold as human EB1 crystallisation trials were performed. The procedures for crystallising the native protein are described in chapter 4.12.5. Since attempts to solve the Bim1p (C-term) structure by molecular replacement with the already known structure of human EB1 (PDB-ID: 1WU9, 1YIB, 1YIG) consistently failed (see chapter 2.1.6), another strategy had to be used to solve the phase problem. Bim1p (C-term) has only one methionine in its amino acid sequence, which is insufficient for phasing by single- (SAD) or multi-wavelength anomalous dispersion (MAD) using selenomethionine labelled protein. Selenomethionine labeling is a standard method in protein crystallography to determine phases. It has been estimated that for solving a protein structure using MAD, one selenomethionine residue is required for ~75-100 residues (Hendrickson 1997). Since Bim1p (C-term) has a total length of 113 residues, additional methionine residues are needed to obtain a higher phasing power and figure of merit (FOM). Therefore additional methionines were introduced by site-directed mutagenesis (see chapter 4.9.1). Four residues (L199M, Y206M, L224M, F264M) were chosen for mutagenesis based on the indirect structural information derived from sequence homology to human EB1 and its solved structure as well as on secondary structure predictions for Bim1p (C-term). The protein was expressed in minimal medium containing selenomethionine (see chapter 4.11.2) and purified like the unlabelled protein. Crystallisation trials yielded only very tiny (20-30 μm x 5-10 μm) needle shaped crystals, which did not show X-ray diffraction at the synchrotron. Therefore, for solving the phase problem, different heavy atom derivatives were used for soaking of the native crystals. As a preliminary experiment, the purified protein was incubated with several heavy atoms in different concentrations (see chapter 4.12.6) and analysed on a native PAGE (Figure 15C). Three heavy atom derivatives showed clearly a band shift of the protein on the native PAGE and have been used for heavy atom derivatisation of Bim1p (C-term) ($\text{K}_2\text{Pt}(\text{NO}_2)_4$, $(\text{PtCl}_2(\text{H}_2\text{NCH}_2\text{CH}_2\text{NH}_2))_2$, $\text{Pt}(\text{NH}_3)_2(\text{NO}_2)_2$).

2.3.4 Structure determination and refinement of Bim1p (C-term)

Plate-like crystals (Figure 15D) were tested at various beamlines at the ESRF in Grenoble. Datasets from the native crystals (Figure 15E) were recorded at beamline ID 29 at a wavelength of 1.254 Å. Although crystals showed X-ray diffraction up to 2.1 Å, processing of the data revealed high-quality diffraction only for the resolution range of 20-2.45 Å. Data was integrated and scaled with XDS and SCALA (Evans ; Kabsch ; Evans 2006). Crystals belong to the spacegroup $\text{P}2_1$ with cell dimensions of $a=28.00$ Å, $b=42.5$ Å, $c=100.5$ Å, $\alpha = \gamma = 90^\circ$, $\beta = 90.3^\circ$. From the unit cell a Matthews's coefficient of 2.99 Å³/dalton of protein was

RESULTS

calculated (Matthews 1968) with one molecule (dimer) per asymmetric unit and a solvent content of 58.89 %.

Single anomalous dispersion (SAD) experiments for the platin-derivatised crystals were recorded at beamline ID 29 (ESRF, Grenoble, France) at a wavelength of 1.071 Å. Crystals showed diffraction up to 2.1 Å and significant anomalous signal up to 3.5 Å. Data were integrated and scaled as for the native datasets and the unit cell has a dimension of $a=28.00$ Å, $b=44.25$ Å, $c=101.25$ Å, $\alpha = \gamma = 90^\circ$, $\beta = 94.7^\circ$. Using *ShelxD* (Sheldrick 2008), two platin positions could be located within the asymmetric unit. Phases were calculated with *SHARP* (Bricogne, Vonrhein et al. 2003) using SAD. The model was built manually with *COOT* (Emsley and Cowtan 2004) and the platin-derivatised dataset. Molecular replacement with *PHASER* (McCoy 2007) has been used to solve the structure of the native dataset with the model of the platin-derivatised dataset as template. Refinement was performed with *BUSTER* (Blanc, Roversi et al. 2004) using Non-Crystallographic Symmetry. The final model on Bim1p (C-term) contains 91 out of 113 amino acids. Final R-factors are $R_{\text{work}} = 0.209$ and $R_{\text{free}} = 0.24$, and the Ramachandran plot shows 97.01 % of the residues in allowed regions. The main crystallographic statistics are listed in Table 4.

Data collection			Refinement (native)	
Data set	Native	Pt Peak		
X-ray source	ID 29 (ESRF)	ID 29 (ESRF)		
Space group	P2 ₁	P2 ₁		
Wavelength (Å)	1.254	1.071		
Data range (Å)	20-2.45	50-2.1		
Observations (unique)	31883 (8834)	90864 (30751)	R_{work} (R_{free})	0.209 (0.240)
I/σ (last shell)	13.12 (2.07)	8.16 (1.71)	RMS bond length (Å)	0.0098
Completeness (last shell)	(%) 98.8 (98.3)	99.0 (63.8)	RMS bond angles (deg)	1.18°
			Ramachandran plot (%)	
			(allowed)	97.0
			(additionally allowed)	1.8
			outliers	1.2
R_{sym} (last shell)	7.8 (71.7)	14.2 (98.5)		

Cell symmetry Native: P2₁ cell constants (Å):

$a=28.00$, $b=42.5$, $c=100.5$, $\alpha=\gamma=90^\circ$, $\beta=90.3^\circ$

Cell symmetry Pt: P2₁ - cell constants (Å):

$a=28.00$, $b=44.25$, $c=101.25$, $\alpha=\gamma=90^\circ$, $\beta=94.7^\circ$

Resolution range of last shell: 2.59-2.45 Å

R_{sym} is the un-weighted R-value on I between symmetry mates.

$R_{\text{work}} = \sum_{\text{hkl}} |F_{\text{obs}}(\text{hkl}) - F_{\text{calc}}(\text{hkl})| / \sum_{\text{hkl}} |F_{\text{obs}}(\text{hkl})|$ for reflections in the working data set.

R_{free} = cross validation R-factor for 5% of reflections against which the model was not refined.

Table 4 Crystallographic statistics for Bim1p (C-term)

RESULTS

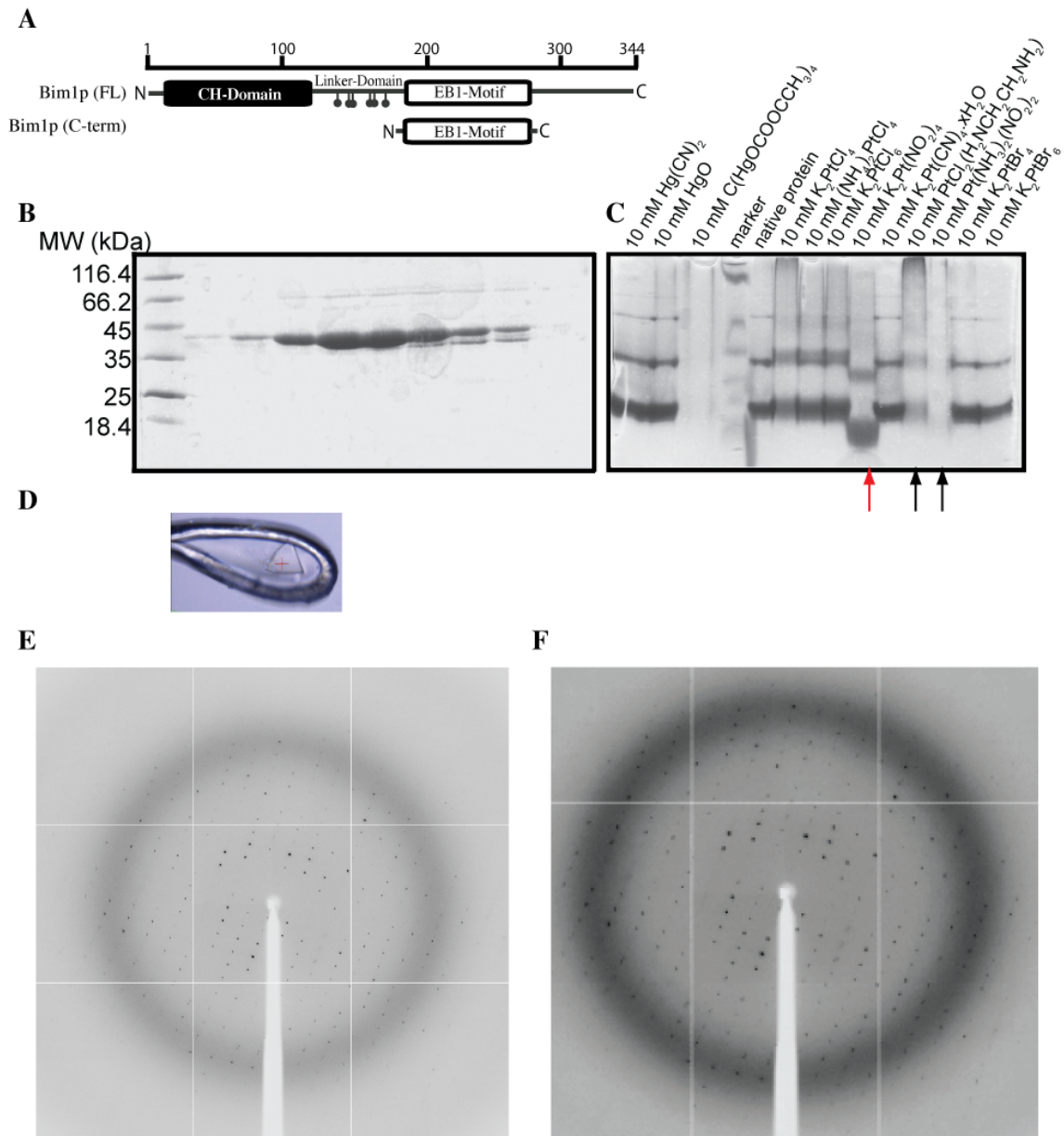


Figure 15 Purification and Crystallisation of Bim1p (FL) and Bim1p (C-term) (A) Domain composition of Bim1p (FL) and Bim1p (C-term). The residues modified by phosphorylation are indicated in the linker region. (B) Purification of Bim1p (FL) after cleavage of the GST-tag and size-exclusion chromatography. (C) Native SDS-PAGE after incubation of purified Bim1p (C-term) with different heavy atom derivatives. Arrows indicate the heavy atom derivatives that showed a band shift on the gel and which have been used for soaking of the crystals. (D) Crystal of Bim1p (C-term). (E) Diffraction pattern of the native crystals. (F) Diffraction pattern after soaking of the crystals with K₂Pt(CN)₄.

2.3.5 Crystal structure of Bim1p (C-term)

The structure of Bim1p (C-term) includes residues 1-68 and 82-105. For 14 residues in the flexible loop region and 8 residues at the very C-terminus no electron density was observed. The missing residues 69-81 are located in a Bim1p-specific sequence insertion of 24 residues (amino acid 240 to 263 in Bim1p (FL) and amino acid 58 to 81 in Bim1p (C-term)) which contains many glycine residues and which is therefore likely to be highly flexible.

RESULTS

The overall structural arrangement is similar to human EB1 and shows that Bim1p (C-term) is a dimer. The C-terminal domain of Bim1p is formed through a coiled-coil followed by a four-helix bundle. Each monomer consists of a long helix (α_1 , residues 1-63) which is followed by a 24-residue loop leading to a short second helix (α_2 , residues 84-102), which is antiparallel to α_1 (Figure 16A). The Bim1p-specific sequence insertion, for which no electron density was visible, is located between the two helices of each monomer.

Although both monomers look similar, their superimposition shows that their respective structures are not identical. One monomer has a kink in the lower third of the long helix, which induces asymmetry (Figure 29A). Residues 43-46 contain a highly conserved FYF motif that might influence the difference in their structure. These residues are also likely involved in the binding to Kar9p and in forming intramolecular contacts. Since the structural asymmetry is found in all molecules of the unit cell, the crystal-packing does not seem to influence the structural difference between the two monomers, (Figure 29B). Despite this difference, the residual mean square deviation (RMSD) from an overlay of both monomers is rather small (1.60 Å).

An analysis of the crystallographic contacts with the PDBe PISA server (www.ebi.ac.uk/pdbe/prot_int/pistart.html) (Krissinel and Henrick 2007) shows that the hydrophobic dimerisation interface involves a large buried surface of 1987 Å², suggesting stable dimerisation in solution. All data obtained from the PDBe PISA server is shown in Table 5.

Assessment of the electrostatic surface potential of Bim1p (C-term) revealed that this domain contains has a rather uncharged overall surface with few pronounced regions of positive or negative charge (Figure 16B).

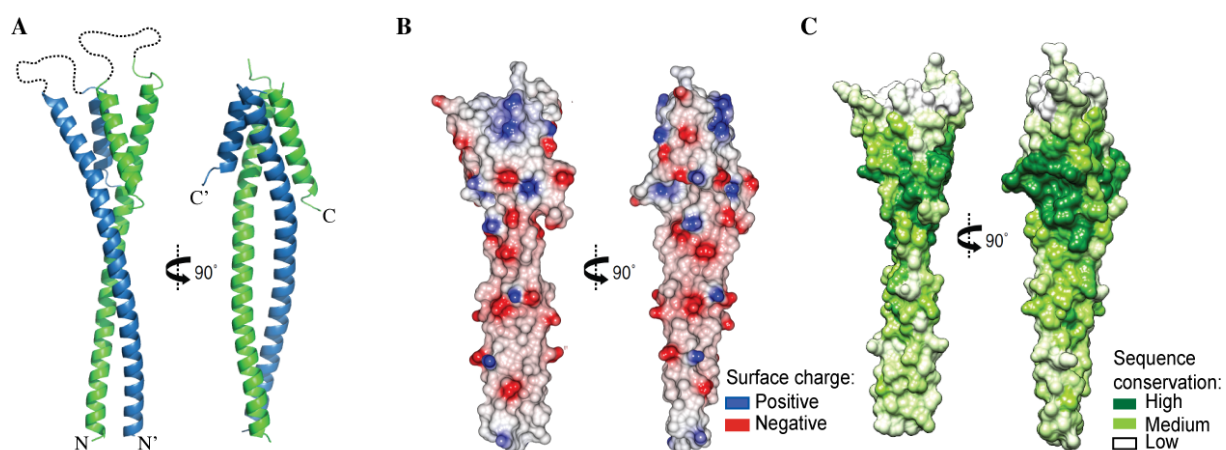


Figure 16 Crystal structure of Bim1p (C-term) (A) Crystal structure of Bim1p (C-term). The domain is formed by two monomers. Each monomer consists of a long α -helix followed by a short α -helix. The coiled-coil is formed by the long helices, whereas the short helices fold back thereby forming a four-helix bundle. Monomers are shown in blue and green. N- and C-termini are labelled with "N" and "C". (B) Surface charge of Bim1p (C-term). No clusters of positively or negatively charged residues are visible. (C) Surface conservation of Bim1p (C-term) based on sequence alignment of different EB1-family members. A highly conserved region lies at the four-helix bundle in the upper part of the structure.

RESULTS

To visualise, which areas in Bim1p (C-term) are highly conserved, the sequence alignment from Figure 30 was plotted onto the surface of the Bim1p structure. A region at the interface of the four-helix bundle shows a high degree of conservation (Figure 16C), but does not overlap with regions of pronounced positive or negative surface charges. The region at the four-helix bundle contains two highly conserved hydrophobic patches, one in the long helix (FYF-motif) and the other at the end of the short helix. It has been shown for EB1 that these two regions mediate the binding to cargo (Honnappa, John et al. 2005; Slep, Rogers et al. 2005; Honnappa, Gouveia et al. 2009). This similarity supports the assumption that Kar9p potentially also binds in this region.

The submission of the Bim1p (C-term) crystal structure to the RSCB protein data bank (PDB) is in preparation.

2.3.6 Structural comparison of the cargo-binding domains of Bim1p and human EB1

An overlay of the crystal structures of the cargo-binding domains from Bim1p (C-term) and human EB1 shows a similar overall fold, with an RMSD of only 1.2 Å (Figure 17). The most obvious difference in both structures is that the large helix of Bim1p is about one-third longer than in human EB1 (total length ~ 93 Å versus ~ 63 Å). The sequence of the protein fragment of Bim1p that was crystallised is also about one-third longer than the corresponding fragment of human EB1 (100 residues versus 66 residues). Another minor difference between the two structures is the kink in one of the long helices of Bim1p (C-term). This difference is a possible explanation as to why molecular replacement approaches with human EB1 failed.

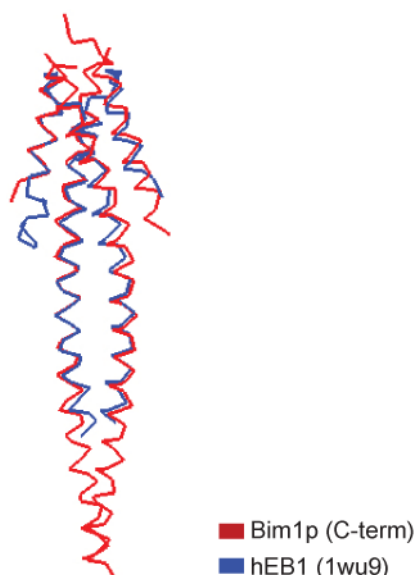


Figure 17 Overlay of the crystal structures of the cargo-binding domains from Bim1p (C-term) and human EB1. Both domains shown and overall similar fold with an RMSD of only 1.2 Å. The long alpha helix of Bim1p is substantially longer than the alpha helix in EB1.

2.3.7 Analysis of Bim1p (C-term) and (FL) by small-angle-X-ray scattering (SAXS)

Small-angle-X-ray Scattering (SAXS) is often used as a complementary technique to X-ray crystallography to observe and verify the conformation and oligomeric state of a protein in solution. It can also be used to calculate surface envelopes of molecules that fail to crystallise and to fit known structural models into the envelopes.

To confirm whether the dimer of Bim1p (C-term) observed in the crystal lattice is also present under nearly physiological conditions, SAXS experiments were performed as described in chapter 4.10.5. The molecular mass determined from the scattering intensity extrapolated to zero angle confirms that Bim1p (C-term) is a dimer in solution (Figure 18A). To obtain information on the shape and size of Bim1p (C-term), the radius of gyration (R_g) was determined from the scattering curves. For Bim1p (C-term) an average R_g of 2.96 nm was calculated, which is quite large for a molecule with this molecular weight, but can be explained by the extended shape (long helices). Furthermore, the *CRY SOL* software was used to calculate a theoretical scattering curve from the crystal structure and to compare it with the experimental scattering curve of the protein in solution. An overlay of both scattering curves of Bim1p (C-term) shows an almost perfect match, confirming that the dimer observed in the crystal structure is likely physiologic (Figure 18B). Bead models of Bim1p (C-term) were calculated with the *DAMMIN* software and show approximately the same dimensions as the molecule in the crystal structure (length of 98.4 Å versus 101.2 Å). The model obtained from the SAXS data seems to have additional density around the four-helix bundle. This difference can be explained by the existence of the flexible loop region, for which no electron density was visible in the crystal structure.

Another question was whether the full-length protein is dimeric in solution too and whether envelopes of Bim1p (FL) can be obtained. The envelopes would then be used to obtain insights into the overall shape of the protein and to fit the known structures of the CH-domain (Slep and Vale 2007) and the C-terminal domain. Analysis of Bim1p (FL) by SAXS confirmed that full-length Bim1p is also a dimer in solution (Figure 18A) and has a radius of gyration of 5.88nm. The scattering curves obtained were however not of sufficient quality to calculate envelopes for fitting of the known structures. Together with the SAXS analysis of Bim1p (C-term) these results confirm that the C-terminus mediates dimerisation of Bim1p.

RESULTS

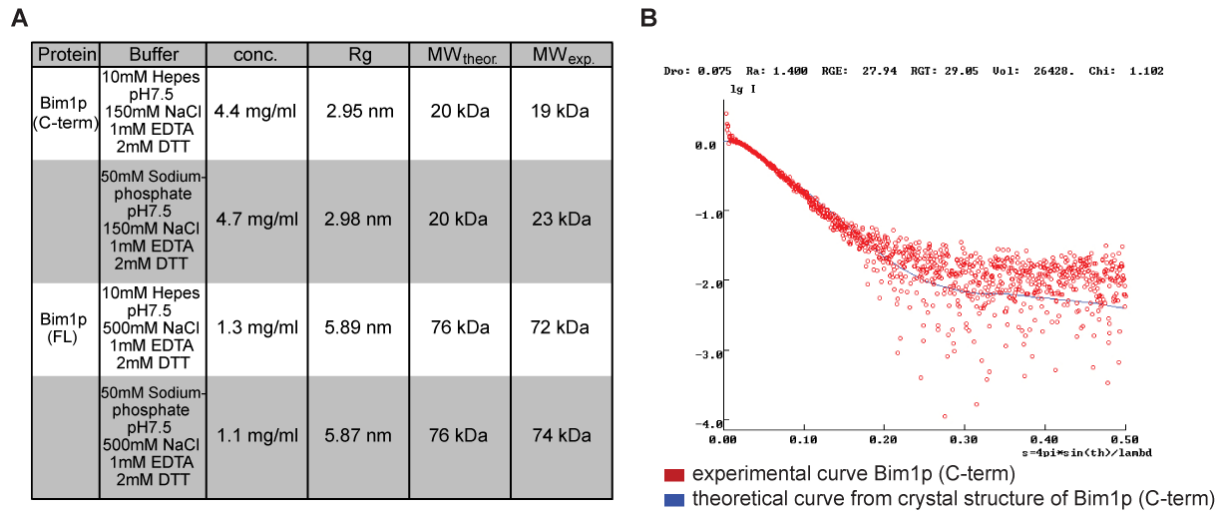


Figure 18 Small-angle-X-ray scattering (SAXS) analysis of Bim1p (A) Table showing the experimental setup, the measured radius of gyration and molecular weight. Conc = protein concentration, Rg= radius of gyration, MW_{theor.} = molecular weight calculated from the amino acid sequence, MW_{exp.} = molecular weight obtained by SAXS-analysis. **(B)** CRYSOLOG analysis of Bim1p (C-term) shows an almost perfect match of the theoretical (blue line) and the measured scattering curve (red dots).

2.4 *In vitro* and *in vivo* analysis of the Bim1p-Kar9p interaction

As already described above (chapter 2.2), the interaction of Bim1p and Kar9p requires sumoylation of Kar9p. Therefore all experiments described in the following section were accomplished with MBP-tagged Bim1p expressed in and purified from *E.coli* and lysate from yeast cells expressing myc-tagged Kar9p.

In order to find out whether Bim1p (C-term) binds to Kar9p, pull-down experiments were performed at different salt concentrations (Figure 19). Bim1p (C-term) can pull-down Kar9p in all reactions as detected by western blot, but the binding to Kar9p is always weaker than compared to Bim1p (FL). The binding of both Bim1p variants to Kar9p gets also weaker with increasing salt concentrations and is almost invisible for Bim1p (C-term) at 500 mM NaCl. This difference in binding suggests that an additional so far undetected region outside the C-terminal domain of Bim1p might contribute to Kar9p binding.

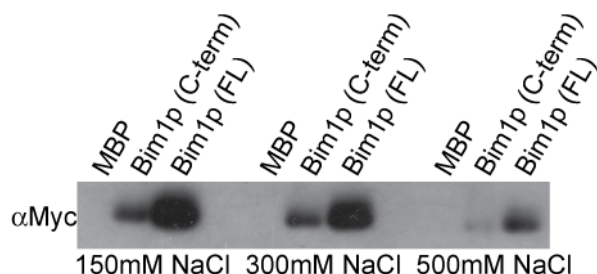


Figure 19 Pull-down experiments with Bim1p (C-term) or Bim1p (FL) and myc-Kar9p from yeast extracts. Bim1p (FL) always binds stronger to Kar9p than the C-terminal EB1 motif alone.

2.4.1 The Bim1p-specific loop is not required for the binding to Kar9p

The C-terminal domain of Bim1p contains a yeast specific insertion of 24 amino acids, connecting the long and the short helix. Since no electron density could be observed in the crystal structure, it would be interesting to find out whether this region is important for Kar9p binding. For EB1 it has been shown that this loop is not involved in cargo binding (Honnappa, John et al. 2005; Slep, Rogers et al. 2005). However, since Bim1p contains a much larger insertion it might indeed contribute to the binding. To test the importance of the loop region for Kar9p binding, mutants of Bim1p (FL) and Bim1p (C-term) with loop deletions of either 12 or 14 amino acids were generated and tested in pull-down experiments. Since recombinant Bim1p ($\Delta 12$) or Bim1p ($\Delta 14$) did not show defects in Kar9p binding (Figure 20A), it can be concluded that the yeast-specific loop in Bim1p is unlikely to be required for Kar9p binding.

2.4.2 Mutational analysis of the Bim1p-Kar9p interaction

Based on the information obtained from the crystal structure of Bim1p (C-term) and interaction studies of human EB1 with different cargoes (Honnappa, John et al. 2005; Slep, Rogers et al. 2005; Honnappa, Gouveia et al. 2009) as well as sequence conservation and surface exposure in Bim1p a total of 20 point mutations were introduced in Bim1p (FL). These mutants were then tested in pull-down experiments for binding to myc-tagged Kar9p from yeast extracts. A detailed overview of the mutated residues and their location in the C-terminal domain of Bim1p is given in Figure 20B,C.

Of the total of 20 mutations, 5 mutations resulted in rapidly degrading proteins, whereas 15 of these mutants were soluble proteins. Most of the mutations resulting in degrading proteins are located in the hydrophobic region of the short alpha helix. The hydrophobic side chains of these residues are oriented towards the hydrophobic residues of the long alpha helix. Replacement of these residues with alanine might induce structural changes of this helix or a better accessibility of those hydrophobic residues to the solvent and could therefore lead to protein unfolding and aggregation. All 15 well-behaving mutated protein versions were tested in pull-down experiments with extracts from myc-tagged Kar9p expressing cells. Reduced binding to Kar9p was observed with mutations R217A, F219A, Y220A, F221A, and H232A in Bim1p (FL) and mutation E228A even abolished Kar9p binding (Figure 20D). An unexpected two-fold enhanced binding to Kar9p could be observed with the mutation E214A. Mutations E218A and N222A also showed a milder increase in Kar9p binding. None of the other mutations (I215A, K223A, R225A, D226A, I227A, I229A) showed a significant effect on binding to Kar9p. To establish whether these mutations have the same effect in Bim1p (C-term), nine of these point mutations were introduced in Bim1p (C-term) and tested in pull-down experiments. The results were consistent with Bim1p (FL) except for mutation I227A, where a slightly increased binding was observed and mutation R225A, where a

RESULTS

slightly reduced binding (Figure 20D) was observed. Since mutation I227A is buried in the hydrophobic core of Bim1p, this effect can be explained by likely structural changes of the protein (Figure 20C).

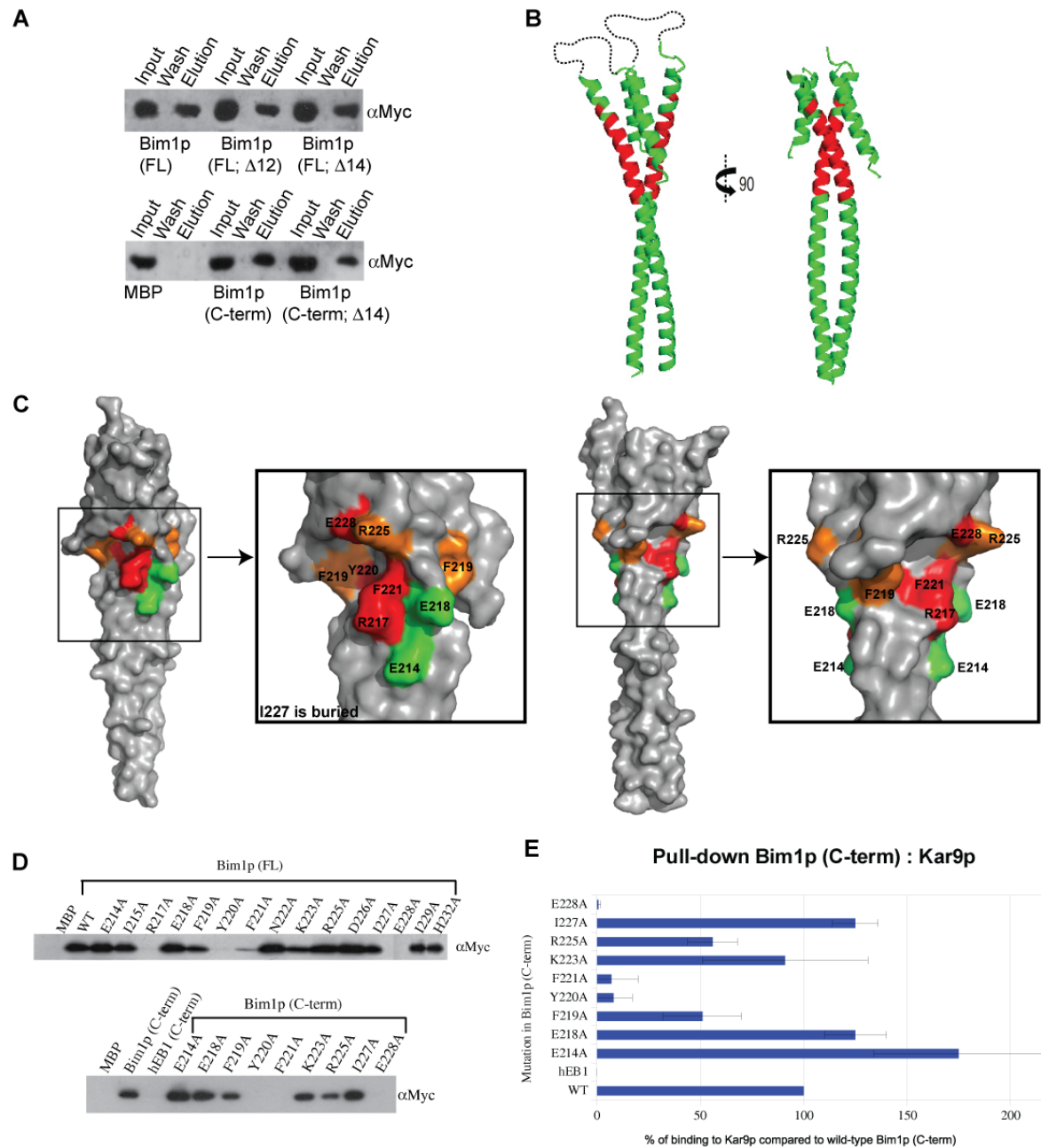


Figure 20 Mutational analysis of the interaction between Bim1p and Kar9p (A) The extended loop region in the C-terminal domain of Bim1p is not required for binding of Kar9p. Deletions of either 12 or 14 residues of this loop in Bim1p do not have an effect on Kar9p-binding in pull-down experiments. (B) Location of the residues mutated in Bim1p on a surface model of its crystal structure. Red: mutated residues. (C) Detailed view of mutations in Bim1p that affect the binding to Kar9p. Red = severely reduced binding, orange = mild binding defects, green = increased binding. I227A is buried, but showed increased binding to Kar9p upon mutation in Bim1p (C-term). (D) Western blots of pull-down experiments with different mutations in Bim1p (FL), Bim1p (C-term) and human EB1. (E) Quantification of western blots from pull-down experiments with mutations in Bim1p (C-term), confirming the results observed in (D).

RESULTS

Western blots from pull-down experiments with mutations in Bim1p (C-term) were also subjected to quantification of the myc-Kar9p signals with a digital imaging system (see chapter 4.10.3). Quantification of the myc-Kar9p signals confirmed what had already been observed in the western blots. In particular, the two-fold increase in binding of mutation E214A or the almost abolished binding of mutation E228A was consistent between Bim1p (FL) and Bim1p (C-term) (Figure 20E).

Since human EB1 shows high similarity to Bim1p (C-term) in terms of structural arrangements and sequence conservation, the C-terminal cargo-binding domain of human EB1 was also tested in pull-down experiments with myc-tagged Kar9p. Since no interaction with Kar9p was observed for human EB1, I concluded that both proteins are likely to bind their cargo in a somewhat different manner.

2.4.3 *In vivo* effects of the Bim1p-mutations

To test the *in vivo* effects of Bim1p mutations six mutations which showed Kar9p-binding defects in the pull-down assay were chosen for expression in yeast. Several yeast strains were generated harbouring mutant versions of Bim1p (FL) fused to an HA-tag under the control of the native *BIM1* promoter in an otherwise Δ *BIM1* background. As for the mutations in Kar9p the yeast cells were incubated with different concentrations of the microtubule-depolymerising drug *Benomyl*. It had already been shown that *bim1*-null mutants are more sensitive to *Benomyl* than wild-type cells. Therefore, if a particular mutation has an effect, the cells should be highly sensitive (Schwartz, Richards et al. 1997; Parsons, Brost et al. 2004; Ye, Peyser et al. 2005). Additionally, wild type and mutant Bim1p-expressing yeast strains were incubated at 23°C, 30°C, and 37°C to assess temperature-induced defects in spindle orientation (Schwartz, Richards et al. 1997). Both assays were performed as colony growth tests on agar plates.

No growth defect was observed in the temperature-sensitivity assays for any of the tested mutations (Figure 21). Despite the impaired binding to Kar9p *in vitro*, the interaction *in vivo* seems to be more robust. Indeed, the dynein-dynactin pathway can partially rescue defects in the Myo2p-Kar9p-Bim1p pathway *in vivo*. However, when probing sensitivity to *Benomyl*, a yeast strain expressing the mutant Bim1p (F219A) did yield growth defects (Figure 21). Bim1p with this mutation had almost completely lost its ability to interact with Kar9p in pull-down experiments (Figure 20D). It suggests that a reduced binding to Kar9p also results in growth defects with *Benomyl*. Surprisingly, Bim1p with the mutation I229A, which showed normal binding to Kar9p in the pull-down experiments (Figure 20D), was less sensitive to *Benomyl* when compared to wild-type Bim1p (Figure 21). No other mutation resulted in a growth defect in this assay.

RESULTS

In comparison to the *in vitro* assays, the experimental readout of the *in vivo* experiments is less straightforward. It either suggests that *in vivo* the complex assembly is more robust or that other mechanisms contribute to the rescue of the defects. Indeed, these findings are consistent with the assumption of a second, partially redundant Kar9p binding site in Bim1p, as already suggested above (see chapter 2.4).

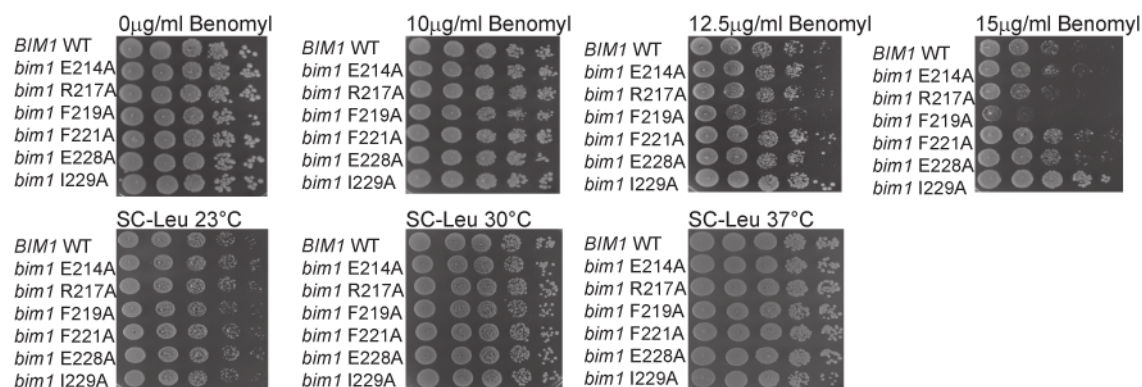


Figure 21 In vivo effects of mutations in Bim1p Yeast strains harbouring mutations in the C-terminal cargo-binding domain of Bim1p were exposed to different concentrations of Benomyl or different temperatures. Only two mutations show effects in the presence of Benomyl, no effect can be observed at different temperatures.

2.4.4 Bim1p has a second binding region for Kar9p

The observation that Bim1p (FL) binds better to Kar9p than to Bim1p (C-term) (Figure 19) suggests a contribution of regions outside the C-terminal cargo-binding domain. To determine the contribution of such additional regions to Kar9p binding, several fragments with deletions of the C-terminal cargo-binding domain (Bim1p (1-187)) or of even larger fragments of the C-terminus (Bim1p (1-154) and Bim1p (1-124)) were tested in pull-down assays with myc-tagged Kar9p from yeast extracts. Bim1p (1-124) consists only of the CH-domain, which mediates binding to microtubules and of which the crystal structure is known (Schwartz, Richards et al. 1997). Bim1p (1-154) contains the CH-domain and part of the unstructured middle domain, connecting the CH-domain and the EB1-like domain. Bim1p (1-187) contains the CH-domain and the middle domain up to the beginning of the EB1-like domain (Figure 22A). With these fragments, no binding to Kar9p was observed in pull-down experiments (Figure 22B). These results argue against the presence of a second Kar9p-binding region in Bim1p.

Taking into account that the crystal structure of Bim1p (C-term) and the SAXS analyses revealed a dimerisation of Bim1p by the EB1-like motif (Figure 16 and Figure 18), a second binding region might also require dimerisation of Bim1p for binding to Kar9p. Therefore, deletion of the C-terminal domain of Bim1p would impair its function.

To find out whether a potential second Kar9p-binding region requires dimerisation of Bim1p, the C-terminal cargo binding domain was replaced by the dimerisation-mediating coiled-coil region of GCN4. This heterologous coiled-coil region is comparable in size to the coiled-coil

RESULTS

of Bim1p. All three Bim1p-GCN4 hybrid fragments (Figure 22B) were tested in pull-down experiments with myc-tagged Kar9p. Indeed, Kar9p could be pulled-down with Bim1p (1-187 GCN4) in comparable amounts to Bim1p (C-term) (Figure 22B). The more residues of the middle domain were deleted, the less interaction with Kar9p could be observed (Bim1p (1-514 GCN4) and Bim1p (1-124 GCN4)) (Figure 22B). These results suggest that the region between the CH domain and the EB1-like motif also mediates binding to Kar9p and that this function requires dimerisation of Bim1p by the C-terminal dimerisation domain. The proportion of Kar9p bound to Bim1p (C-term) and Bim1p (1-187 GCN4) furthermore suggests that both regions equally contribute to the binding. The proportion of Kar9p bound by Bim1p (FL) seems to be more than the amount of both regions alone taken together.

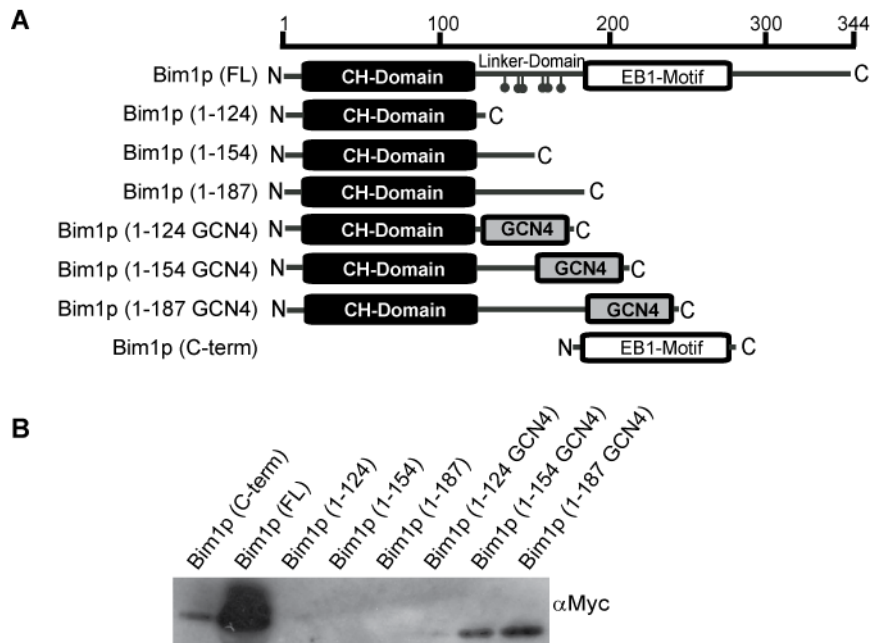


Figure 22 The middle domain of Bim1p binds to Kar9p (A) Cartoon representation of the different fragments used for pull-down experiments. A dimerisation domain of GCN4 replaced the C-terminal dimerisation domain. **(B)** Western blot from pull-down experiments with the different fragments of Bim1p. Fragments of Bim1p without a dimerisation domain cannot bind to Kar9p, whereas fragments dimerised by the unrelated GCN4-domain can bind to Kar9p. Together these results suggest the presence of a second binding region in Bim1p.

2.4.5 *In vivo* effects of Bim1p lacking the EB1-like motif

Since the binding by each individual Kar9p-binding domain of Bim1p is considerably weaker than compared to full-length Bim1p (Figure 22), it would be of great interest to find out whether this previously undetected Kar9p-binding region of Bim1p alone is sufficient to mediate spindle orientation *in vivo*. A yeast strain harbouring a plasmid expressing Bim1p (1-187 GCN4) in a *bim1*-deletion background was generated and tested for *Benomyl* and temperature sensitivity. If Bim1p (1-187 GCN4) would rescue the effects of a *bim1* deletion, this should lead to reduced sensitivity to high temperature or *Benomyl*. Growth tests

RESULTS

on plates containing *Benomyl* or at different temperatures showed that Bim1p (1-187 GCN4) only marginally rescues the deletion of *bim1*. The effects are very weak and the growth rates are more comparable to a *bim1*-deletion than to wild-type *BIM1* (Figure 23). This observation further supports the assumption of a cooperative binding of both Kar9p-binding domains.

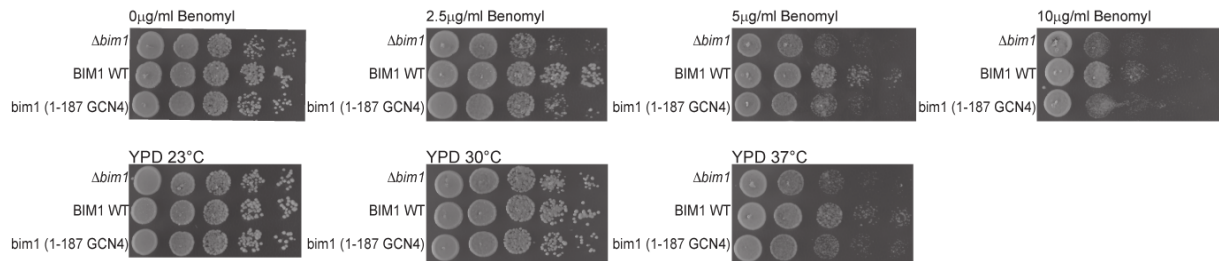


Figure 23 In vivo analysis of Bim1p lacking the C-terminal EB1-like motif Growth tests of a yeast strain expressing Bim1p (1-187 GCN4) at different Benomyl concentrations and temperatures. The phenotype of a *bim1*-deletion can only marginally be rescued by the expression of Bim1p (1-187 GCN4).

2.4.6 Aurora B/Ipl1p dependent phosphorylation of Bim1p impairs binding to Kar9p

A recent publication has shown that the middle domain of Bim1p is phosphorylated at six serine residues (amino acid positions 139, 148, 149, 165, 166, and 176) by the Aurora B kinase Ipl1p (Zimniak, Stengl et al. 2009) (Figure 15A). This phosphorylation occurs specifically during anaphase and is required for proper spindle mid-zone disassembly (Zimniak, Stengl et al. 2009). Since these residues are located in the novel Kar9p-binding region identified in this study, phosphorylation of these residues could also play a role in Kar9p-binding.

In order to test whether phosphorylation of Bim1p directly affects the interaction with Kar9p, pull-down experiments with four different phosphomimetic mutants in the middle domain of Bim1p were performed. Zimniak and colleagues have shown that mutations of these serines into glutamic acids efficiently mimic phosphorylation of Bim1p and reduce microtubule binding (Zimniak, Stengl et al. 2009). A strongly impaired binding to Kar9p was observed with the phosphomimetic double mutant Bim1p (FL; S165D S166D), whereas Kar9p binding with Bim1p (FL; S148D S149D) was comparable to wild-type Bim1p (FL). A less reduced interaction with Kar9p was observed with the other two mutations of Bim1p (FL; S139D) and Bim1p (FL; S176D).

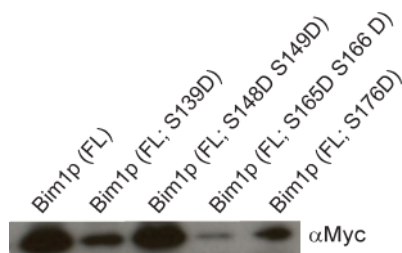


Figure 24 Phosphorylation of Bim1p by Aurora B / Ipl1p affects binding to Kar9p Western blots of pull-down experiments with phosphomimetic mutations in the middle-domain of Bim1p. Three of four mutant versions of Bim1p show a reduced binding to Kar9p.

RESULTS

These results further support the finding that the middle domain has an additional Kar9p binding site. It also suggests that Aurora B/Ipl1p-dependent phosphorylation of the Bim1p middle domain regulates its binding to Kar9p. This interpretation is consistent with the observation that Aurora B/Ipl1p kinase-dependent phosphorylation of Bim1p is required for normal progression of mitosis (Zimniak, Stengl et al. 2009).

3 Discussion

3.1 Crystallisation of Kar9p

The function of Kar9p is well understood *in vivo*, but the molecular details of how the protein is folded and how it interacts with other proteins are unknown (Bloom 2000; Hwang, Kusch et al. 2003). Given that Kar9p has limited sequence similarities to its homologue APC (Bienz 2001), a crystal structure of Kar9p would help to improve our understanding of Kar9p and maybe even APC function.

In this study, crystals of Kar9p were obtained for the full-length protein as well as for several Kar9p variants (Table 1). Most of the crystals diffracted X-rays not better than 7 Å and only crystals of Kar9p (1-398) showed some additional spots up to 4-5 Å (Figure 9C). This indicates that the protein generally tends to crystallise and represents therefore a promising starting point. Since several cryo-protection approaches have been tried without great differences, the poor X-ray diffraction properties are rather likely to be due to suboptimal crystal packing (see chapter 2.1.2 and 2.1.4).

Common causes of suboptimal crystal packing are flexible or unstructured parts of a protein. Structure predictions of Kar9p obtained from *HHPred Server* (Soding, Biegert et al. 2005) showed that the C-terminal part of Kar9p is completely unstructured, whereas the N-terminal part is structured (Figure 8A).

When large parts of the C-terminus were deleted, the protein yield was much higher than for Kar9p (FL) and additional spots around 4-5 Å appeared in the diffraction pattern of crystals of Kar9p (1-398). On the other hand, deletions of the N-terminal part of Kar9p led to rapid degradation of the proteins (see chapter 2.1.3). Additionally, fragments of the N terminal part of Kar9p were not digested by limited proteolysis, whereas the C-terminal part was prone to proteolysis.

Taken together, these results indicate that the N-terminal part of Kar9p is structured, whereas the C-terminal part is not, further supporting the preliminary structural model obtained by *HHPred Server* (Soding, Biegert et al. 2005). The unstructured part of Kar9p might therefore hinder crystallisation of Kar9p (FL). A crystal structure of the N-terminal part of Kar9p based on these findings appears possible, but would require additional optimisation of the fragments as well as the crystal-growth conditions and cryo-protection. However, since multiple attempts to improve such conditions failed to result in well-diffracting crystals, this might not be an easy task.

3.2 Role of posttranslational modifications of Kar9p

Several studies have shown that Kar9p is posttranslationally modified *in vivo* by phosphorylation and sumoylation (Liakopoulos, Kusch et al. 2003; Maekawa, Usui et al. 2003; Maekawa and Schiebel 2004; Moore, D'Silva et al. 2006; Moore and Miller 2007; Leisner, Kammerer et al. 2008; Meednu, Hoops et al. 2008). Both types of modifications independently promote asymmetric localisation of Kar9p to the mother SPB (Leisner, Kammerer et al. 2008). Combining mutations in phosphorylation- and sumoylation-sites abrogates the asymmetric distribution of Kar9p more extensively than each mutation alone (Leisner, Kammerer et al. 2008). It will be therefore important to identify the molecular mechanisms underlying those types of regulations to gain further insights into Kar9p regulation and function. Of particular importance is the role of posttranslational modifications on the association of Kar9p with other proteins such as Bim1p.

3.2.1 Phosphorylation of Kar9p

Phosphorylation of Kar9p occurs at serines 197 and 496 in a Clb4p/Cdc28p-dependent manner (Liakopoulos, Kusch et al. 2003; Maekawa, Usui et al. 2003; Maekawa and Schiebel 2004; Moore, D'Silva et al. 2006; Moore and Miller 2007). Two models have been proposed how this phosphorylation event could mediate asymmetry in Kar9p association with the mother SPB. Liakopoulos and colleagues have suggested that phosphorylation of Kar9p by Clb4p/Cdc28p disrupts the interaction between Kar9p and Bim1p and thereby prevents its loading onto the corresponding spindle pole (Liakopoulos, Kusch et al. 2003). In an alternative model, Moore and Miller have suggested that Kar9p is phosphorylated at both spindle poles, but that a factor present only at one of the two poles would associate with Kar9p (Moore and Miller 2007).

Using *in-vitro* pull-down experiments, the research presented here demonstrates that mutations preventing phosphorylation of Kar9p at serine 197 and/or 496 show no defects in Bim1p binding (Figure 11). This observation suggests that Clb4p/Cdc28p-dependent phosphorylation is not directly involved in modulating the Bim1p interaction. These results are also in agreement with previous *in vivo* experiments elsewhere, which have demonstrated that phosphorylation of Kar9p is not required for association with Bim1p (Moore and Miller 2007). To gain further insights on the function of phosphorylation *in vivo*, yeast strains harbouring mutations of Kar9p at both or either phosphorylation site were generated. When tested for growth on *Benomyl* or at different temperatures, the strain harbouring the double mutation was less sensitive than compared to the wild-type, suggesting that this protein is less active (Figure 12 and Table 2). Given that the association with Bim1p is not impaired by this mutation, other mechanisms or microtubule-associated proteins must influence the activity of Kar9p (S197A; S496A). Therefore, future work will be

required to show whether the previously proposed unknown, asymmetric factor (Moore and Miller 2007) indeed exists to modulate the function of Kar9p at only one pole or whether phosphorylation of Kar9p is required for association with other microtubule-associated proteins.

To identify such a potential asymmetric factor, co-immunoprecipitation (co-IP) experiments with myc-tagged Kar9p were performed with all mutations of phosphorylation sites, followed by mass-spectrometric analysis of the co-immunoprecipitating protein bands (see chapter 2.2.3). The proteins co-immunoprecipitating with Kar9p were similar in all experiments and no obvious difference in the overall composition was observed (see chapter 7.2). This either indicates that such an asymmetric factor is not present or, when considering that the cells were asynchronous, the detection of such an asymmetric factor requires synchronisation of the cells. Since the localisation of Kar9p to the mother SPB occurs within a short time frame of the cell-cycle such an asymmetric factor might only associate with Kar9p in a well-defined time frame. Therefore, co-IPs from synchronised yeast cultures might be required to detect the presence of such an asymmetric factor.

3.2.2 Sumoylation of Kar9p

Sumoylation is a highly conserved process and a major regulator of protein function in a wide range of cellular events (Hay 2005; Wilkinson and Henley 2010). Covalent attachment of SUMO (Smt3p in budding yeast) to lysine residues of target proteins involves an enzymatic cascade analogous to the ubiquitination pathway (Wilkinson and Henley 2010). Modifications of target proteins by sumoylation exert regulatory effects on protein-protein interactions, protein localisation and protein stabilisation (Johnson 2004; Meednu, Hoops et al. 2008). Furthermore, sumoylation might alter protein function at a molecular level by masking or adding interaction surfaces and by inducing conformational changes that result in altered protein-protein interactions (Meulmeester and Melchior 2008).

Sumoylation of Kar9p has been reported to begin in metaphase, which is the time point when the Myo2p-Kar9p-Bim1p complex is active (Leisner, Kammerer et al. 2008). Is sumoylation therefore a possible regulator of complex assembly? To answer this question, the role of the individual sumoylation sites identified in the previous study (Leisner, Kammerer et al. 2008) was investigated in pull-down experiments and *in vivo* studies. In pull-down experiments, mutations of Kar9p (K333R) had only mild defects in binding to Bim1p and almost no effect was observed with Kar9p (K301R) and Kar9p (K529R), whereas strong defects were observed with Kar9p (K333E) and Kar9p (K381R). Combinations of these mutations resulted in an additive decrease in binding (Figure 13). The observation that Kar9p sumoylation in the majority of the four reported modification sites is required for efficient Bim1p interaction is also suited to explain why no interaction of the proteins with recombinant proteins expressed

DISCUSSION

in bacteria was observed. When testing these mutations *in vivo* in the already described dominant negative-overexpression assay for *Benomyl* and temperature sensitivity, the results did not always correlate in every detail with the *in vitro* results (Figure 14 and Table 3). However, a clear correlation between the number of mutated sumoylation sites and decreased binding to Bim1p as well as to reduced sensitivity towards *Benomyl* and higher temperatures was observed. One can therefore assume that a more complex mechanism might exist *in vivo*. The overall outcome of the experiments suggests that sumoylation plays an important role in Bim1p binding and that the effect is additive. Of particular importance is residue K381 that upon mutation almost abolishes binding to Bim1p. Whether sumoylation of this residue alone contributes to association of Kar9p with Bim1p or if the other sumoylated residues play also play a role remains unclear and requires further experiments such as *in vivo* co-localisation of these mutant proteins with Bim1p and other Kar9p associated proteins.

A more indirect confirmation of these results comes from an observation of Miller and colleagues (Miller, Cheng et al. 2000). After pull-down experiments from yeast with HA-tagged Kar9p, the authors always detected two bands of Kar9p in western-blot that differed by 4000-5000 Da in apparent molecular weight. On the other hand when they pulled-down Bim1p, only the higher molecular weight band of Kar9p was observed (Miller, Cheng et al. 2000). This shift in molecular weight suggests that there might be a significant functional or regulatory difference between the two bands of Kar9p. In conjunction with the results from this study, the observations strongly suggest that sumoylation of Kar9p is required for the interaction with Bim1p. If sumoylation of Kar9p at K381 is sufficient for the regulated association with Bim1p or if the other residues are also important remains unclear. The results of Miller and colleagues rather suggest that a single sumo-modification of Kar9p may be sufficient.

Taken together, the results of the present study suggest that assembly of the spindle-orientation complex is induced by Kar9p sumoylation. Because sumoylation of Kar9p is prominent also in anaphase (Leisner, Kammerer et al. 2008) desumoylation-independent mechanisms must be in place to mediate disassembly of the Myo2p-Kar9p-Bim1p complex at the onset of anaphase.

3.3 Crystal structure of Bim1p

3.3.1 Comparison of the crystal structure of Bim1p with human EB1

The functions of the C-terminal domains of EB1 and Bim1p are related (Miller, Cheng et al. 2000; Honnappa, John et al. 2005; Slep, Rogers et al. 2005). In EB1 the C-terminal domain represents a general landing platform for a number of different +TIPS such as APC or spectraplakins (Lansbergen and Akhmanova 2006). Bim1p on the other hand interacts with Kar9p, the CLIP-170 homologue Bik1p, Stu2p, Dam1p and other proteins (Miller, Cheng et al. 2000; Shang, Hazbun et al. 2003; Wolyniak, Blake-Hodek et al. 2006). However, whether these interactions happen in all cases via the C-terminal domain is not yet known. Given that this domain in both orthologs exhibit similar functions, they are also likely to form very similar structures.

To gain further insights into the regulation of Kar9p binding to Bim1p, the crystal structure of Bim1p (C-term) was solved in this study. The overall structural arrangement of Bim1p is similar to human EB1 and shows that Bim1p (C-term) is also a dimer (Figure 16 and Figure 17). The RMSD value for the C-terminal domains between hEB1 and Bim1p is only 1.2 Å, indicating significant similarity of both overall folds. One very obvious difference is the length of the long alpha-helix, which is in Bim1p about one third longer than in hEB1 (Figure 17). Sequence alignments with EB1-like proteins from different species revealed that Bim1p contains a sequence insertion of 24 residues (amino acid 240 to 263 in Bim1p (FL) and amino acid 58 to 81 in Bim1p (C term) (Figure 30). This sequence insertion was not visible in the electron density presumably because of its high content in glycine residues and the resulting flexibility. This Bim1p-specific sequence insertion connects the long and the short helix. Pull-down experiments with Kar9p and deletions of this extended loop region showed no difference in binding to Kar9p (Figure 20A). These results clearly indicate that the extended loop region is not required for association of Kar9p with Bim1p. Why budding yeast has evolved such an extended loop region is not clear. One possibility is that other proteins interact with Bim1p via this unstructured loop.

Sequence alignments between several EB1 family members revealed highly conserved residues in their C-terminal EB1-like domains (Figure 30). A surface plot of this alignment onto the Bim1p (C-term) structure shows that the majority of the highly conserved residues lie at the four-helix bundle forming a hydrophobic core (Figure 16C). This hydrophobic core contains a highly conserved „FYF“-motif, which has been shown for human EB1 to mediate binding to APC (Honnappa, John et al. 2005; Slep, Rogers et al. 2005). It is widely accepted that residues, which mediate protein-protein contacts are conserved between different species (Ma, Elkayam et al. 2003). Therefore, this region is very likely to mediate association with Kar9p. Furthermore, this region contains several highly conserved acidic residues,

contributing a net negative charge (Figure 16B). This conserved solvent-exposed region with hydrophobic and charged character might serve as cargo-binding site in Bim1p.

3.3.2 The C-terminal domain of Bim1p mediates dimerisation of the protein

The crystal structure of Bim1p (C-term) revealed that this domain is formed by a dimer. Several recent studies have shown that dimerisation via this domain is required for proper function of EB1-like proteins (Slep and Vale 2007; Honnappa, Gouveia et al. 2009; Komarova, De Groot et al. 2009; Zimniak, Stengl et al. 2009; De Groot, Jelesarov et al. 2010). Dimer formation of EB1 enables the protein to track microtubule plus-ends (Slep and Vale 2007). In addition, dimerisation of the CH-domain of Bim1p potentially promotes microtubule nucleation (Slep and Vale 2007; Zimniak, Stengl et al. 2009) and microtubule binding (Zimniak, Stengl et al. 2009). To gain insight into dimer formation and the overall composition of Bim1p (FL), I performed small-angle X ray scattering (SAXS) experiments. The molecular weights calculated from the measured data clearly show that Bim1p (C-term) and Bim1p (FL) are dimeric in solution (Figure 18A). Crysol analysis of the theoretical scattering curve calculated from the crystal structure and comparison with the measured data shows an almost perfect match (chi-value of 1.1) (Figure 18B). Together these results confirm that the dimer observed in the crystal structure is also present at near-physiological conditions in solution.

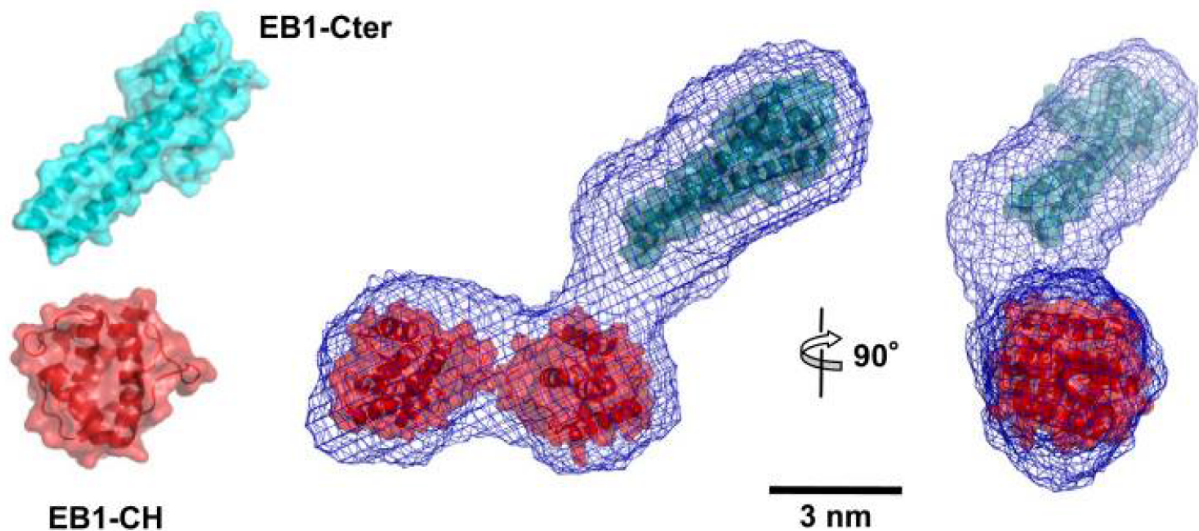


Figure 25 Low resolution model of human EB1. Calculated SAXS envelope (blue mesh) of human EB1. The crystal structures of the CH-domain (EB1-CH, red, PDB-ID: 1PA7) and the C-terminal domain (blue, PDB-ID: 1WU9) of EB1 were manually docked into the map (Zimniak, Stengl et al. 2009). Picture taken from (Buey, Mohan et al. 2011)

While SAXS experiments were performed for Bim1p, a study was published indicating similar properties of human EB1 (Buey, Mohan et al. 2011). In this study a low-resolution structure of the full-length EB1 protein was obtained by SAXS. Their model of EB1 depicts an elongated and globally asymmetric molecule, which resembles the shape of a golf club (Figure 25) (Buey, Mohan et al. 2011). The known X-ray structures of the CH-domain (Slep and Vale 2007) and the EB1 dimerisation domain (Honnappa, John et al. 2005; Slep, Rogers et al. 2005) were docked manually into the molecular envelope (Buey, Mohan et al. 2011). Both domains are in close proximity, suggesting that the linker domain is partially folded and interacts with both the CH-domain and the C-terminal EB1-like domain to form a complex interaction surface (Buey, Mohan et al. 2011). The overall structural arrangement requires the C-terminal dimerisation domain, since no dimers were observed for the isolated CH-linker domain fragments (Sandblad, Busch et al. 2006; Buey, Mohan et al. 2011). Thus dimerisation by the C-terminal EB1-like domain is likely to be a general feature of this class of proteins.

3.4 Kar9p and APC share common binding features to Bim1p and EB1

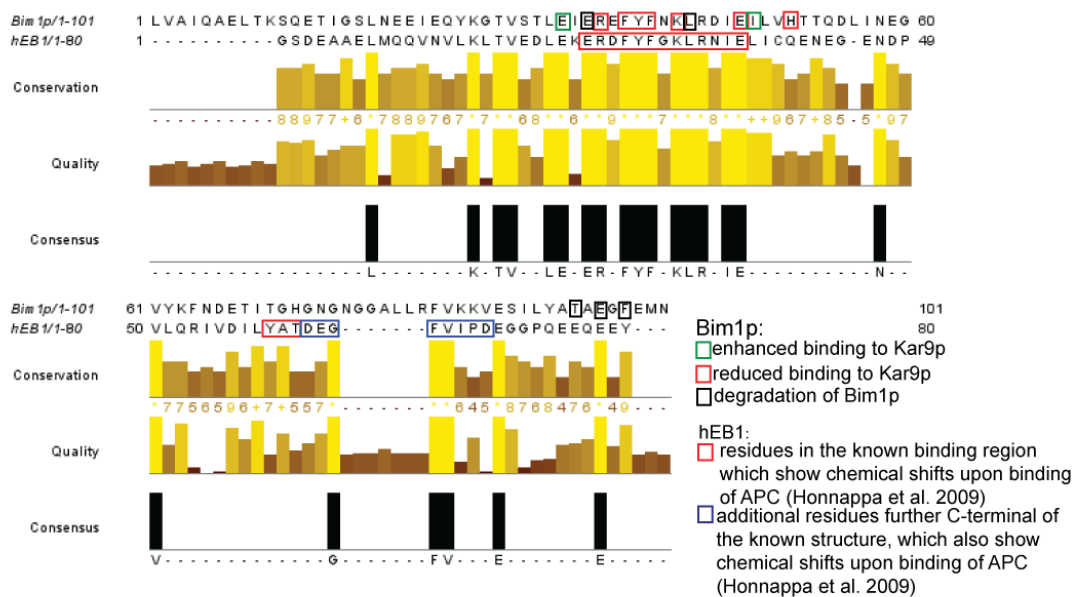
To gain further insights into the Kar9p-Bim1p complex assembly, structure-guided mutations were introduced in the C-terminal domain of Bim1p and tested for Kar9p binding. Pull-down experiments revealed several residues that either decreased or increased binding to Kar9p upon mutation to alanine (Figure 20B-E). Surprisingly, two point mutations (E218A, E214A) result in an almost two-fold increase in binding to Kar9p (Figure 20C-E). When plotting the interaction-modulating mutations onto the surface of the structure of the C-terminal domain of Bim1p, a patch within the highly conserved hydrophobic core can be observed (Figure 20C and Figure 16C). Both mutations enhancing binding to Kar9p are close to each other, but also in vicinity to two mutations that strongly decrease binding to Kar9p (R217A, F221A). This observation suggests that the region might be of particular importance for Kar9p binding. Alteration of the acidic residues obviously alters the net charge of the protein leading to an increased binding.

When testing several mutations *in vivo*, sensitivity towards *Benomyl* and higher temperature was observed only for mutation F219A (Figure 21). The considerably weak effect *in vivo* suggests that either *in vivo* the complex assembly is more robust or that other mechanisms contribute to the rescue of the defects. Other mechanisms could include a second binding region or the partially redundant dynein-dynactin pathway, which can rescue defects in Bim1p-dependent spindle orientation. Therefore a synthetic lethality assay with a knockout of dynein is in preparation to assay if the defects of the mutations become more pronounced in absence of redundancy.

DISCUSSION

The availability of a co-structure of EB1 with an APC peptide and MACF (Honnappa, Gouveia et al. 2009) made a direct comparison of the results obtained in this study with structural information of these homologues possible (Figure 26). The analysis revealed that Kar9p also binds within the same highly conserved region of Bim1p that has been shown for EB1 to bind its cargoes (Honnappa, John et al. 2005; Slep, Rogers et al. 2005; Honnappa, Gouveia et al. 2009). Several of the corresponding residues in both proteins are identical and others lie in close vicinity (Figure 26), suggesting that the overall mode of interaction is similar for both EB1-like domains.

Comparison of identified residues in the interaction between Bim1p and Kar9p and the interaction between hEB1 and APC



Comparison of identified residues in the interaction between Bim1p and Kar9p and the interaction between hEB1 and MACF

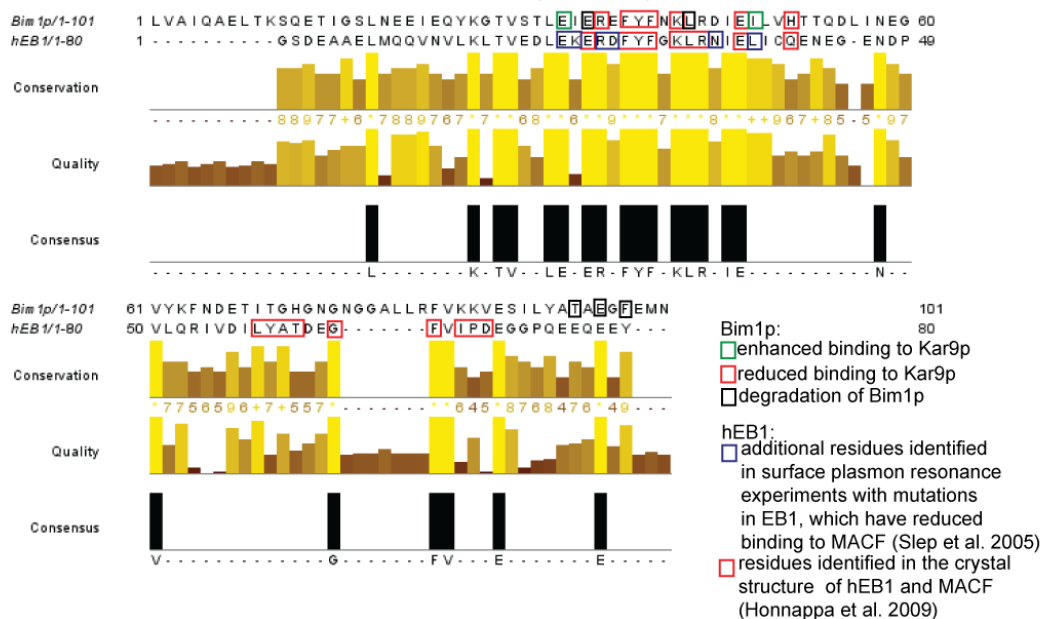


Figure 26 Comparison of the residues mediating binding to different cargoes in EB1 and Bim1p. The residues mediating binding of Kar9p to Bim1p are identical or lie in close vicinity to the residues in EB1 required for binding to APC and MACF, suggesting that the mode of cargo binding is similar.

DISCUSSION

However, when testing the binding of human EB1 C-terminus with yeast Kar9p an interaction was not observed (Figure 20D,E). This finding indicates that despite their similarities cargo binding is not identical. However, for fission yeast it has been shown that human EB1 can substitute the function of the endogenous homolog Mal3p (Beinhauer, Hagan et al. 1997; Browning, Hackney et al. 2003). Mal3p can furthermore mimic the interaction of EB1 with APC *in vitro*, although an APC homologue has not been identified yet in fission yeast (Nakamura, Zhou et al. 2001). Nakamura and colleagues further showed that Mal3p can promote microtubule polymerisation *in vitro* in the presence of the C-terminal EB1-binding domain of APC (Nakamura, Zhou et al. 2001).

These results indicate that the EB1-family members are not only conserved based on protein sequence and structural considerations but also at a functional level. Why an interaction with the C-terminal domain of human EB1 and Kar9p failed remains unclear. It might be that the full-length proteins contain additional binding regions required for the association with their homologous proteins. The identification of a second Kar9p-binding region in Bim1p in the present study indeed suggests that cargo interaction is more complex than previously anticipated. It would be interesting to see whether this new Kar9p-binding region in Bim1p is also functional and required in human EB1 for the binding of APC, MACF or its other binding partners.

Interaction studies between the C-terminal domain of human EB1 and APC used a small peptide of APC, with which an interaction could be observed (Honnappa, John et al. 2005; Slep, Rogers et al. 2005; Honnappa, Gouveia et al. 2009). The peptide of APC mediating binding to EB1 is completely unstructured in solution, but the region binding to EB1 becomes ordered upon complex formation with EB1 (Honnappa, Gouveia et al. 2009). Moore and colleagues (Moore and Miller 2007) have identified a minimal binding region in Kar9p that still binds to Bim1p in a yeast-two hybrid assay (residue 534-580) (Figure 27). This region is located in the highly unstructured basic and proline rich C-terminal domain of Kar9p. It is therefore likely that Kar9p adopts a similar fold as APC upon binding to Bim1p. Although this region lies outside the sequence, which shows sequence conservation to APC (Figure 5B), several other general features are present that have been observed to be required for binding to EB1. Slep and colleagues identified repeat binding motifs in APC and MACF as well as other general features required for cargo binding of EB1 (Slep, Rogers et al. 2005). These general features are the presence of several hydrophobic residues (mainly prolines) and a net positive charge (Slep, Rogers et al. 2005). Despite Kar9p does not have a repeat motif architecture similar to APC or MACF (Slep, Rogers et al. 2005), the common features required for binding to EB1 are present in the region mapped by the yeast-two hybrid assay. Another hint that the binding of Kar9p to Bim1p is similar to APC and EB1 is the identification of an EB1-binding motif in APC and MACF (Honnappa, Gouveia et al. 2009). This short

DISCUSSION

polypeptide motif (Serine-x-Isoleucine-Proline (SxIP)) is used by numerous + TIPs for their localisation to microtubule plus-ends in an EB1-dependent manner (Honnappa, Gouveia et al. 2009). The SxIP-motif establishes an interaction network between the serine, isoleucine and proline motif and the hydrophobic core of the C-terminal domain of EB1 (Honnappa, Gouveia et al. 2009). Intriguingly, this motif is also found in the minimal region of Kar9p binding to Bim1p. This leads to a speculation that this motif might also mediate the binding to Bim1p as has been shown for APC and MACF (Honnappa, Gouveia et al. 2009). Additional experiments will be required to delineate the role of this Kar9p region in binding to Bim1p. First of all a direct interaction between a peptide of the minimal Bim1p binding region of Kar9p and Bim1p has to be demonstrated. If this will be possible is arguable, since sumoylation of full-length Kar9p is required for the interaction with Bim1p and all identified sumoylation sites (Leisner, Kammerer et al. 2008) are outside this minimal region. Nevertheless, K529 is in close vicinity, which might argue for a potential role of this residue in regulating binding to Bim1p.

```
1 MDNDGPRSMT IGDDFQENFC ERLERIHNTL HSINDCNLSL ESTTSISETL
51 LVQFYDDLLEN VASVIPDLVN KKRLGKDDIL LFMDWLLLKK YMLYQFISDV
101 HNIEEGFAHL LDLLEDEFSK DDQDSDKYNR FSPMFDVIEE STQIKTQLEP
151 WLTNLKELLD TSLEFNEISK DHMDTLHKII NSNISYCLEI QEERFASPIR
201 HTPSFTLEQL VKLLGTHTET TEPKVPKFSP AEDILSRKFL NLKKNIPPIE
251 KSLTDILPQR IVQFGHRNIT NITTLQILQ KKYELIMKDY RFMNSEFREL
301 KVELIDKRWN ILFINLNHEL LYILDEIERL QSKLLTTYKT KDITIRLERQ
351 LERKSKTVSK TFNIIYRALE FSLLDAGVAS KTNELAQRWL NIKPTADKIL
401 IKSSASNKIA TSKKKIPKPK SLGFGRPNSV IGTITQDFQE RVAINEGDSN
451 KTPENSTTVA LKGKKLGKAL LQKMNIKPAT SPNSSNAINP FFDPESPNKG
501 KLILSSVPPL PYDEDETTL RVSRGENEKS PDSFITSRHE NKVQITETPL
551 MAKNKSVALDI EKDKWNHYRS LPSRIPYKD KVVKVTVENT PIAKVFQTPP
601 TKITTPNSQV WVPSTRRRRTR LRPPTPLSQL LSPREGRLDK TPTY*
```

Figure 27 Sequence of Kar9p. Blue: minimal sequence of Kar9p that has been mapped by yeast-two hybrid to bind to Bim1p (Moore and Miller 2007). The SxIP-motif found in APC and MACF to be required for binding to EB1 is also present in this region (red) (Honnappa, Gouveia et al. 2009).

3.5 Role of the middle domain of Bim1p in protein binding

My observation that full-length Bim1p binds to Kar9p considerably stronger than its C-terminal EB1-like motif suggested additional features in Bim1p to participate in this interaction. Indeed, a second Kar9p binding site in the middle domain of Bim1p was identified (Figure 22A,B). However, the middle domain of Bim1p was only capable of Kar9p binding when the protein was dimerised. Full binding to Kar9p was only observed when the whole middle domain was present, whereas binding decreased when parts of the middle domain were deleted (Figure 22B). This binding to Kar9p via the Bim1p-middle domain is comparable in strength to the interaction of the EB1-like domain alone with Kar9p. Thus, the C-terminal EB1-like motif not only functions as Kar9p binding site but also provides the dimerisation required for Kar9p binding by the middle domain.

DISCUSSION

However, Bim1p (1-187 GCN4) only marginally counters the growth defects of a *bim1* deletion *in vivo*. This observation further supports the assumption of a cooperative binding of both Kar9p binding domains. The simultaneous binding to two regions is furthermore likely to increase the strength and the specificity for a given interaction. It should also be noted that the GCN4 fragments not only lacked the EB1-like motif but also 57 residues C-terminal to the EB1-like motif. It has been shown that these two regions together mediate binding of the Aurora B/Ipl1p kinase (Zimniak, Stengl et al. 2009) and thus might also be required to rescue the $\Delta bim1$ phenotype independent of their role in Kar9p binding.

Secondary structure predictions and sequence alignments indicate that the middle domain is rather unstructured. It is also only weakly conserved, compared to other regions of Bim1p. Since protein-interaction surfaces are often highly conserved (Ma, Elkayam et al. 2003), it is likely that the mode of interaction between the middle domain of Bim1p and Kar9p follows a rather unique and unusual mechanism. On the other hand considering that this middle domain is also required for efficient microtubule binding in EB1 and Bim1p, the function of this domain seems to be conserved despite its weak conservation (Slep and Vale 2007; Zimniak, Stengl et al. 2009). It would be therefore interesting to see if this middle domain is also involved in cargo binding in EB1.

Phosphorylation of the middle domain was shown to be important for the regulation of microtubule binding of Bim1p (Zimniak, Stengl et al. 2009). This region is phosphorylated by the Aurora B/Ipl1p kinase in a well-defined time window starting in anaphase (Zimniak, Stengl et al. 2009). To gain insight into the regulation of Kar9p binding, phosphomimetic mutants of Bim1p were tested in pull-down experiments. Compared to wild-type Bim1p (FL), the double mutant Bim1p (FL; S165D S166D) showed strongly reduced binding, whereas mutations of S139 and S176 had only mild defects. Aurora B/Ipl1p kinase-dependent phosphorylation of Bim1p occurs at a time point when the spindle is finally oriented and when the Myo2p-Kar9p-Bim1p complex has to disassemble.

For the vertebrate homolog EB1 of Bim1p it has recently been reported that its binding to Aurora B kinase protects it from inactivation (Sun, Gao et al. 2008). In this context, it would be interesting to see whether phosphorylated EB1 or Bim1p shows increased binding to AuroraB/Ipl1p kinase, thereby protecting it from inactivation. If true, this feedback loop could constitute a novel entry point for inhibitory approaches.

3.6 Model of the cell-cycle dependent regulation of Bim1p-Kar9p complex assembly and disassembly

The findings of this study suggest a model that explains the cell-cycle dependent regulation of the assembly and disassembly of the Myo2p-Kar9p-Bim1p complex. Given its role in spindle orientation, this complex should not assemble before metaphase and should be inactivated again at the beginning of anaphase. Leisner and colleagues showed that sumoylation occurs during metaphase and that a Kar9p version with all four lysine residues mutated fails to localise exclusively to the mother SPB (Leisner, Kammerer et al. 2008). Other studies have furthermore shown that the Bim1p-Kar9p complex assembles before loading onto the microtubules via the spindle pole bodies (Cuschieri, Miller et al. 2006). The present findings therefore suggest that sumoylation induces the assembly of the Bim1p Kar9p complex prior loading onto the spindle poles.

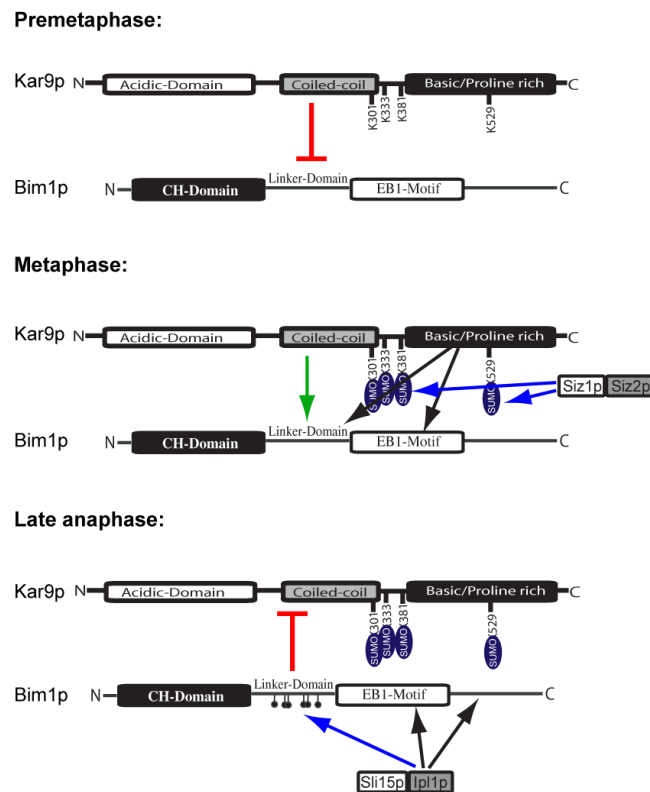


Figure 28 Model for the assembly and disassembly of the Bim1p-Kar9p complex. In premetaphase, Kar9p is not sumoylated and therefore cannot bind to Bim1p. Kar9p becomes sumoylated in metaphase to regulate the binding to Bim1p. For complex disassembly in late anaphase, Bim1p becomes phosphorylated, thereby reducing binding to Kar9p. Arrows color code: green= binding when modified, black= binding regions, blue= phosphorylation/sumoylation events, red= reduced binding upon modification/without modification.

Because sumoylation of Kar9p is prominent also in anaphase (Leisner, Kammerer et al. 2008), desumoylation-independent mechanisms must be in place to mediate disassembly of the Myo2p-Kar9p-Bim1p complex at the onset of anaphase. Since phosphorylation of Kar9p had no effect on the complex assembly (Figure 11), additional regulatory events were investigated. Bim1p is phosphorylated in its middle domain in late

DISCUSSION

anaphase by the Aurora B/Ipl1p kinase. Mimicking phosphorylation at these residues results in decreased Kar9p binding. Therefore the findings of this study suggest a cell-cycle dependent inactivation of the Bim1p-Kar9p interaction by phosphorylation of Bim1p in its middle domain. This inactivation would pave the way for the subsequent spindle elongation by the dynein-dependent complex. It is also consistent with the observation that Aurora B/Ipl1p kinase-dependent phosphorylation of Bim1p is required for spindle elongation to occur with normal kinetics and for efficient disassembly of the spindle midzone (Zimniak, Stengl et al. 2009).

In summary, the present study not only offers a mechanism for the cell cycle-dependent regulation of the Bim1p interaction to Kar9p. It also provides a testable hypothesis for the regulation of the human EB1 interaction with its binding partners by EB1 phosphorylation through Aurora B kinase in its middle domain.

4 Materials and Methods

4.1 Consumables and chemicals

All commonly used chemicals were purchased in the highest available purity from Roth (Karlsruhe, Germany), Merck (Darmstadt, Germany), or Sigma (Deisenhofen, Germany), unless stated otherwise. Enzymes and nucleotides for molecular biology and molecular weight markers for electrophoretic analyses were obtained from Fermentas (St. Leon-Rot, Germany), New England Biolabs (Frankfurt, Germany) or Agilent Technologies (Waldbronn, Germany). Components to prepare media for bacterial and yeast cultivation were purchased from Becton Dickinson (Heidelberg, Germany) and Sigma Aldrich (Deisenhofen, Germany). Media for insect cell culture were obtained from Thermo Scientific (Bonn, Germany) and Sigma Aldrich (Deisenhofen, Germany). Chromatographic equipment, columns, media and autoradiography films for western blots were purchased from GE Healthcare (Munich, Germany), except for Amylose resin material, which was purchased from New England Biolabs. Transfer membranes for western blotting were obtained from Roth (Karlsruhe, Germany). Crystallisation screens, crystallisation grade reagents, and crystallisation tools were obtained from Hampton Research (Aliso Viejo, USA), Qiagen (Hilden, Germany), and Jena Bioscience (Jena, Germany). DNA oligonucleotides were ordered from Thermo Fisher (Ulm, Germany).

4.2 Oligonucleotides

4.2.1 Oligonucleotides for biochemical characterization

1	5'AAA AAGCTAGCATGGATAATGATGGACCCAG3'
3	5'AAAGGATCCATGAGTGC GGATCGGAGAATC3'
11	5'AAAGAGCTCTCAATAAGTTGGGGTTTTATCTAAACG3'
12	5'AAACTCGAGTTAAAAAGTTTCCTCGTCGATGATCAAG3'
15	5'AAAGCGGCCCGCCAGGGGCCCTGGAACAGAACTTCC3'
16	5'AAAGCGGCCCGCATGGATAATGGACCCAG3'
17	5'AAATCTAGATCAATAAGTTGGGGTTTTATCTAAACG3'
18	5'AAAGGATCCATGTCCCTATACTAGGTTATTGG3'
19	5' AAAGGATCCTTGGTAGCGATACAAGCGGA 3'
20	5'AAAGGATCCACTTTAGAGATTGAAAGAGA3'
21	5'AAACTCGAGATTCATTTCAAATCCTTCTG3'
22	5'AAACTCGAGTTACTACCTTCGTTACCAT3'
23	5'AAA AAGTCGACATGGATAATGATGGACCCAG3'
26	5'AAA AAGTCGACAAATGGATAATGATGGACCCAG3'
27	5'AAAAAAGAGCTCTCATTTAATATTCATCTTCTGCAG3'
28	5'AAAAAAGAGCTCTCATTTCATCGGTTTCGTCATAAGG3'
29	5'AAA AAAGAGCTCTCATTTATCCGCTGTAGGCTTGAT3'
30	5'AAAAAGCTAGCGGGGATGACTCCAAGAGAAC3'
31	5'AAAAAGAGCTCTCACTTTGCTATCGGTGTGTTTTTC3'
32	5'AAAAAGAGCTCTCATCTTGGTAAAGTAAGTGTG3'
33	5'AAAAAGCTAGCACCATTGGGGATGACTTCCAAG3'

174	5'AAAGTCGACATGGATAATGATGGACCCAG3'
175	5'AAAGCGGAAGCTCAATAAGTTGGGGTTTTATC3'
176	5'AAACTCGAGATATCTCTAAATGAATTG3'
177	5'AAATCTAGAGGCAGTGCTACTGAAATC3'
178	5'AAATCTAGAATGGATAATGATGGACCC3'
181	5'AAAGTCGACATAAGTTGGGGTTTTATC3'
184	5'AAAGCGGCCCGCATACTAACCTAAAAGTGTATAC3'
185	5'AAAGAGCTCGCCAATGTATCCTAGCGAA3'
186	5'AAAGTCGACTCCGGTTCTGCTGCTAGTGG3'
187	5'AAAGCGGCCGCTTAGCTAGTGGATCCGTTTC3'
198	5'GTACTTTAGCGATTGAAAG3'
199	5'CTTTCAATCGCTAAAGTAC3'
200	5'CTTTAGAGGCTGAAAGAG3'
201	5'CTCTTTCAGCCTCTAAAG3'
202	5'TAGAGATTGCAAGAGAATT3'
203	5'AATTCTCTTGCAATCTCTA3'
204	5'GAGATTGAAGCAGAATTTTAC3'
205	5'GTAATTTCTGCTCAATCTC3'
206	5'TTGAAAGAGCATTACTTTC3'
207	5'GAAGTAAATGCTCTTCAA3'
208	5'GAAAGAGAAGCTTACTTCAAC3'

MATERIALS AND METHODS

34	5'AAAAAGCTAGCAGATCTATGACCATTGGGGATG3'
35	5'AAAAAGCTAGCGGACCAGATCTATGACCATTGG3'
36	5'AAAGAGCTCTCATTATCTAAACGCCCTTCTC3'
37	5'AAAGAGCTCTCAACGCCCTTCTCTTGGTGAAAG3'
40	5'AAAGGTACCAAATGAGTGCGGGTATCGGAGA3'
41	5'AAACTCGAGTAAAAAGTTTCTCGTCTGA3'
55	5'AAAAAGCTAGCATGATACAGGTACCTAACGCG3'
56	5'AAAAACTCGAGTCATGATAAGTTAAGAAGATC3'
57	5'AAAAAGAATTCAAATGATACAGGTACCTAACGCG3'
58	5'AAAAAGCTAGCATGAGCAACCATGAGTTGACG3'
59	5'AAAAACTCGAGTCAAAAAGGACGTCTCTGGAAG3'
60	5'AAAAAGTCGACAATGAGCAACCATGAGTTGACG3'
61	5'AAAAAGCGGCCCTCAAAAAGGACGTCTCTGGAAG3'
91	5'AGGTTTCGCGGCCCGATACGG3'
92	5'CCGTATCGGGGCCGCAACCT3'
93	5'GATCCGGAGGCGCCAAACAAA3'
94	5'TTTGTTTGGCGCCTCCGGATC3'
95	5'AGGGAATTGAGAGTCGAACTA3'
96	5'TAGTTCGACTCTCAATTCCT3'
97	5'TTGCAGTCGAGATTACTGACA3'
98	5'TGTCAGTAATCTCGACTGCAA3'
99	5'TTGCAGTCGGAATTACTGACA3'
100	5'TGTCAGTAATCCGACTGCAA3'
101	5'GTCGCATCGAGGACAAATGAA3'
102	5'TTCATTTGTCCTCGATGCGAC3'
103	5'GAAAATGAAAGGTCACCAGAC3'
104	5'GTCTGGTGACCTTTTCATTTTC3'
105	5'AAAAAGCTAGCAGGAATTGAAAGTCGAACTAATC3'
106	5'AAAAAGCTAGCAAACGTTGGAATATACTCTTTATT3'
107	5'AAA AAGTCGACAAAATATCCCTCCAATTGAAAAAG3'
108	5'AAA AAGTCGACAAGAAAAAGTTTACTGATATCC3'
109	5'AAAAAGTCGACAAAGGGAATTGAAAGTCGAACTAATC3'
110	5'AAAAAGTCGACAAAACGTTGGAATATACTCTTTATT3'
127	5' CATTTCATTACCATGGCCACCTTCATTTATTAATC 3'
128	5' CTCCCCATTTCCATTACCACCTTCATTTATTAATC 3'
129	5' GATTTAATAAATGAAGGTGGCCATGGTAATGAAATGG 3'
130	5' GATTTAATAAATGAAGGTGGTAATGAAATGGGGGAG 3'
135	5'AAAGAGCTCTCATTGTGCGATTAGTTCGACTTT3'
136	5'AAAGAGCTCTCATTGTGTCAGTAATTCG3'
137	5'AAAGAGCTCTCATTATTACTGTCACCTTCATT3'
138	5'AAAGCGCCGCTCATTGTGCGATTAGTTCGACTTT3'
139	5'AAAGCGCCGCTCATTGTGTCAGTAATTCG3'
140	5'AAAGCGCCGCTCATTATCCGCTGTAGGCTTGAT3'
141	5'AAAGCGCCGCTCATTATTACTGTCACCTTCATT3'
146	5'AAAGCGCCGCTCATGATTTTCTCTCCAATTGCCTCTC3'
149	5'AAAGAGCTCTCAAACACTATTCGGTCGCCAAAGCC3'
155	5'AAAAGTCGACATGCATCATCATCATCAGATAATGATG GACCCAGATC3'
165	5'AAAGAGCTCTCATGTAGGCTTGATATTCAGCC3'
166	5'AAAGAGCTCTCAGATTAGAATTTTATCCGCTG3'

209	5'GTTGAAGTAAGCTTCTCTTTC3'
210	5'GAGAATTTGCCTTCAACAA3'
211	5'TTGTGAAGGCAAATTC3'
212	5'GAATTTTACGCCAACAACT3'
213	5'AGTTTGTGGCGTAAAAATTC3'
214	5'TTACTTCGCCAACTACG3'
215	5'CGTAGTTTGGCGAAGTAA3'
216	5'ACTTCAACGCACTACGCGAC3'
217	5'GTCGCGTAGTGCCTGAAGT3'
218	5'TCAACAAAGCACGCGACAT3'
219	5'ATGTCGCGTGCTTTGTTGA3'
220	5'ACAACTAGCCGACATAGA3'
221	5'TCTATGTCGGCTAGTTTGT3'
222	5'AACTACGCGCCATAGAAAT3'
223	5'ATTTCTATGGCGGTAGTT3'
224	5'TACGCGACGCAGAAATCCT3'
225	5'AGGATTTCTGCGTCGCGTA3'
226	5'GCGACATAGCAATCCTGGT3'
227	5'ACCAGGATTGCTATGTCGC3'
228	5'ACATAGAAGCCCTGGTCCA3'
229	5'TGGACCAGGGCTTCTATGT3'
230	5'ACATAGAAGCCCTGGTCCA3'
231	5'TGGACCAGGGCTTCTATGT3'
237	5'AAAAAGCTTCGGGGCGTAATCACCTAAC3'
238	5'AAAGAATTCTGGCTACGCTTACTCCAGG3'
239	5'GAGGAACTTTTTCTAGATAAGTTGAGAAC3'
240	5'GTTCTCACTTATCTAGAAAAAGTTTCTC3'
241	5'AAATCTAGATCCGGTTCTGCTGCTAGATAC3'
242	5'AAATCTAGATTAGCTAGAAGCGTAATCTGG3'
250	5'TTTATATGCTGCTGCAGAAG3'
251	5'CTTCTGCAGCAGCATATAAA3'
252	5'GCTACTGCAGAAGGATTTGAA3'
253	5'TTCAAATCCTGCTGCAGTAGC3'
254	5'GCAGAAGGAGCTGAAATGAAT3'
255	5'CATTCAATTCAGCTCCTTCTG3'
263	5'TTTCTCGAGTTATTGTATCGCTACCAACTGACC3'
264	5'TTTCTCGAGTTAACTCCCAGTGCCTGTGCATGA3'
265	5'TTTCTCGAGTTAACGATACTTGCCTTGCATC3'
268	5'AAAAAGCTTAGAATGAAACAACCTGAAGAC3'
269	5'AAACTCGAGTCAGCGTTCCGCAACTAATTC3'
305	5'AAATCTAGAGGAATCCGGAATCTTTACCCA3'
306	5'AAATCTAGACTAGCACTGAGCAGCGTAATC3'
307	5'AAAGCTAGCAGAATGAAACAACCTGAAGAC3'
308	5'AAATCTAGAGCGTTCCGCAACTAATTTCTT3'
309	5'AAATCTAGATGCCGCGTAGCTTGATCGCTACCAA CTGACCTTGGG3'
314	5'CGTACAGTAGACAACCCCTACC3'
315	5'GGTAGGTTGTTACTGTACG3'
316	5'GCAAGAGGTCAGATGACACAGGCACTGGG3'
317	5'CCCAGTGCCTGTGCATCTGACCTCTTTC3'

MATERIALS AND METHODS

167	5'AAAGAGCTCTCAGGAGGATTTGATTAGAATTT3'
168	5'AAAGAGCTCTCATTGTTTGAAGCGGAGGATT3'
171	5'GCTAGCATGCATCATCATCATCACTCATCAAGTGC GGGTATCGGAGAATC3'
172	5'AAAGGTACCTTAATTCATTTCAAATCCTTCTGC3'
173	5'AAAGGTACCTTAAAAAGTTTCCTCGTCG3'

318	5'GCAACAAGACATGATGACCTGGGAATAAAC3'
319	5'GTTATTCCCAGGTCATCATGTCTTGTTC3'
320	5'AGAAAAACCGATGTTACCCAA3'
321	5'TTGGGTAACATCGGTTTTTCT3'

4.2.2 Oligonucleotides for homologous recombination in *S. cerevisiae*

53 (S2 Kar9)	5'GAGGGAGGATATATAAAAATGTATAAGTATACAGTTTTAGTTAGTATCAATCGATGAATTCGAG CTCG 3'
54 (S3 Kar9)	5'CACAGTTACTTTACCAAGAGAAGGGCGTTTAGATAAAACCCCAACTTATCGTACGCTGCAGGT CGAC 3'
68 (S1 Kar9)	5'CACGAATCTTTGTCTGTAACAGCCTTAAAGATTTAGTAGCACTGCCATGCGTACGCTGCAGTCC GAC 3'
69 (S1 Bim1)	5'CAGACTCAAAAGCAAGGATAATATTCCACCAAATCAGGGACGAAGCAATG CGTACGCTGCAGGTCGAC 3'
70 (S2 Bim1)	5'AAAAATAATACATATTCGAAAAACAATACTGCTTTTTAGTTCTCACTTAATCGATGAATTCGAGCT CG 3'

4.3 Plasmids

4.3.1 Plasmids for protein expression in *E. coli*

	Insert	Vector	Template	Primer	Enzyme	Reference
pDH001	Bim1 (FL)	pGEX-6P-1	Genomic DNA	3+12	BamHI/XhoI	This study
pDH003	Kar9 (FL)	pET28a-TEV	Genomic DNA	1+11	NheI/SacI	This study
pDH004	pFastBac1-GST	pFastBac1	pGEX6P-1	15+18	BamHI/NotI	This study
pDH005	pFastBac1 Bim1 (FL)	pFastBac1	Genomic DNA	3+12	BamHI/XhoI	This study
pDH008	pFastBac1 Kar9 (FL)	pFastBac1	Genomic DNA	16+17	NotI/XbaI	This study
pDH009	pDH004 Kar9(FL)	pDH004	Genomic DNA	16+17	NotI/XbaI	This study
pDH010	Bim1 (C-term) 182-282	pGEX-6P-1	Genomic DNA	19+21	BamHI/XhoI	This study
pDH011	Bim (C-term) 182-319	pGEX-6P-1	Genomic DNA	19+22	BamHI/XhoI	This study
pDH012	Bim1 (C-term) 182-344	pGEX-6P-1	Genomic DNA	19+12	BamHI/XhoI	This study
pDH013	Bim1 (C-term) 212-282	pGEX-6P-1	Genomic DNA	20+21	BamHI/XhoI	This study
pDH014	Bim1 (C-term) 212-319	pGEX-6P-1	Genomic DNA	20+22	BamHI/XhoI	This study
pDH015	Bim1 (C-term) 212-344	pGEX-6P-1	Genomic DNA	20+12	BamHI/XhoI	This study
pDH016	Kar9 (FL)	pGEX-6P-1	Genomic DNA	23+26	NotI/SalI	This study
pDH017	Kar9 (1-478)	pET28a-TEV	Genomic DNA	1+27	NheI/SacI	This study
pDH018	Kar9 (1-517)	pET28a-TEV	Genomic DNA	1+28	NheI/SacI	This study
pDH019	Kar9 (1-398)	pET28a-TEV	Genomic DNA	1+29	NheI/SacI	This study
pDH020	Kar9 (12-644)	pET28a-TEV	Genomic DNA	11+30	NheI/SacI	This study
pDH021	Kar9 (1-608)	pET28a-TEV	Genomic DNA	1+31	NheI/SacI	This study
pDH022	Kar9 (1-635)	pET28a-TEV	Genomic DNA	1+32	NheI/SacI	This study
pDH023	Kar9 (12-608)	pET28a-TEV	Genomic DNA	30+31	NheI/SacI	This study
pDH024	Kar9 (12-635)	pET28a-TEV	Genomic DNA	30+32	NheI/SacI	This study

MATERIALS AND METHODS

	Insert	Vector	Template	Primer	Enzyme	Reference
pDH025	Kar9 (10-644)	pET28a-TEV	Genomic DNA	11+33	NheI/SacI	This study
pDH026	Kar9 (7-644)	pET28a-TEV	Genomic DNA	11+34	NheI/SacI	This study
pDH027	Kar9 (5-644)	pET28a-TEV	Genomic DNA	11+35	NheI/SacI	This study
pDH028	Kar9 (1-640)	pET28a-TEV	Genomic DNA	1+36	NheI/SacI	This study
pDH029	Kar9 (1-637)	pET28a-TEV	Genomic DNA	1+37	NheI/SacI	This study
pDH030	Kar9 (10-640)	pET28a-TEV	Genomic DNA	33+36	NheI/SacI	This study
pDH031	Kar9 (10-637)	pET28a-TEV	Genomic DNA	33+37	NheI/SacI	This study
pDH032	Kar9 (7-640)	pET28a-TEV	Genomic DNA	34+36	NheI/SacI	This study
pDH033	Kar9 (7-637)	pET28a-TEV	Genomic DNA	34+37	NheI/SacI	This study
pDH034	Kar9 (5-640)	pET28a-TEV	Genomic DNA	35+36	NheI/SacI	This study
pDH035	Kar9 (5-637)	pET28a-TEV	Genomic DNA	35+37	NheI/SacI	This study
pDH036	Kar9 (10-635)	pET28a-TEV	Genomic DNA	33+32	NheI/SacI	This study
pDH037	Kar9 (7-635)	pET28a-TEV	Genomic DNA	34+32	NheI/SacI	This study
pDH038	Kar9 (5-635)	pET28a-TEV	Genomic DNA	35+32	NheI/SacI	This study
pDH043	ACR023W 1-769	pET28a-TEV	Genomic DNA	55+56	NheI/XhoI	This study
pDH044	ACR023W 1-769	pGEX-6P-1	Genomic DNA	56+57	EcoRI/XhoI	This study
pDH045	CAGLOA01155g 1-609	pET28a-TEV	Genomic DNA	58+59	NheI/XhoI	This study
pDH046	CAGLOA01155g 1-609	pGEX-6P-1	Genomic DNA	60+61	Sall/NotI	This study
pDH051	Bim1 (FL)	pETM40 with modified linker	Genomic DNA	3+12	BamHI/Xho1	This study
pDH052	Bim1 (C-term) 182-282	pETM40 with modified linker	Genomic DNA	19+21	BamHI/XhoI	This study
pDH061	Kar9 (245-644)	pET28a-TEV	Genomic DNA	103+11	NheI/SacI	This study
pDH062	Kar9 (250-644)	pET28a-TEV	Genomic DNA	104+11	NheI/SacI	This study
pDH063	Kar9 (298-644)	pET28a-TEV	Genomic DNA	105+11	NheI/SacI	This study
pDH064	Kar9 (307-644)	pET28a-TEV	Genomic DNA	106+11	NheI/SacI	This study
pDH065	Kar9 (245-644)	pGEX-6P-1	Genomic DNA	107+24	NotI/Sall	This study
pDH066	Kar9 (250-644)	pGEX-6P-1	Genomic DNA	108+24	NotI/Sall	This study
pDH067	Kar9 (298-644)	pGEX-6P-1	Genomic DNA	109+24	NotI/Sall	This study
pDH068	Kar9 (307-644)	pGEX-6P-1	Genomic DNA	110+24	NotI/Sall	This study
pDH069	Kar9 (1-307)	pET28a-TEV	Genomic DNA	1+135	NheI/SacI	This study
pDH070	Kar9 (1-338)	pET28a-TEV	Genomic DNA	1+136	NheI/SacI	This study
pDH071	Kar9 (1-451)	pET28a-TEV	Genomic DNA	1+137	NheI/SacI	This study
pDH072	Kar9 (1-307)	pGEX-6P-1	Genomic DNA	26+138	NotI/Sall	This study
pDH073	Bim1 (C-term) Δ241-253	pETM40 with modified linker	Genomic DNA	19, 21, 127, 129	BamHI/XhoI	This study
pDH075	Bim1 (FL) Δ241- 253	pETM40 with modified linker	Genomic DNA	3, 12 127, 129	BamHI/XhoI	This study
pDH076	Bim1 (FL) Δ241- 253	pETM40 with modified linker	Genomic DNA	3, 12, 128, 130	BamHI/XhoI	This study
pDH077	Kar9 (1-338)	pGEX-6P-1	Genomic DNA	26+139	NotI/Sall	This study
pDH078	Kar9 (1-355)	pGEX-6P-1	Genomic DNA	26+146	NotI/Sall	This study
pDH079	Kar9 (1-398)	pGEX-6P-1	Genomic DNA	26+140	NotI/Sall	This study
pDH080	Kar9 (1-451)	pGEX-6P-1	Genomic DNA	26+141	NotI/Sall	This study
pDH081	Kar9 (1-373)	pGEX-6P-1	Genomic DNA	26+147	NotI/Sall	This study
pDH082	Kar9 (1-429)	pGEX-6P-1	Genomic DNA	26+148	NotI/Sall	This study
pDH083	Kar9 (1-429)	pET28a-TEV	Genomic DNA	1+149	NheI/SacI	This study
pDH084	Kar9 (1-395)	pET28a-TEV	Genomic DNA	11+165	NheI/SacI	This study

MATERIALS AND METHODS

	Insert	Vector	Template	Primer	Enzyme	Reference
pDH085	Kar9 (1-401)	pET28a-TEV	Genomic DNA	11+166	NheI/SacI	This study
pDH086	Kar9 (1-404)	pET28a-TEV	Genomic DNA	11+167	NheI/SacI	This study
pDH087	Kar9 (1-408)	pET28a-TEV	Genomic DNA	11+168	NheI/SacI	This study
pDH089	Kar9 (10-395)	pET28a-TEV	Genomic DNA	33+165	NheI/SacI	This study
pDH090	Kar9 (12-395)	pET28a-TEV	Genomic DNA	30+165	NheI/SacI	This study
pDH091	Kar9 (10-398)	pET28a-TEV	Genomic DNA	33+29	NheI/SacI	This study
pDH092	Kar9 (12-398)	pET28a-TEV	Genomic DNA	30+29	NheI/SacI	This study
pDH093	Kar9 (10-401)	pET28a-TEV	Genomic DNA	33+166	NheI/SacI	This study
pDH094	Kar9 (12-401)	pET28a-TEV	Genomic DNA	30+166	NheI/SacI	This study
pDH095	Kar9 (FL) + Bim1(FL)	pET-Duet	Genomic DNA	174+175 (Kar9) 40+41 (Bim1)	Sall/NotI KpnI/XhoI	This study
pDH096	Kar9 (FL)-6xHis Bim1 (FL)	pFastBacDual	Genomic DNA	155+175 (Kar9) 79+172 (Bim1)	Sall/NotI KpnI/NheI	This study
pDH097	Kar9 (FL) Bim1 (FL)-6xHis	pFastBacDual	Genomic DNA	174+175 (Kar9) 171+173 (Bim1)	Sall/NotI KpnI/NheI	This study
pDH098	Kar9 (FL)-6xHis Bim1 (C-term)	pFastBacDual	Genomic DNA	155+175 (Kar9) 79+172 (Bim1)	Sall/NotI KpnI/NheI	This study
pDH099	Kar9 (FL) Bim1 (C-term)- 6xHis	pFastBacDual	Genomic DNA	174+175 (Kar9) 170+172 (Bim1)	Sall/NotI KpnI/NheI	This study
pDH123	Bim1 (FL) E214A	pETM40 with modified linker	Genomic DNA	3, 12, 198, 199	BamHI/XhoI	This study
pDH124	Bim1(FL) I215A	pETM40 with modified linker	Genomic DNA	3, 12, 200, 201	BamHI/XhoI	This study
pDH125	Bim1(FL) E216A	pETM40 with modified linker	Genomic DNA	3, 12, 202, 203	BamHI/XhoI	This study
pDH126	Bim1(FL) R217A	pETM40 with modified linker	Genomic DNA	3, 12, 204, 205	BamHI/XhoI	This study
pDH127	Bim1(FL) E218A	pETM40 with modified linker	Genomic DNA	3, 12, 206, 207	BamHI/XhoI	This study
pDH128	Bim1(FL) F219A	pETM40 with modified linker	Genomic DNA	3, 12, 208, 209	BamHI/XhoI	This study
pDH129	Bim1(FL) Y220A	pETM40 with modified linker	Genomic DNA	3, 12, 210, 211	BamHI/XhoI	This study
pDH130	Bim1(FL) F221A	pETM40 with modified linker	Genomic DNA	3, 12, 212, 213	BamHI/XhoI	This study
pDH131	Bim1(FL) N222A	pETM40 with modified linker	Genomic DNA	3, 12, 214, 215	BamHI/XhoI	This study
pDH132	Bim1(FL) K223A	pETM40 with modified linker	Genomic DNA	3, 12, 216, 217	BamHI/XhoI	This study
pDH133	Bim1(FL) L224A	pETM40 with modified linker	Genomic DNA	3, 12, 218, 219	BamHI/XhoI	This study
pDH134	Bim1(FL) R225A	pETM40 with modified linker	Genomic DNA	3, 12, 220, 221	BamHI/XhoI	This study
pDH135	Bim1(FL) D226A	pETM40 with modified linker	Genomic DNA	3, 12, 222, 223	BamHI/XhoI	This study
pDH136	Bim1(FL) I227A	pETM40 with modified linker	Genomic DNA	3, 12, 224, 225	BamHI/XhoI	This study
pDH137	Bim1(FL) E228A	pETM40 with modified linker	Genomic DNA	3, 12, 226, 227	BamHI/XhoI	This study
pDH138	Bim1(FL) I229A	pETM40 with modified linker	Genomic DNA	3, 12, 228, 229	BamHI/XhoI	This study
pDH139	Bim1(FL) H232A	pETM40 with modified linker	Genomic DNA	3, 12, 230, 231	BamHI/XhoI	This study

MATERIALS AND METHODS

	Insert	Vector	Template	Primer	Enzyme	Reference
pDH141	Bim1(FL) T275A	pETM40 with modified linker	Genomic DNA	3, 12, 250, 251	BamHI/XhoI	This study
pDH142	Bim1(FL) E277A	pETM40 with modified linker	Genomic DNA	3, 12, 252, 253	BamHI/XhoI	This study
pDH143	Bim1(FL) F279A	pETM40 with modified linker	Genomic DNA	3, 12, 253, 254	BamHI/XhoI	This study
pDH151	Bim1 (C-term) E214A	pETM40 with modified linker	Genomic DNA	19, 21, 198, 199	BamHI/XhoI	This study
pDH152	Bim1 (C-term) E218A	pETM40 with modified linker	Genomic DNA	19, 21, 206, 207	BamHI/XhoI	This study
pDH153	Bim1 (C-term) F219A	pETM40 with modified linker	Genomic DNA	19, 21, 208, 209	BamHI/XhoI	This study
pDH154	Bim1 (C-term) Y220A	pETM40 with modified linker	Genomic DNA	19, 21, 210, 211	BamHI/XhoI	This study
pDH155	Bim1 (C-term) F221A	pETM40 with modified linker	Genomic DNA	19, 21, 212, 213	BamHI/XhoI	This study
pDH156	Bim1 (C-term) K223A	pETM40 with modified linker	Genomic DNA	19, 21, 216, 217	BamHI/XhoI	This study
pDH157	Bim1 (C-term) R225A	pETM40 with modified linker	Genomic DNA	19, 21, 220, 221	BamHI/XhoI	This study
pDH158	Bim1 (C-term) I227A	pETM40 with modified linker	Genomic DNA	19, 21, 224, 225	BamHI/XhoI	This study
pDH159	Bim1 (C-term) E228A	pETM40 with modified linker	Genomic DNA	19, 21, 226, 227	BamHI/XhoI	This study
pDH160	Bim1 (1-187)	pETM40 with modified linker	Genomic DNA	3, 263	BamHI/XhoI	This study
pDH161	Bim1 (1-154)	pETM40 with modified linker	Genomic DNA	3, 264	BamHI/XhoI	This study
pDH162	Bim1 (1-124)	pETM40 with modified linker	Genomic DNA	3, 265	BamHI/XhoI	This study
pDH163	Bim1 (1-187) GCN4	pETM40 with modified linker	Genomic DNA	3, 270 (Bim1) 268, 269 (GCN4)	BamHI/XhoI/ HindIII	This study
pDH164	Bim1 (1-154) GCN4	pETM40 with modified linker	Genomic DNA	3, 271 (Bim1) 268, 269 (GCN4)	BamHI/XhoI/ HindIII	This study
pDH165	Bim1 (1-124) GCN4	pETM40 with modified linker	Genomic DNA	3, 272 (Bim1) 268, 269 (GCN4)	BamHI/XhoI/ HindIII	This study
pDH178	Bim1(FL) S133D	pETM40 with modified linker	Genomic DNA	3, 12, 314, 315	BamHI/XhoI	This study
pDH179	Bim1 (FL) S143D S144D	pETM40 with modified linker	Genomic DNA	3, 12, 316, 317	BamHI/XhoI	This study
pDH180	Bim1 (FL) S160D S161D	pETM40 with modified linker	Genomic DNA	3, 12, 318, 319	BamHI/XhoI	This study
pDH181	Bim1 (FL) S171D	pETM40 with modified linker	Genomic DNA	3, 12, 320, 321	BamHI/XhoI	This study

4.3.2 Plasmids for protein expression in *S. cerevisiae*

	Insert	Vector	Template	Primer	Enzyme	Reference
pDH112-Gal1	<i>GAL1</i> Kar9 (S197A)-9xmyc	pRS403	Genomic DNA	91, 92, 178, 181	XbaI, Sall	This study
pDH113-Gal1	<i>GAL1</i> Kar9 (S496A)-9xmyc	pRS403	Genomic DNA	93, 94, 178, 181	XbaI, Sall	This study
pDH114-Gal1	<i>GAL1</i> Kar9 (S197A;S296A)-9xmyc	pRS403	pDH113-Gal1	91, 92, 178, 181	XbaI, Sall	This study
pDH115-Gal1	<i>GAL1</i> Kar9 (K301R)-9xmyc	pRS403	Genomic DNA	95, 96, 178, 181	XbaI, Sall	This study
pDH119-Gal1	<i>GAL1</i> Kar9 (K301R;K381R)-9xmyc	pRS403	pDH115-Gal1	101, 102, 178, 181	XbaI, Sall	This study
pDH120-Gal1	<i>GAL1</i> Kar9 (K301R;K381R;K529R)-9xmyc	pRS403	pDH119-Gal1	103, 104, 178, 181	XbaI, Sall	This study
pDH121-Gal1	<i>GAL1</i> Kar9 (K301R;K381R;K529R;K3333R)-9xmyc	pRS403	pDH121-Gal1	97, 98, 178, 181	XbaI, Sall	This study
pDH122-Gal1	<i>GAL1</i> Kar9 (WT)-9xmyc	pRS403	Genomic DNA	176, 177 (Promotor); 178, 181 (Kar9); 184, 185 (Terminator) 186, 187 (Myc-Tag)	ApaI, XbaI (Promotor) XbaI, Sall (Kar9) NotI, SacI (Terminator) Sall, NotI (Myc-Tag)	This study
pDH172	Gal1-Kar9 (K333R)	pRS403	Genomic DNA	97, 98, 178, 181	XbaI, Sall	This study
pDH173	Gal1-Kar9 (K333E)	pRS403	Genomic DNA	99, 100, 178, 181	XbaI, Sall	This study
pDH174	Gal1-Kar9 (K381R)	pRS403	Genomic DNA	101, 102, 178, 181	XbaI, Sall	This study
pDH175	Gal1-Kar9 (K529R)	pRS403	Genomic DNA	103, 104, 178, 181	XbaI, Sall	This study
pDH185	Bim1 (1-187 GCN4)-HA	pRS405	Genomic DNA	237, 305, 306, 307, 308, 309	HindIII, XbaI (Bim1) NheI, XbaI (GCN4), XbaI (HA-Tag)	This study
pDH188	Bim1 (FL)	pRS405	Genomic DNA	237, 238, 239, 240, 241, 242	HindIII, EcoRI (Bim1) XbaI (HA-Tag)	This study
pDH189	Bim1 (FL) E214A	pRS405	pDH189	198, 199	Quickchange (Stratagene)	This study
pDH190	Bim1 (FL) R217A	pRS405	pDH189	204, 205	Quickchange (Stratagene)	This study
pDH191	Bim1 (FL) F219A	pRS405	pDH189	208, 209	Quickchange (Stratagene)	This study
pDH192	Bim1 (FL) F221A	pRS405	pDH189	212, 213	Quickchange (Stratagene)	This study
pDH193	Bim1 (FL) E228A	pRS405	pDH189	226, 227	Quickchange (Stratagene)	This study
pDH194	Bim1 (FL) I229A	pRS405	pDH189	228, 229	Quickchange (Stratagene)	This study

4.4 *E. coli* strains

Strain	Essential genotype	Source
XL-1 blue	<i>recA endA1 gyrA96 thi-1 hsdR17 supE44 relA1 lac</i> [F' <i>proAB lac^f ZΔM15 Tn10 (Tet^r)</i>]	Stratagene (La Jolla, USA)
BL21 Star (DE3)	F- <i>ompT hsdSB (rB-mB-) gal dcm me131</i> (DE3)	Invitrogen (Karlsruhe, Germany)
B834 (DE3)	F- <i>ompT gal met rBmB</i>	Novagen; Schwalbach, Germany
Rosetta (DE3) pLysS	F- <i>ompT hsdS_B (rB_B-mB_B-) gal dcm</i> (DE3) pLysSRARE (Cam ^R)	Novagen; Schwalbach, Germany

4.5 *S. cerevisiae* strains

Strain	Essential Genotype	Reference
YDH001	MATa; <i>his3Δ1; leu2Δ0; met15Δ0; ura3Δ0; Kar9-9xmyc::HIS3</i>	this study
YDH002	MATa; <i>his3Δ 1; leu2Δ 0; met15Δ 0; ura3Δ 0; Δkar9::ClonNat</i>	this study
YDH003	MATa; <i>his3Δ1; leu2Δ0; met15Δ0; ura3Δ0; Δkar9::ClonNat; pDH112-Gal1::HIS3</i>	this study
YDH004	MATa; <i>his3Δ 1; leu2Δ 0; met15Δ 0; ura3Δ 0; Δkar9::ClonNat; pDH113-Gal1::HIS3</i>	this study
YDH005	MATa; <i>his3Δ1; leu2Δ0; met15Δ0; ura3Δ0; Δkar9::ClonNat; pDH114-Gal1::HIS3</i>	this study
YDH006	MATa; <i>his3Δ 1; leu2Δ 0; met15Δ 0; ura3Δ 0; Δkar9::ClonNat; pDH115-Gal1::HIS3</i>	this study
YDH007	MATa; <i>his3Δ1; leu2Δ0; met15Δ0; ura3Δ0; Δkar9::ClonNat; pDH119-Gal1::HIS3</i>	this study
YDH008	MATa; <i>his3Δ 1; leu2Δ 0; met15Δ 0; ura3Δ 0; Δkar9::ClonNat; pDH120-Gal1::HIS3</i>	this study
YDH009	MATa; <i>his3Δ1; leu2Δ0; met15Δ0; ura3Δ0; Δkar9::ClonNat; pDH121-Gal1::HIS3</i>	this study
YDH010	MATa; <i>his3Δ 1; leu2Δ 0; met15Δ 0; ura3Δ 0; Δkar9::ClonNat; pDH122-Gal1::HIS3</i>	this study
YDH011	MATa; <i>ura3-52; trp1Δ2; leu2-3; his3-11; ade2-1; can1-100; Δbim1::ClonNat</i>	this study
YDH012	MATa; <i>ura3-52; trp1Δ2; leu2-3,112; his3-11; ade2-1; can1-100; Δbim1::ClonNat; pDH189::LEU2</i>	this study
YDH013	MATa; <i>ura3-52; trp1Δ2; leu2-3; his3-11; ade2-1; can1-100; Δbim1::ClonNat; pDH190::LEU2</i>	this study
YDH014	MATa; <i>ura3-52; trp1Δ2; leu2-3,112; his3-11; ade2-1; can1-100; Δbim1::ClonNat; pDH191::LEU2</i>	this study
YDH015	MATa; <i>ura3-52; trp1Δ2; leu2-3; his3-11; ade2-1; can1-100; Δbim1::ClonNat; pDH192::LEU2</i>	this study
YDH016	MATa; <i>ura3-52; trp1Δ2; leu2-3,112; his3-11; ade2-1; can1-100; Δbim1::ClonNat; pDH193::LEU2</i>	this study
YDH017	MATa; <i>ura3-52; trp1Δ2; leu2-3; his3-11; ade2-1; can1-100; Δbim1::ClonNat; pDH194::LEU2</i>	this study
YDH018	MATa; <i>his3Δ1; leu2Δ0; met15Δ0; ura3Δ0; Δkar9::ClonNat; pDH172-Gal1::HIS3</i>	this study
YDH019	MATa; <i>his3Δ1; leu2Δ0; met15Δ0; ura3Δ0; kar9::ClonNat; pDH173-Gal1::HIS3</i>	this study
YDH020	MATa; <i>his3Δ1; leu2Δ0; met15Δ0; ura3Δ0; Δkar9::ClonNat; pDH174-Gal1::HIS3</i>	this study
YDH021	MATa; <i>his3Δ1; leu2Δ0; met15Δ0; ura3Δ0; kar9::ClonNat; pDH175-Gal1::HIS3</i>	this study
YDH028	MATa; <i>ura3-52; trp1Δ2; leu2-3,112; his3-11; ade2-1; can1-100; Δbim1::ClonNat; pDH185::LEU2</i>	this study
YDH030	MATa; <i>ura3-52; trp1Δ2; leu2-3; his3-11; ade2-1; can1-100; Δbim1::ClonNat; pDH188::LEU2</i>	this study

4.6 Media for *E. coli* and *S. cerevisiae*

Medium	Composition	Purpose
LB medium	1 % (w/v) bacto tryptone, 0.5 % (w/v) bacto yeast extract, 0.5 % (w/v) NaCl (+1.5 % (w/v) agar and /or for plates)	Growth medium for <i>E. coli</i>
DH10Bac	1 % (w/v) bacto tryptone, 0.5 % (w/v) bacto yeast extract, 0.5 % (w/v) NaCl, 7 mg/mL gentamycin, 10 mg/mL tetracycline, 50 mg/mL kanamycin for plates + 1.5 % (w/v) agar, 1 M IPTG, 100 µg/mL bromo-chloro-galactopyranoside (X-Gal),	Medium growth of DH10Bac
SOC	2 % (w/v) bacto tryptone, 0.5 % (w/v) bacto yeast extract, 10 mM NaCl, 2.5 mM KCl, 10 mM MgCl ₂ , 10 mM MgSO ₄ , pH 7.0	Medium for regeneration of DH10Bac after transformation
Minimal Medium	7,5 mM (NH ₄) ₂ SO ₄ , 8,5 mM NaCl, 55 mM KH ₂ PO ₄ , 100 mM K ₂ HPO ₄ , 1 mM MgSO ₄ , 20 mM glucose, 1 mg/l CaCl ₂ , 1 mg/l FeCl ₂ , 1 µg/l of the following trace element: Cu ²⁺ ; Mn ²⁺ ; Zn ²⁺ ; MoO ₄ ²⁻ , 1 mg/l Thiamine, 1 mg/l Biotin, 100 mg/l of the following amino acids (L-alanine, L-arginine, L-aspartic acid, L-cysteine, L-glutamate, L-glycine, L-histidine, L-isoleucine, L-leucine, L-lysine, L-phenylalanine, L-proline, L-serine, L-threonine, L-tyrosine, L-valine, SeMet)	Medium for expression of L-selenomethionine labeled proteins
YPD medium	1 % (w/v) yeast extract, 2 % (w/v) bacto peptone, 2 % (w/v) glucose (+2 % (w/v) agar for plates)	Growth medium for <i>S. cerevisiae</i>
Synthetic Complete (SC) medium	0.67 % (w/v) yeast nitrogen base (w/o amino acids), 2 % (w/v) glucose, 0.06 % (w/v) dropout mix (includes all essential amino acids and nucleobases except the amino acids or nucleobases used as auxotrophy markers, i.e. histidine, leucine, uracil, tryptophane)	Selective growth medium for <i>S. cerevisiae</i>

4.7 Antibodies

Primary antibody (AB)	Source	Dilution / Application	Supplier
anti-HA (3F10)	rat	1:1000 / Western Blot	Roche Applied Science (Mannheim, Germany)
anti-myc (9E10)	mouse	1:1000 / Western Blot	Roche Applied Science (Mannheim, Germany)
anti-myc (9E11)	mouse	100 µg AB coupled to 250 µl protein-G beads / Co-IP	Acris Antibodies (Herford, Germany)

Secondary antibody	Source	Dilution / Application	Supplier
anti-mouse-IgG-HRPO	goat	1:3000 / Western	BioRad (Munich, Germany)
anti-rat-IgG-HRPO	rabbit	1:10000 / Western	Abcam (Cambridge, USA)

4.8 General buffers and solutions

	Application	Composition
4x stacking gel buffer	SDS-PAGE	0.5M Tris, 0.4% (w/v) SDS, pH 6.8
4x resolving gel buffer	SDS-PAGE	3 M Tris, 0.4% (w/v) SDS, pH 8.5
running buffer	SDS-PAGE	0.5 M Tris, 1 % (w/v) SDS, 1.9 M glycine
4x loading dye	SDS-PAGE	110 mM Tris/HCl pH 6.8, 40 % (v/v) glycerol, 0.5 % (w/v) bromophenol blue, 4 % (w/v) SDS, 40 mM DTT
Coomassie staining solution	SDS-PAGE	50 % (v/v) ethanol, 7 % (v/v) acetic acid, 0.2 % Coomassie Brilliant blue R-250
4x stacking gel buffer	Native PAGE	0.5M Tris pH 6.8
4x resolving gel buffer	Native PAGE	1.5M Tris pH 8.9
running buffer	Native PAGE	0.1 M Tris, 0.35 M Glycine, pH 8.9
5x loading dye	Native PAGE	50 % (v/v) glycerol, 0.5 M Tris pH 6.8, 0.5 % (w/v) Bromphenolblue
1x TBE	Agarose gel electrophoresis	8.9 mM Tris, 8.9 mM boric acid, 2 mM EDTA (pH 8.0)
1x TE	DNA	10 mM Tris pH 7.5, 1 mM EDTA
1x TBS	Agarose gel electrophoresis	500 mM Tris pH 7.5, 1.5 M NaCl
6x loading dye	Agarose gel electrophoresis	1.5 g/l bromophenol blue, 1.5 g/l xylene cyanol, 50% (v/v) glycerol
HU-buffer	Western blotting	8 M urea, 5% SDS, 200 mM Tris pH 8.8, 1 mM EDTA, 1.5% DTT, 0.01 % bromophenol blue
10x transfer buffer	Western blotting	10 mM NaHCO ₃ , 3 mM NaCO ₃
1x TBS-T	Western blotting	10 mM Tris pH 8.0, 150 mM NaCl, 0.05 % Tween 20
1x PBS	Western blotting	2 mM KH ₂ PO ₄ , 4 mM Na ₂ HPO ₄ , 140 mM NaCl, 3 mM KCl, pH 7.4

4.9 Molecular Biology

4.9.1 Cloning

Genes of interest were cloned according to the standard methods for molecular biology (Sambrook and Russell 2001). This includes amplification of DNA fragments by polymerase chain reaction, restriction digest of DNA, separation of DNA-fragments by agarose gel electrophoresis and ligation of DNA fragments. DNA-fragments were purified using the Nucleospin Extract II Kit (Macherey & Nagel, Düren, Germany). Restriction enzymes and buffers were used according to the manufacturer's instructions. Digested Plasmid-DNA was additionally treated with alkaline phosphatase (FastAP, Fermentas, St. Leon-Roth, Germany). Point mutations were introduced using either the QuickChange II Site-Directed Mutagenesis Kit (Agilent Technologies, Waldbronn, Germany) or by PCR-based site-directed mutagenesis (Ho, Hunt et al. 1989). Cloning strategies for all plasmids used in this study and the sequences of the corresponding oligonucleotides are described in chapter 4.3 and in chapter 4.2, respectively.

4.9.2 Transformation of *E. coli* and isolation of plasmid DNA

Transformation-competent *Escherichia coli* (*E. coli*) cells were prepared and transformed according to the standard chemical methods (Hanahan 1983). Isolation of plasmid DNA from *E. coli* cells was performed using the NucleoSpin-Plasmid from Macherey-Nagel (Düren,

Germany). Plasmid-DNA was sequenced by GATC-Biotech (Konstanz, Germany) or by Eurofins-MWG (Ebersberg, Germany).

4.9.3 Transformation of *S. cerevisiae*

Genes of interest were deleted or tagged using a PCR-based method (Janke, Magiera et al. 2004). Plasmids harbouring mutations in *BIM1* or *KAR9* were linearised with NheI (pRS403) or AflII (pRS405) prior transformation to allow for homologous recombination in the *HIS3* or *LEU2* locus. Yeast cells were transformed using the lithiumacetate-method (Knop et al., 1999). After transformation, the cells were either resuspended in sterile PBS and plated directly on SC-plates lacking the respective amino acids or for antibiotic selection, the cells were resuspended in 2 ml of YPD-medium and incubated at 30°C on a shaker for at least 5-6 h before plating. Transformants were incubated on plates for 2 days, and then streaked as single colonies on fresh selection plates. Positive clones were identified by western-blot analysis using TCA-extracts (chapter 4.14.1) or by colony-PCR (chapter 4.9.5).

4.9.4 Isolation of genomic DNA from *S. cerevisiae*

Cells from a stationary 5ml culture were sedimented, washed once with 0.5ml ddH₂O and resuspended in 200 µl breaking buffer (2 % (v/v) Triton X-100, 1 % (v/v) SDS, 100 mM NaCl, 10 mM Tris-HCl pH 8.0, 1 mM EDTA pH 8.0). After addition of 200 µl phenol/chloroform/isoamyl alcohol (24:24:1) and 200 µl of glass beads (Ø ~ 0.5 mm), the mixture was vortexed vigorously for 3 - 4 min. Subsequently, 400 µl of TE buffer were added and the mixture was gently vortexed. After centrifugation for 5 min at 14000 rpm at room temperature, the aqueous phase was transferred to a new reaction tube and the DNA was precipitated by the addition of 1 ml of 96 % ethanol, following centrifugation for 3 min at 14000 rpm at room temperature. The pellet was resuspended in 200 µl 10 mM Tris pH 8.5 and RNA was digested by the addition of 7 µl RNase A and incubation at 37°C for 15 min. To precipitate again the DNA 20 µl of 4 M ammonium acetate and 500 µl of 96 % ethanol were added, gently mixed and centrifuged for 3 min at 14000 rpm at room temperature. The pellet was air dried and resuspended in 50 µl 10 mM Tris pH 8.5. A 5 µl sample was taken and analysed on an agarose gel.

4.9.5 Colony PCR for *S. cerevisiae*

Colony PCR to verify the correct insertion of a PCR cassette was either performed with the respective primers on isolated chromosomal DNA or with whole yeast cells. For the second method, yeast cells from a freshly streaked plate were scraped off with a pipette tip (amount ~ size of a pinhead) and resuspended in 50 µl 0,01 % sarkosyl + 0.2 N NaOH. The mixture

was incubated at 95 °C for 10 min to disrupt the cells. 0.5 µl of the yeast-cell suspension was taken to perform a colony PCR with the standard protocol (chapter 4.9.1).

4.10 Methods for protein analysis

4.10.1 Protein separation by SDS-PAGE

Protein samples were analysed by sodium dodecylsulfate polyacrylamide gel electrophoresis (SDS-PAGE) as described (Laemmli, 1970). Electrophoretic separation was achieved on 8 – 19 % polyacrylamid gels depending on the size of the protein. The gels were either stained with coomassie-blue staining solution (see chapter 4.8) or with a silver stain kit (Pierce by Thermo Fisher Scientific, Bonn, Germany) or further used for western blot analysis. After coomassie-blue staining the gels were destained with water.

4.10.2 Protein separation by native PAGE

To analyse proteins in their native state, e.g. after incubation with heavy atoms or after methylation, a native PAGE was carried out. For the analysis of Bim1p (C-term) after incubation with different heavy atoms, a 10% native PAGE resolving gel with a 4% stacking gel was prepared. The loading dye was added to the samples and the samples were immediately loaded on the gel in the cold-room. Electrophoretic separation was performed for ~ 1 h at 230 V in the cold-room. Gels were stained with coomassie-blue staining solution.

4.10.3 Western blotting

After protein separation by SDS-PAGE, proteins were transferred onto a PVDF membrane for 2 h at 60 V (Power Pac 300, Bio Rad, Munich, Germany) and 4°C using the wet-blot method. After transfer, the membrane was blocked in TBS-T (chapter 4.8) with 10 % (w/v) milk powder. Then the membrane was added to the primary antibody (diluted in 1x PBS containing 2 % milk (w/v) powder) and incubated for 2 h or overnight at 4 °C. The membrane was washed three times with TBS-T and subsequently incubated with the secondary antibody (diluted in 1x TBS-T containing 2 % milk powder) for 1 h at room temperature. Six washing steps with TBS-T removed unbound antibody. Visualisation of the immuno-stained proteins was achieved using the Pierce ECL substrate (Pierce by Thermo Fisher Scientific, Bonn, Germany). The membrane was then exposed to light-sensitive films (GE Healthcare, Munich, Germany), which were subsequently developed with a Kodak Xomat M35 developing machine. For quantification of the signals, ECL-treated (SuperSignal West Dura Extended Duration Substrate, Pierce by Thermo Fisher Scientific, Bonn, Germany) membranes were directly analyzed with the LAS-3000 mini imaging system (FUJIFILM, Düsseldorf, Germany) and quantification of the signals was done using the Multi-Gauge software.

4.10.4 Dynamic Light Scattering

Dynamic Light Scattering (DLS) is used to determine the hydrodynamic diameter and the size distribution of particles in solution. This technique was used to find appropriate buffer conditions for small angle X-ray scattering (SAXS) experiments. After centrifugation for 20 min at 13200 rpm and 4°C, a sample of 50 µl of the respective sample was transferred into a fluorescence ultra-micro cuvette and measured at 20 °C in an 802 DLS spectrometer (Viskotech Corp., Houston, USA). This way, purified Bim1p and Kar9p fragments in various buffers and different salt concentrations were tested at a concentration range of 1-7.5 mg/ml for concentration-dependent oligomerisation or aggregation. Each sample was measured ten times for 4 s each and the data were analysed with the OmniSIZE 3.0 software.

4.10.5 Small angle X-ray scattering (SAXS)

SAXS data were collected at the ID14-3 beamline (ESRF, Grenoble, France). Bim1p (FL), Bim1p (C-term) and Kar9p (FL) were measured in different buffers and concentrations (see table below). Scattering curves were measured with exposure times of ten times 30 seconds. Before and after each measurement, a blank measurement with sample buffer was taken. For the determination of molecular masses (Mylonas and Svergun 2007), the reference proteins bovine serum albumine (4.5 mg/ml) and lysozyme (9.4 mg/ml and 2.4 mg/ml) were measured in buffer containing 50 mM HEPES (pH 7.5) and 2 mM DTT. Data were evaluated and processed with different programs from the ATSAS 2.1 software package (Konarev, Petoukhov et al. 2006). Primary analysis of the data was done with PRIMUS (Konarev, Volkov et al. 2003). To calculate the radius of gyration R_g , the Guinier approximation was used with the constraint $s \cdot R_g < 1.3$ (Guinier 1955). The indirect transform package GNOM was used to compute the pair-distribution function $p(r)$ and the maximum dimension of the particle D_{max} . *Ab initio* models of Bim1p (C-term) were calculated with the program DAMMIN assuming P2-symmetry (Svergun, Barberato et al. 1995; Svergun 1995). Theoretical scattering curves of the Bim1p (C-term) crystal structure were calculated with the program CRY SOL (Svergun, Petoukhov et al. 2001).

Buffer	Bim1p (C-term)	Bim1p (FL)
10 mM Hepes pH 7.5; 500 mM NaCl; 1 mM EDTA; 1 mM DTT	1.0, 1.9, 4.4 mg/ml	
10 mM Sodiumphosphate pH 7.5; 500 mM NaCl; 1 mM EDTA; 1 mM DTT	2.4 mg/ml	
10 mM Sodiumphosphate pH 7.5; 150 mM NaCl; 1 mM EDTA; 1 mM DTT	2.0, 4.6, 4.9 mg/ml	
10 mM Hepes pH 7.5; 500 mM NaCl; 1 mM EDTA; 1 mM DTT; 5 % Glycerol		1.3 mg/ml
Buffer	Kar9p (FL)	
10 mM Tris pH 7.5; 500 mM NaCl; 1 mM EDTA; 1 mM DTT	2.38; 4.88 mg/ml	

4.10.6 Limited proteolysis

Different proteases (endoproteinase Glu-C, endoproteinase Lys-C, trypsin or chymotrypsin) were added to protein samples in varying ratios (50:1, 100:1, 20:1 w/w) and incubated at room temperature or on ice. Samples of 10 μ l were taken at time points 0 s, 30 s, 1 min, 2 min, 5 min, 10 min, 30 min, 60 min, 90 min and the reaction was immediately stopped by the addition of 3 μ l 4x loading dye. Protein fragments were separated on a SDS-PAGE and clearly visible bands were cut out, blotted on a PVDF membrane via passive adsorption and subjected to Edman sequencing (Messer et al., 1997). To determine the mass of the protein fragments, a second sample was prepared as described above, but instead of adding loading dye, the sample was flash frozen in liquid nitrogen and subjected to mass-spectrometric analysis.

4.10.7 Pull-down assays

Cells from logarithmically growing yeast cultures were lysed by vortexing with glass beads (4x3 min) in lysis buffer (50mM Tris-HCl pH 7.5; 300mM NaCl; 5% glycerol; 0.2% Triton-X-100; 1mM DTT). Cell debris was removed by centrifugation (13200 rpm, 20 min) and the clear supernatant subsequently used for pull-down experiments. Equimolar amounts of each analysed protein were incubated with equal amounts of yeast extract and 50 μ l of amylose resin (NEB) for 20 min in lysis buffer. After incubation, the amylose resin was washed five times with 1ml lysis buffer. Bound proteins were eluted with 35 μ l of elution buffer (lysis buffer + 10mM maltose) and 1/3 of the elution volume was analysed by western blotting with myc-antibody.

4.11 Protein expression and Purification

4.11.1 Recombinant protein expression in *E. coli*

Different fragments of Kar9p- and Bim1p-fusion proteins were recombinantly expressed in *E. coli* BL21 Star (DE3) or Rosetta cells. Cells were grown at 37 °C in LB medium with the appropriate antibiotics to an OD₆₀₀ of 0.4-0.6 and then cooled down to 18 °C. Protein expression was induced by the addition of 0.25 mM IPTG. After further incubation at 18 °C for 12-16 hours, the cells were harvested by centrifugation at 4 °C. Cell pellets were resuspended in the appropriate lysis buffer, flash frozen in liquid nitrogen, and stored at -80 °C.

4.11.2 Selenomethionine labeling of proteins

L- selenomethionine (SeMet) labeled protein was expressed with the *E. coli* strain B834 (DE3). Cells were grown in minimal medium, containing SeMet identical to the procedure described above (see chapter 4.11.1).

4.11.3 Recombinant protein expression in *S. cerevisiae*

For expression of myc-tagged Kar9p, cells were streaked on SC-His- plates. 50 ml of YPD were used to inoculate a culture over night at 30°C. The next morning, the culture was diluted in 1.5l of YPD and the cells were grown at 30°C until mid-logarithmic phase. For overexpression of Kar9p, cells were grown in YP + raffinose until OD₆₀₀ of 1 and protein expression was induced by addition of 20 % galactose (final concentration 2 %) for 3-4 h at 30°C.

4.11.4 Recombinant protein expression in insect cells

To express recombinant proteins in insect cells, the Bac-to-Bac baculovirus expression system (Ciccarone et al., 1998) was used according to the manufacturer's instructions (Invitrogen, Karlsruhe, Germany). The genes of interest were cloned into pFastBac1-GST (pDH004, this study), pFastBac1, pFastBacDual or pFastBac-28 (kind gift from AG Hopfner, Gene Centre Munich). The plasmids were amplified in XL-1 Blue cells and isolated using the NucleoSpin Plasmid Kit (Macherey & Nagel, Düren, Germany). To generate recombinant bacmid DNA, the plasmids were transformed into DH10Bac *E.coli* cells (Luckow et al., 1993). After the heat-shock at 42°C and incubation on ice for 3 min, the cells were incubated in 1 ml of SOC medium for 6 h at 37°C. To select the right transformants, a blue-white selection was carried out on agar plates at 37°C for 48 h. Single white colonies were picked from the plate and incubated over night at 37°C in 5 ml LB-medium containing 7 mg/mL gentamycin, 10 mg/mL tetracycline and 50 mg/mL kanamycin. Recombinant bacmid DNA was isolated with the buffers from the NucleoSpin Plasmid Kit (Macherey & Nagel, Düren, Germany), but the DNA was precipitated with isopropanol instead of purification via the provided columns. Sf9 and High Five insect cells were transfected using 2 µg recombinant bacmid DNA and 3 µl FuGeneHD reagent (Roche, Basel, Switzerland). 300 µl of medium were incubated for 45 min at room temperature with the transfection reagent and the bacmid DNA: Cells were diluted to 0.4 million/ml and 2 ml of cell suspension were transferred to each well of a 6-well plate. After incubation of the cells at 27.5°C for 30 min, the transfection mix was added. Transfected cells were incubated at 27.5°C for 3-4 days and inspected regularly for signs of infection. When cells showed signs of infection, the medium was recovered and centrifuged (10 min, 3000 rpm) and the supernatant (P0 virus) filter sterilised and stored at 4°C. The virus was amplified in 10 ml cell culture (1 million cells/ml) by adding 1 ml of the P0 virus and incubation for 3-4 days at 27.5°C. Regular inspection and counting of the cells was performed until the cells stopped growing. To collect the virus, the culture was centrifuged (10 min, 3000rpm) and the supernatant (P1 virus) filter sterilised and stored at 4°C. To generate P2 virus, the whole procedure was repeated with 250 ml of cells (0.4 million/ml) and 0.5 ml of P1 virus. For protein expression 1 l of High Five cell culture (1 million cells/ml) was

infected with 20 – 50 ml of P2 virus and incubated at 27.5°C for 3 days. Cells were harvested by centrifugation (15 min, 3000 rpm) and frozen in liquid nitrogen. Protein expression was verified by SDS-PAGE.

4.11.5 Purification of recombinant His-tagged Kar9p

His-tagged Kar9p was either expressed in *Escherichia coli* or in insect cells. Cells were harvested by centrifugation and the pellet was resuspended in lysis buffer. *E. coli* cells were lysed by sonication whereas insect cells were lysed by the addition of 1 % NP40 to the lysis buffer and stirring in a beaker for 30 min at 4 °C, followed by short sonication. Cell debris was removed by centrifugation (15000 rpm, 30 min, 4°C, SS34 rotor). The lysate from insect cells was additionally filtered through a 0.2 µm syringe filter unit (Millex-FG, Millipore, Schwalbach, Germany). The lysate was loaded onto a pre-equilibrated 5 ml His-Trap FF column (GE Healthcare, Munich). Subsequently, the column was washed with 10 column volumes of wash buffer, and the protein eluted in a stepwise gradient with elution buffer (5 column volumes 75 mM imidazole, linear gradient from 150 mM to 500 mM imidazole for 5 column volumes). Peak fractions were analysed by SDS-PAGE, pooled and diluted with storage buffer (only for Kar9p (FL)). The solution was subsequently loaded onto a pre-equilibrated HiTrap-Q column (GE Healthcare, Munich), to remove contaminating DNA; Kar9p itself does not bind to the HiTrap-Q column. The flow-through was concentrated with centrifugal filter devices (Amicon Ultra, Millipore, Billerica, US) and loaded onto a Superdex S200 16/60 size exclusion chromatography column equilibrated with gel filtration buffer. Peak fractions were again analysed by SDS-PAGE and concentrated. The purified protein was subsequently used for crystallisation experiments.

lysis buffer	50 mM Sodiumphosphate pH 7.5; 500 mM NaCl; 5 mM imidazole; 1 mM DTT
wash buffer	50 mM Sodiumphosphate pH 7.5; 1 M NaCl; 50 mM imidazole; 1 mM DTT
elution buffer	50 mM Sodiumphosphate pH 7.5; 500 mM NaCl; 500 mM imidazole; 1 mM DT
storage buffer	50 mM Sodiumphosphate pH 7.5; 100 mM NaCl; 50 mM Glutamic acid; 50 mM Arginine; 5 % Glycerol; 1 mM DTT
gelfiltration buffer	10 mM Tris-HCl pH 7.5; 200 mM NaCl; 1 mM EDTA; 1 mM DTT

4.11.6 Purification of recombinant GST-tagged Kar9p

GST-tagged Kar9p variants were expressed in *Escherichia coli* and insect cells as described above (chapter 4.11.1 and 4.11.4). The cells were harvested by centrifugation and resuspended in lysis buffer. After lysis of the cells by sonication, cell debris was removed by centrifugation (15000 rpm, 30 min, 4°C, SS34 rotor). The supernatant was loaded onto a 5 ml GST-Trap FF column (GE Healthcare, Munich, Germany), pre-equilibrated in lysis buffer. After loading of the supernatant, the column was washed for 20 column volumes with lysis buffer. Elution of the protein was done in 20 ml of elution buffer. GST-tags were removed by protease cleavage with 50 µg PreScission-protease (GE Healthcare, Munich), which was added to the eluted protein and dialysed for 12 h at 4°C against dialysis buffer.

GST-tags were removed by protease cleavage with 50 µg PreScission-protease (GE Healthcare, Munich), which was added to the eluted protein and dialysed for 12 h at 4°C against dialysis buffer. The cleaved tag was removed from the mixture by loading the dialysis fraction onto a GST-Trap FF column. The flow through fraction, which contains the untagged Kar9p, was loaded onto a pre-equilibrated (buffer A) HiTrap-Q column (GE Healthcare, Munich). Elution of the protein was performed with a linear gradient over 10 column volumes, ranging from buffer A to buffer B. Peak fractions were analysed by SDS-PAGE, pooled and concentrated using centrifugal filter devices (Amicon Ultra, Millipore, Billerica, US). The concentrated protein solution was loaded onto a Superdex S200 16/60 size exclusion chromatography column equilibrated with gel filtration buffer. Peak fractions were again analysed by SDS-PAGE and concentrated. The purified protein was subsequently used for crystallisation experiments.

lysis buffer	10 mM Tris-HCl pH 7.5; 500 mM NaCl, 1 mM EDTA, 1 mM DTT
elution buffer	10 mM Tris-HCl pH 7.5; 500 mM NaCl, 1 mM EDTA, 1 mM DTT; 25 mM Glutathion
dialysis buffer/buffer A	10 mM Tris-HCl, pH 7.5; 250 mM NaCl, 1 mM EDTA, 1 mM DTT
buffer B	10 mM Tris-HCl, pH 7.5; 1 M NaCl, 1 mM EDTA, 1 mM DTT
gel filtration buffer	10 mM Tris-HCl, pH 7.5; 200 mM NaCl, 1 mM EDTA, 1 mM DTT

4.11.7 Purification of recombinant GST-tagged Bim1p

GST-tagged Bim1p variants were expressed and purified via a 5 ml GST-Trap FF column as described for Kar9p (chapter 4.11.6). The protein solution after the anion exchange chromatography was loaded onto a Superdex S200 16/60 or Superose 12 10/300 GL size exclusion chromatography column equilibrated with gel filtration buffer. Peak fractions were analysed by SDS-PAGE and concentrated. Subsequently, the purified protein was either used for crystallisation experiments or flash frozen in liquid nitrogen and stored at -80 °C.

lysis buffer	10 mM Tris-HCl, pH 7.5; 500 mM NaCl, 1 mM EDTA, 1 mM DTT
buffer A/dialysis buffer	10 mM Tris-HCl, pH 7.5; 100 mM NaCl, 1 mM EDTA, 1 mM DTT
buffer B	10 mM Tris-HCl, pH 7.5; 100 mM NaCl, 1 mM EDTA, 1 mM DTT
gel filtration buffer	10 mM Tris-HCl pH 7.5; 100 mM NaCl, 1 mM EDTA, 1 mM DTT

4.11.8 Purification of recombinant MBP-tagged Bim1p

MBP-tagged Bim1p (C-term) and Bim1p (FL) were expressed in *E. coli* and the cells treated as described above (chapter 4.11.6). After centrifugation, the supernatant was loaded onto a 3 ml amylose resin (New England Biolabs, Frankfurt, Germany), pre-equilibrated with lysis buffer. The column was washed extensively with 60 ml lysis buffer and bound proteins were eluted with elution buffer. The maltose was subsequently removed on a Superose-12 10/300 GL column (GE Healthcare, Munich), pre-equilibrated with gel filtration buffer. Peak fractions were analysed by SDS-PAGE, concentrated and flash frozen in liquid nitrogen for storage at -80°C.

lysis buffer	20 mM Tris-HCl pH 7.4; 200 mM NaCl; 1 mM EDTA; 1 mM DTT
elution buffer	20 mM Tris-HCl pH 7.4; 200 mM NaCl; 1 mM EDTA; 1 mM DTT, 10 mM Maltose
gel filtration buffer	10 mM Tris-HCl pH 7.5; 100 mM NaCl, 1 mM EDTA, 1 mM DTT

4.12 Crystallisation

All crystallisation experiments were carried out with freshly prepared protein samples, which were centrifuged before set up of crystallisation screens (20 min, 13 200 rpm and 4 °C). Initial crystallisation screens were set up with a nanoliter crystallisation robot (Phoenix, Art Robbins Instruments, Sunnyvale USA) at the crystallisation facility of the Max-Planck-Institute for Biochemistry (Martinsried, Germany). A drop size of 0.5 µl and a 1:1 mixture of protein and crystallisation solution were used for sitting-drop vapour-diffusion experiments in a 96-well plate format. Crystallisation drops were imaged at regular time intervals using an Xtafocus visualisation system (Tecan, Männedorf, Switzerland and Leica, Wetzlar, Germany). Refinement was done manually using hanging-drop vapour diffusion technique with a drop size of 2 µl and a 1:1 mixture of protein and crystallisation solution and a total reservoir volume of 500 µl using the 24-well EasyXtal CrystalSupport (Qiagen, Hilden, Germany).

4.12.1 Crystallisation of Kar9p (FL)

Recombinant full-length Kar9p was concentrated in gel filtration buffer to concentrations up to 6 mg/ml. Initial screens were set up with different concentrations of protein solution (1-6 mg/ml) at room temperature and 4°C. Crystals of Kar9p (FL) appeared after 1-2 days. After refinement, crystals of Kar9p (FL) were grown at 21°C by hanging-drop vapor-diffusion using a 1:1 mixture of protein (1-6 mg/ml) and crystallisation solution containing 0.1M Hepes pH 8.0, 21 % PEG 2000 MME, 125 mM serine or 0.1 M potassium citrate, 20 % PEG 3350, 125 mM serine. Needle-like shaped crystals with cracked ends appeared within 1-2 days. Cryo-protection was achieved with different cryo-protectants (glycerol, ethylene glycol, PEG 400), concentrations and incubation times. To slow down crystal growth, paraffine oil and silicone oil were used in different ratios (50:50, 65:35) to cover the reservoir solution. Isopropanol and glycerol were added in concentrations of 4-6 % to the precipitant solution. Proteases as Trypsin and Endoproteinase Glu-C were added to the protein solution in different ratios (w/w, 1:1000, 1:500, and 1:200) prior setting up crystal screens. For selenomethionine-derivatised protein, 1 mM TCEP was added to the protein solution prior crystal set up.

4.12.2 Crystallisation of Kar9p variants

Different Kar9p variants were crystallised as described for Kar9p (FL). Initial screens were set up with concentrations of 1-6 mg/ml for Kar9p variants lacking some amino acids at the very N-terminus (1-12) or C-terminus and with concentrations of 1-2 mg/ml for Kar9p fragments lacking large parts of the C-terminus (1-398; 1-401). Different cryoprotectants

(MPD; ethylenglycol, PEG 400, glycerol, sucrose, glucose) and incubation times with cryoprotectants were used.

4.12.3 Methylation of Kar9p

Reductive methylation of lysine residues is usually performed to improve the crystallisability of proteins. Many solvent exposed residues on the surface of proteins such as lysine, arginine, aspartic acid or glutamic acid have long flexible side chains. This flexibility can cause intrinsic disorders, which hinder formation of a crystal lattice. Addition of methyl groups to the side chains of lysine residues can immobilize these side chains and therefore promote crystallisation. It can also change the biophysical properties such as pI, solubility and hydrophathy and therefore enhance the interaction with other molecules. Reductive methylation of Kar9p was performed as described (Kim et al., 2008). 1 ml of protein solution (conc. < 10 mg/ml) was mixed with 40 μ l 1 M formaldehyde and 20 μ l of freshly prepared 1 M dimethylborane complex (ABC). After incubation at 4 °C for 2 h, the procedure was repeated and the mixture incubated again on ice for 2 h. At the end of incubation, 10 μ l of 1 M ABC were added and the reaction was left over night at 4 °C. To quench the reaction, 0.67 M glycine (final conc. 13.3 mM) and 1 M DTT (final conc. 5 mM) were added followed by size-exclusion chromatography on a Superdex S200 16/60 column in buffer containing 10 mM Tris-HCl pH 7.5, 200 mM NaCl, 1 mM EDTA and 1 mM DTT. The protein was concentrated again to 6 mg/ml and directly used for crystallisation screens. Initial screens were set up at concentrations of 2, 4 and 6 mg/ml.

4.12.4 Co-crystallisation of Bim1p and Kar9p (FL)

Kar9p (FL), Bim1p (C-term) and Bim1p (FL) were concentrated separately in gel filtration buffer. Prior crystallisation, the proteins were mixed in different molar ratios. Initial screens were performed either with Kar9p (FL) + Bim1p (FL) or Kar9p (FL) + Bim1p (C-term). Crystals appeared only in the screens with Kar9p (FL) + Bim1p (C-term) after 2-3 days.

4.12.5 Crystallisation of Bim1p

Different protein fragments were concentrated in gel filtration buffer to concentrations up to 20 mg/ml (for Bim1p (C-term)) and up to 7 mg/ml (for Bim1p (FL)). Initial screens were performed with different concentrations of protein solution (1-15 mg/ml). Crystals of Bim1p (C-term) appeared after 2-3 days in various conditions. After refinement, crystals of Bim1p (C-term) were grown at 21°C by hanging-drop vapor-diffusion using a 1:1 mixture of protein (2 mg/ml) and crystallisation solution containing 0.1M Bis-Tris pH 8.0, 20% PEG 5000MME, 40% γ -butyrolactone. Plate-like shaped crystals appeared within 2-3 days. For

selenomethionine-substituted protein, 1 mM TCEP was added to the protein solution prior crystal set up.

4.12.6 Heavy atom derivatisation by soaking

To screen for suitable heavy atom reagents (Hampton Research, Heavy atom screens Pt, Au, Hg, Aliso Viejo, USA) that can be used for derivatisation of Bim1p (C-term) in crystals, a binding assay with the protein in solution was performed. 1 µl of heavy atom reagent solution at different concentrations (10 mM and 100 mM) was incubated with 20 µg of protein in a buffer containing 10 mM Tris pH 7.5, 100 mM NaCl for 1h on ice. After addition of native loading dye, the proteins were resolved on a native PAGE (see 4.10.2). Heavy atom conditions, which showed a band shift of the protein on the native PAGE (Potassium tetranioplatinate(II), Potassium tetrabromoplatinate(II), Platinum potassium iodide) were used for soaking of crystals of Bim1p (C-term). Different concentrations of the heavy atom reagent solutions (10 mM, 5 mM and 1 mM) were prepared, added to the crystallisation drop and incubated for 1 min, 2 min, 5 min, 10 min, 30 min, 1 h and 12 h. For heavy atom derivatisation of Kar9p (FL), 5-Amino-2,4,6-triiodoisophtahalic acid (JBS Magic Triangle) and Hexatantalum tetradecabromide (JBS Tantalum Cluster) were tested (Beck et al., 2008 Knablein et al., 1997) (Jena Bioscience, Jena, Germany). The heavy atom reagent solutions were added directly to the crystals in the way described for Bim1p (C-term) without previous binding assays.

4.12.7 Structure determination of Bim1p (C-term)

Cryoprotection was achieved by adding 20% ethylene glycol and the crystals were subsequently mounted onto nylon loops and flash frozen in liquid nitrogen. Single anomalous dispersion (SAD) experiments were recorded at beamline ID-29 (ESRF, Grenoble France) and native datasets at beamline ID14-4 (ESRF, Grenoble France). The data was integrated and scaled using XDS (Kabsch) . Phases were obtained with SHELX (Sheldrick 2008) using SAD. The platin-derivatised dataset was used to build the model manually with COOT (Emsley and Cowtan, 2004). The native protein structure was solved by molecular replacement using PHASER (McCoy, 2007) and the platin-derivatised protein structure as search model. Refinement was performed with BUSTER (Blanc et al., 2004), using non-crystallographic symmetry.

4.13 Bioinformatics

4.13.1 Protein parameters

Programs that are available via the ExPASy Proteomics Server (<http://ca.expasy.org/sitemap.html>) were used to calculate protein parameters. ProtParam (Wilkins, Gasteiger et al. 1999) (www.expasy.org/tools/protparam.html) was used to calculate physical and chemical parameters of proteins such as isoelectric point, molecular mass and the molar extinction coefficient. The probability of coiled-coil formation was calculated with the program COILS (http://www.ch.embnet.org/software/COILS_form.html) (Lupas, Van Dyke et al. 1991).

4.13.2 Sequence alignments and structure predictions

DNA and protein sequences were either obtained from the *Saccharomyces* genome database (www.yeastgenome.org) or from the NCBI database (www.ncbi.nlm.nih.gov). The NCBI Basic Local Alignment Search Tool (BLAST) server (Altschul, Madden et al. 1997) (www.ncbi.nlm.nih.gov/BLAST) was used to perform homology searches. Multiple sequence alignments were performed with ClustalW (Larkin, Blackshields et al. 2007) (www.ebi.ac.uk/Tools/msa/clustalw2) and visualized with Jalview (Waterhouse, Procter et al. 2009) (www.jalview.org). Secondary structures were predicted using the program JPred (<http://www.compbio.dundee.ac.uk/www-jpred/>) (Cole, Barber et al. 2008). The structure prediction of Kar9p (FL) was performed with the program HHPred (Cole, Barber et al. 2008) (<http://toolkit.tuebingen.mpg.de/hhpred#>).

4.13.3 Structure visualisation and analysis

All figures of protein structures were generated with the program PyMOL (Schrodinger 2010) (DeLano, Palo Alto, USA). The UCSF Chimera package (University of California, San Francisco) (Pettersen et al., 2004) was used to visualize the sequence conservation on the surface of the Bim1p protein structure. Superimposition of the homologous Bim1p and human EB1 structures and RMSD calculation was performed with PyMOL and LSQMAN (<http://xray.bmc.uu.se/usf/>). Calculation and representation of the electrostatic surface was done with CCP4mg (Collaborative Computational Project, 1994). Buried surface areas were calculated using AREAIMOL (Collaborative Computational Project, 1994).

4.14 Yeast methods

4.14.1 Preparation of yeast whole-cell extracts

To analyse the protein-expression level of individual transformants, whole-cell extracts were prepared. Cells were grown overnight until stationary phase in 5 ml of appropriate medium. Next morning, the cells were diluted in fresh medium to an OD₆₀₀ of 0.15 and grown at 30°C until an OD₆₀₀ of 1. Cells were harvested by centrifugation, washed once in PBS and lysed by the addition of 1 ml alkaline solution (1ml 1.85 M NaOH + 8.5 ml ddH₂O). After incubation on ice for 10 min, 150 µl trichloroacetic acid (55 % w/v) was added to precipitate proteins. The reaction was incubated on ice for 10 minutes. Following sedimentation (13000 rpm, 15 minutes, 4 °C), the pellet was resuspended in 100 µl HU buffer (chapter 4.8) per 1 absorption unit at OD₆₀₀. Samples were stored at -20°C and the proteins were denatured by incubation at 65 °C for 10 min and analysed by western blot.

4.14.2 Co-immunoprecipitations

Myc-tagged Kar9p was immunoprecipitated with α-myc antibody from cell extracts. 100 µg of monoclonal α-myc antibody 9E11 (Acris Antibodies) was covalently coupled to 250 µl magnetic Protein-G beads (Dynabeads, Invitrogen) using dimethyl pimelimidate (DMP) as a cross linker according to the manufacturer's instructions. The beads were stored in TBS at 4°C until use. 20 µl of beads were equilibrated with lysis buffer (50 mM Tris-HCl, pH 7.5; 150 mM NaCl, 5 % Glycerol, 0,2 % Triton-X 100). For precipitation of overexpressed Kar9p and Kar9p-mutants, a 50 ml culture with an OD₆₀₀ of 4 was used. For precipitation of Kar9p expressed under the native promoter, a 1.5 l culture with an OD₆₀₀ of 3 was used. The cells were lysed in lysis buffer by vortexing with glass-beads for 3 x 4 min. The lysate was cleared by centrifugation at 13200 rpm for 20 min and the supernatant incubated with the beads for at least 4 h at 4°C on a rotating wheel. After incubation, the beads were washed with lysis buffer 3 x for 5 min on a rotating wheel. To reduce unspecific binding of proteins, an additional washing step with 300 mM NaCl was performed. The beads were finally washed again with lysis buffer. To elute bound proteins and to avoid contamination with the antibody, 10 µl of 100 mM Glycine pH 2.8 were added and incubated shortly (1-2 min) with the beads. The supernatant was transferred to a new tube and the beads were neutralized with 10 µl of 1 M Tris-HCl pH 8.5. The whole process was repeated twice and the elution fractions collected in one tube. After addition of 4 x loading buffer, the sample was boiled at 98°C and the proteins separated on a 4 – 20 % Mini-protean TGX pre-cast gel (Bio-Rad, München, Germany). Proteins were visualized using a silver-stain kit (Pierce by Thermo Fisher Scientific). Desired proteins bands were cut out with a clean scalpel and analysed by mass-spectrometry to identify proteins co-immunoprecipitating with Kar9p.

4.14.3 Benomyl- and temperature-sensitivity

To analyse Bim1p and Kar9p mutations *in vivo*, yeast cells that were deleted for either *BIM1* or *KAR9*, were transformed with the respective plasmids carrying the mutation. Temperature sensitivity of the mutants was assayed in a colony growth test on agar-plates. 5 µl of logarithmically growing yeast cells were applied to SC-His (for Kar9p) or SC-Leu (for Bim1p) agar plates in serial 1:10 dilutions and incubated at 25 °C, 30°C and 37°C for 2 days. Benomyl is a fungicide that binds to microtubules and destabilizes them (Stearns, Hoyt et al. 1990). It is routinely used to assay mutations of proteins that affect the cell cycle. The assay was carried out as described for the temperature sensitivity on YPD agar plates containing 0, 2.5, 5, 7.5, 10, 12.5, 15 or 20 µg/ml of benomyl at 30°C for two days.

5 Summary

Accurate positioning of the mitotic spindle relative to the plane of cytokinesis ensures proper distribution of the genetic material and of cell fate determinants. Failure in spindle orientation and migration can cause severe defects such as aberrant chromosome numbers, which is often correlated with the development of cancer.

In all eukaryotes, spindle positioning is accomplished through interactions between cytoplasmic microtubules, actin filaments and the cell cortex. Many of the relevant proteins are conserved from yeast to human and the *in vivo* functions of the proteins are well understood in yeast. Therefore, budding yeast is a powerful model system to investigate the molecular details and control mechanisms required for accurate spindle positioning. In yeast, the spindle is aligned along the axis of division by a complex consisting of the type-V myosin Myo2p, the adapter Kar9p and the microtubule-binding protein Bim1p.

The goal of this study was to elucidate the molecular principles underlying mitotic spindle positioning in budding yeast. In order to reach this goal, different structural techniques such as X-ray crystallography and small angle X-ray scattering (SAXS) were combined with various *in vitro* and *in vivo* assays to study the regulation of the Kar9p-Bim1p interaction.

In this study, crystals of full-length Kar9p and Kar9p variants were obtained, but the X-ray diffraction properties were not sufficient to solve a three-dimensional structure. Yet, the crystal structure of the C-terminal cargo-binding domain of Bim1p was determined. The crystal structure revealed that the C-terminal domain of Bim1p is formed by a dimer. SAXS analysis confirmed that Bim1p is dimeric in solution. Structure-guided mutational analysis of Bim1p resulted in the identification of residues that either reduced or increased the interaction with Kar9p. Remarkably, the residues involved in cargo-binding in Bim1p are within a highly conserved region on the surface of the protein. Other studies have shown that this highly conserved region mediates cargo binding in the Bim1p homolog EB1, suggesting that both proteins interact with their cargo in a similar manner.

To gain further insight into the regulation of complex assembly, the role of posttranslational modifications of both proteins was analysed. Sumoylation of Kar9p is required for binding to Bim1p, whereas phosphorylation of Kar9p is not. Furthermore, a yet unknown binding region for Kar9p in Bim1p was identified in the unstructured middle region. The middle region of Bim1p was only capable of Kar9p binding when the protein was dimerised and it was shown that the interaction via this region is regulated by phosphorylation by Aurora B.

These results in combination with findings from other studies lead to a model that explains the cell-cycle dependent regulation of the assembly and disassembly of the Myo2p-Kar9p-Bim1p complex. Complex assembly during metaphase is regulated by sumoylation of Kar9p, whereas the complex disassembly in late anaphase is regulated by phosphorylation of Bim1p by Aurora B.

6 References

- Adames, N. R. and J. A. Cooper (2000). "Microtubule interactions with the cell cortex causing nuclear movements in *Saccharomyces cerevisiae*." J Cell Biol **149**(4): 863-74.
- Adams, A. E. and J. R. Pringle (1984). "Relationship of actin and tubulin distribution to bud growth in wild-type and morphogenetic-mutant *Saccharomyces cerevisiae*." J Cell Biol **98**(3): 934-45.
- Akhmanova, A. and C. C. Hoogenraad (2005). "Microtubule plus-end-tracking proteins: mechanisms and functions." Curr Opin Cell Biol **17**(1): 47-54.
- Akhmanova, A. and M. O. Steinmetz (2008). "Tracking the ends: a dynamic protein network controls the fate of microtubule tips." Nat Rev Mol Cell Biol **9**(4): 309-22.
- Akhmanova, A. and M. O. Steinmetz (2011). "Microtubule end binding: EBs sense the guanine nucleotide state." Curr Biol **21**(8): R283-5.
- Altschul, S. F., T. L. Madden, et al. (1997). "Gapped BLAST and PSI-BLAST: a new generation of protein database search programs." Nucleic Acids Res **25**(17): 3389-402.
- Anand, K., D. Pal, et al. (2002). "An overview on 2-methyl-2,4-pentanediol in crystallization and in crystals of biological macromolecules." Acta Crystallogr D Biol Crystallogr **58**(Pt 10 Pt 1): 1722-8.
- Aoki, K. and M. M. Taketo (2007). "Adenomatous polyposis coli (APC): a multi-functional tumor suppressor gene." J Cell Sci **120**(Pt 19): 3327-35.
- Beach, D. L., J. Thibodeaux, et al. (2000). "The role of the proteins Kar9 and Myo2 in orienting the mitotic spindle of budding yeast." Curr Biol **10**(23): 1497-506.
- Beck, T., A. Krasauskas, et al. (2008). "A magic triangle for experimental phasing of macromolecules." Acta Crystallogr D Biol Crystallogr **64**(Pt 11): 1179-82.
- Beinhauer, J. D., I. M. Hagan, et al. (1997). "Mal3, the fission yeast homologue of the human APC-interacting protein EB-1 is required for microtubule integrity and the maintenance of cell form." J Cell Biol **139**(3): 717-28.
- Bergfors, T. (2003). "Seeds to crystals." J Struct Biol **142**(1): 66-76.
- Betschinger, J. and J. A. Knoblich (2004). "Dare to be different: asymmetric cell division in *Drosophila*, *C. elegans* and vertebrates." Curr Biol **14**(16): R674-85.
- Bieling, P., L. Laan, et al. (2007). "Reconstitution of a microtubule plus-end tracking system in vitro." Nature **450**(7172): 1100-5.
- Bienz, M. (2001). "Spindles cotton on to junctions, APC and EB1." Nat Cell Biol **3**(3): E67-8.
- Blanc, E., P. Roversi, et al. (2004). "Refinement of severely incomplete structures with maximum likelihood in BUSTER-TNT." Acta Crystallogr D Biol Crystallogr **60**(Pt 12 Pt 1): 2210-21.
- Bloom, K. (2000). "It's a kar9ochore to capture microtubules." Nat Cell Biol **2**(6): E96-8.

REFERENCES

- Bretscher, A. (2003). "Polarized growth and organelle segregation in yeast: the tracks, motors, and receptors." J Cell Biol **160**(6): 811-6.
- Bricogne, G., C. Vonrhein, et al. (2003). "Generation, representation and flow of phase information in structure determination: recent developments in and around SHARP 2.0." Acta Crystallogr D Biol Crystallogr **59**(Pt 11): 2023-30.
- Browning, H., D. D. Hackney, et al. (2003). "Targeted movement of cell end factors in fission yeast." Nat Cell Biol **5**(9): 812-8.
- Bu, W. and L. K. Su (2003). "Characterization of functional domains of human EB1 family proteins." J Biol Chem **278**(50): 49721-31.
- Buey, R. M., R. Mohan, et al. (2011). "Insights into EB1 structure and the role of its C-terminal domain for discriminating microtubule tips from the lattice." Mol Biol Cell **22**(16): 2912-2923.
- Byers, B., K. Shriver, et al. (1978). "The role of spindle pole bodies and modified microtubule ends in the initiation of microtubule assembly in *Saccharomyces cerevisiae*." J Cell Sci **30**: 331-52.
- Carminati, J. L. and T. Stearns (1997). "Microtubules orient the mitotic spindle in yeast through dynein-dependent interactions with the cell cortex." J Cell Biol **138**(3): 629-41.
- Caydasi, A. K., B. Ibrahim, et al. (2010). "Monitoring spindle orientation: Spindle position checkpoint in charge." Cell Div **5**: 28.
- Chayen, N. E. (1997). "The role of oil in macromolecular crystallization." Structure **5**(10): 1269-74.
- Cheng, L. and Y. Mao (2011). "mDia3-EB1-APC: A connection between kinetochores and microtubule plus ends." Commun Integr Biol **4**(4): 480-2.
- Ciccarone, V. C., D. A. Polayes, et al. (1998). "Generation of Recombinant Baculovirus DNA in *E. coli* Using a Baculovirus Shuttle Vector." Methods Mol Med **13**: 213-35.
- Cole, C., J. D. Barber, et al. (2008). "The Jpred 3 secondary structure prediction server." Nucleic Acids Res **36**(Web Server issue): W197-201.
- Cowan, C. R. and A. A. Hyman (2004). "Asymmetric cell division in *C. elegans*: cortical polarity and spindle positioning." Annu Rev Cell Dev Biol **20**: 427-53.
- Cuschieri, L., R. Miller, et al. (2006). "Gamma-tubulin is required for proper recruitment and assembly of Kar9-Bim1 complexes in budding yeast." Mol Biol Cell **17**(10): 4420-34.
- De Groot, C. O., I. Jelesarov, et al. (2010). "Molecular insights into mammalian end-binding protein heterodimerization." J Biol Chem **285**(8): 5802-14.
- Dong, A., X. Xu, et al. (2007). "In situ proteolysis for protein crystallization and structure determination." Nat Methods **4**(12): 1019-21.
- Egger, B., J. M. Chell, et al. (2008). "Insights into neural stem cell biology from flies." Philos Trans R Soc Lond B Biol Sci **363**(1489): 39-56.
- Emsley, P. and K. Cowtan (2004). "Coot: model-building tools for molecular graphics." Acta Crystallogr D Biol Crystallogr **60**(Pt 12 Pt 1): 2126-32.

REFERENCES

- Eshel, D., L. A. Urrestarazu, et al. (1993). "Cytoplasmic dynein is required for normal nuclear segregation in yeast." Proc Natl Acad Sci U S A **90**(23): 11172-6.
- Etienne-Manneville, S., J. B. Manneville, et al. (2005). "Cdc42 and Par6-PKCzeta regulate the spatially localized association ofDlg1 and APC to control cell polarization." J Cell Biol **170**(6): 895-901.
- Evans, P. (2006). "Scaling and assessment of data quality." Acta Crystallogr D Biol Crystallogr **62**(Pt 1): 72-82.
- Evans, P. R. (2011). "An introduction to data reduction: space-group determination, scaling and intensity statistics." Acta Crystallogr D Biol Crystallogr **67**(Pt 4): 282-92.
- Fraschini, R., M. Venturetti, et al. (2008). "The spindle position checkpoint: how to deal with spindle misalignment during asymmetric cell division in budding yeast." Biochem Soc Trans **36**(Pt 3): 416-20.
- Gardner, M. K., J. Haase, et al. (2008). "The microtubule-based motor Kar3 and plus end-binding protein Bim1 provide structural support for the anaphase spindle." J Cell Biol **180**(1): 91-100.
- Glotzer, M. (2004). "Cleavage furrow positioning." J Cell Biol **164**(3): 347-51.
- Gonczy, P. (2008). "Mechanisms of asymmetric cell division: flies and worms pave the way." Nat Rev Mol Cell Biol **9**(5): 355-66.
- Grava, S., F. Schaerer, et al. (2006). "Asymmetric recruitment of dynein to spindle poles and microtubules promotes proper spindle orientation in yeast." Dev Cell **10**(4): 425-39.
- Guinier, A., and Fournet, F. (1955). "Small Angle Scattering of X-rays." Wiley Interscience, New York.
- Gusnowski, E. M. and M. Srayko (2011). "Visualization of dynein-dependent microtubule gliding at the cell cortex: implications for spindle positioning." J Cell Biol **194**(3): 377-86.
- Half, E., D. Bercovich, et al. (2009). "Familial adenomatous polyposis." Orphanet J Rare Dis **4**: 22.
- Hanahan, D. (1983). "Studies on transformation of Escherichia coli with plasmids." J Mol Biol **166**(4): 557-80.
- Hay, R. T. (2005). "SUMO: a history of modification." Mol Cell **18**(1): 1-12.
- Hayashi, I. and M. Ikura (2003). "Crystal structure of the amino-terminal microtubule-binding domain of end-binding protein 1 (EB1)." J Biol Chem **278**(38): 36430-4.
- Hendrickson, W. A. a. O. C. M. (1997). "Phase determination from multiwavelength anomalous diffraction measurements." Methods Enzymol **276**: 494-523.
- Ho, S. N., H. D. Hunt, et al. (1989). "Site-directed mutagenesis by overlap extension using the polymerase chain reaction." Gene **77**(1): 51-9.
- Honnappa, S., S. M. Gouveia, et al. (2009). "An EB1-binding motif acts as a microtubule tip localization signal." Cell **138**(2): 366-76.

REFERENCES

- Honnappa, S., C. M. John, et al. (2005). "Structural insights into the EB1-APC interaction." EMBO J **24**(2): 261-9.
- Hotz, M. and Y. Barral (2010). "Cytokinesis: the Ubc of positioning." Curr Biol **20**(14): R602-4.
- Huisman, S. M., O. A. Bales, et al. (2004). "Differential contribution of Bud6p and Kar9p to microtubule capture and spindle orientation in *S. cerevisiae*." J Cell Biol **167**(2): 231-44.
- Hwang, E., J. Kusch, et al. (2003). "Spindle orientation in *Saccharomyces cerevisiae* depends on the transport of microtubule ends along polarized actin cables." J Cell Biol **161**(3): 483-8.
- Inoue, S. and E. D. Salmon (1995). "Force generation by microtubule assembly/disassembly in mitosis and related movements." Mol Biol Cell **6**(12): 1619-40.
- Janke, C., M. M. Magiera, et al. (2004). "A versatile toolbox for PCR-based tagging of yeast genes: new fluorescent proteins, more markers and promoter substitution cassettes." Yeast **21**(11): 947-62.
- Jaspersen, S. L. and M. Winey (2004). "The budding yeast spindle pole body: structure, duplication, and function." Annu Rev Cell Dev Biol **20**: 1-28.
- Jenal, U. (2000). "Signal transduction mechanisms in *Caulobacter crescentus* development and cell cycle control." FEMS Microbiol Rev **24**(2): 177-91.
- Johnson, E. S. (2004). "Protein modification by SUMO." Annu Rev Biochem **73**: 355-82.
- Kabsch, W. (2010). "Xds." Acta Crystallogr D Biol Crystallogr **66**(Pt 2): 125-32.
- Kammerer, D., L. Stevermann, et al. (2010). "Ubiquitylation regulates interactions of astral microtubules with the cleavage apparatus." Curr Biol **20**(14): 1233-43.
- Khmelniskii, A. and E. Schiebel (2008). "Assembling the spindle midzone in the right place at the right time." Cell Cycle **7**(3): 283-6.
- Kilmartin, J. V. and A. E. Adams (1984). "Structural rearrangements of tubulin and actin during the cell cycle of the yeast *Saccharomyces*." J Cell Biol **98**(3): 922-33.
- Kim, D. W. and F. Hirth (2009). "Genetic mechanisms regulating stem cell self-renewal and differentiation in the central nervous system of *Drosophila*." Cell Adh Migr **3**(4): 402-11.
- Kim, Y., P. Quartey, et al. (2008). "Large-scale evaluation of protein reductive methylation for improving protein crystallization." Nat Methods **5**(10): 853-4.
- Knablein, J., T. Neuefeind, et al. (1997). "Ta6Br(2+)₁₂, a tool for phase determination of large biological assemblies by X-ray crystallography." J Mol Biol **270**(1): 1-7.
- Knop, M., K. Siegers, et al. (1999). "Epitope tagging of yeast genes using a PCR-based strategy: more tags and improved practical routines." Yeast **15**(10B): 963-72.
- Komarova, Y., C. O. De Groot, et al. (2009). "Mammalian end binding proteins control persistent microtubule growth." J Cell Biol **184**(5): 691-706.

REFERENCES

- Konarev, P. V., M. V. Petoukhov, et al. (2006). "ATSAS 2.1, a program package for small-angle scattering data analysis." *Journal of Applied Crystallography* **39**(2): 277-286.
- Konarev, P. V., V. V. Volkov, et al. (2003). "PRIMUS: a Windows PC-based system for small-angle scattering data analysis." *Journal of Applied Crystallography* **36**(5): 1277-1282.
- Korinek, W. S., M. J. Copeland, et al. (2000). "Molecular linkage underlying microtubule orientation toward cortical sites in yeast." *Science* **287**(5461): 2257-9.
- Krissinel, E. and K. Henrick (2007). "Inference of macromolecular assemblies from crystalline state." *J Mol Biol* **372**(3): 774-97.
- Kurihara, L. J., C. T. Beh, et al. (1994). "Nuclear congression and membrane fusion: two distinct events in the yeast karyogamy pathway." *J Cell Biol* **126**(4): 911-23.
- Kusch, J., D. Liakopoulos, et al. (2003). "Spindle asymmetry: a compass for the cell." *Trends Cell Biol* **13**(11): 562-9.
- Kusch, J., A. Meyer, et al. (2002). "Microtubule capture by the cleavage apparatus is required for proper spindle positioning in yeast." *Genes Dev* **16**(13): 1627-39.
- Laemmli, U. K. (1970). "Cleavage of structural proteins during the assembly of the head of bacteriophage T4." *Nature* **227**(5259): 680-5.
- Lansbergen, G. and A. Akhmanova (2006). "Microtubule plus end: a hub of cellular activities." *Traffic* **7**(5): 499-507.
- Larkin, M. A., G. Blackshields, et al. (2007). "Clustal W and Clustal X version 2.0." *Bioinformatics* **23**(21): 2947-8.
- Lee, L., J. S. Tirnauer, et al. (2000). "Positioning of the mitotic spindle by a cortical-microtubule capture mechanism." *Science* **287**(5461): 2260-2.
- Leisner, C., D. Kammerer, et al. (2008). "Regulation of mitotic spindle asymmetry by SUMO and the spindle-assembly checkpoint in yeast." *Curr Biol* **18**(16): 1249-55.
- Liakopoulos, D., J. Kusch, et al. (2003). "Asymmetric loading of Kar9 onto spindle poles and microtubules ensures proper spindle alignment." *Cell* **112**(4): 561-74.
- Louie, R. K., S. Bahmanyar, et al. (2004). "Adenomatous polyposis coli and EB1 localize in close proximity of the mother centriole and EB1 is a functional component of centrosomes." *J Cell Sci* **117**(Pt 7): 1117-28.
- Lu, B., F. Roegiers, et al. (2001). "Adherens junctions inhibit asymmetric division in the *Drosophila* epithelium." *Nature* **409**(6819): 522-5.
- Luckow, V. A., S. C. Lee, et al. (1993). "Efficient generation of infectious recombinant baculoviruses by site-specific transposon-mediated insertion of foreign genes into a baculovirus genome propagated in *Escherichia coli*." *J Virol* **67**(8): 4566-79.
- Luedeke, C., S. B. Frei, et al. (2005). "Septin-dependent compartmentalization of the endoplasmic reticulum during yeast polarized growth." *J Cell Biol* **169**(6): 897-908.
- Lupas, A., M. Van Dyke, et al. (1991). "Predicting coiled coils from protein sequences." *Science* **252**(5010): 1162-4.

REFERENCES

- Ma, B., T. Elkayam, et al. (2003). "Protein-protein interactions: structurally conserved residues distinguish between binding sites and exposed protein surfaces." Proc Natl Acad Sci U S A **100**(10): 5772-7.
- Maekawa, H. and E. Schiebel (2004). "Cdk1-Clb4 controls the interaction of astral microtubule plus ends with subdomains of the daughter cell cortex." Genes Dev **18**(14): 1709-24.
- Maekawa, H., T. Usui, et al. (2003). "Yeast Cdk1 translocates to the plus end of cytoplasmic microtubules to regulate bud cortex interactions." EMBO J **22**(3): 438-49.
- Matthews, B. W. (1968). "Solvent content of protein crystals." J Mol Biol **33**(2): 491-7.
- Mayer, M. L., I. Pot, et al. (2004). "Identification of protein complexes required for efficient sister chromatid cohesion." Mol Biol Cell **15**(4): 1736-45.
- McCarthy, E. K. and B. Goldstein (2006). "Asymmetric spindle positioning." Curr Opin Cell Biol **18**(1): 79-85.
- McCoy, A. J. (2007). "Solving structures of protein complexes by molecular replacement with Phaser." Acta Crystallogr D Biol Crystallogr **63**(Pt 1): 32-41.
- Meednu, N., H. Hoops, et al. (2008). "The spindle positioning protein Kar9p interacts with the sumoylation machinery in *Saccharomyces cerevisiae*." Genetics **180**(4): 2033-55.
- Merlini, L. and S. Piatti (2011). "The mother-bud neck as a signaling platform for the coordination between spindle position and cytokinesis in budding yeast." Biol Chem **392**(8-9): 805-12.
- Messer, M., M. Griffiths, et al. (1997). "Lactose synthesis in a monotreme, the echidna (*Tachyglossus aculeatus*): isolation and amino acid sequence of echidna alpha-lactalbumin." Comp Biochem Physiol B Biochem Mol Biol **118**(2): 403-10.
- Meulmeester, E. and F. Melchior (2008). "Cell biology: SUMO." Nature **452**(7188): 709-11.
- Miller, R. K., S. C. Cheng, et al. (2000). "Bim1p/Yeb1p mediates the Kar9p-dependent cortical attachment of cytoplasmic microtubules." Mol Biol Cell **11**(9): 2949-59.
- Miller, R. K., S. D'Silva, et al. (2006). "The CLIP-170 orthologue Bik1p and positioning the mitotic spindle in yeast." Curr Top Dev Biol **76**: 49-87.
- Miller, R. K. and M. D. Rose (1998). "Kar9p is a novel cortical protein required for cytoplasmic microtubule orientation in yeast." J Cell Biol **140**(2): 377-90.
- Mimori-Kiyosue, Y., N. Shiina, et al. (2000). "Adenomatous polyposis coli (APC) protein moves along microtubules and concentrates at their growing ends in epithelial cells." J Cell Biol **148**(3): 505-18.
- Mimori-Kiyosue, Y., N. Shiina, et al. (2000). "The dynamic behavior of the APC-binding protein EB1 on the distal ends of microtubules." Curr Biol **10**(14): 865-8.
- Mitchison, T. and M. Kirschner (1984). "Dynamic instability of microtubule growth." Nature **312**(5991): 237-42.
- Mitchison, T. J. and E. D. Salmon (2001). "Mitosis: a history of division." Nat Cell Biol **3**(1): E17-21.

REFERENCES

- Moore, J. K. and J. A. Cooper (2010). "Coordinating mitosis with cell polarity: Molecular motors at the cell cortex." Semin Cell Dev Biol **21**(3): 283-9.
- Moore, J. K., S. D'Silva, et al. (2006). "The CLIP-170 homologue Bik1p promotes the phosphorylation and asymmetric localization of Kar9p." Mol Biol Cell **17**(1): 178-91.
- Moore, J. K. and R. K. Miller (2007). "The cyclin-dependent kinase Cdc28p regulates multiple aspects of Kar9p function in yeast." Mol Biol Cell **18**(4): 1187-202.
- Moritz, M., M. B. Braunfeld, et al. (2000). "Structure of the gamma-tubulin ring complex: a template for microtubule nucleation." Nat Cell Biol **2**(6): 365-70.
- Morrison, E. E. (2007). "Action and interactions at microtubule ends." Cell Mol Life Sci **64**(3): 307-17.
- Munro, E. and B. Bowerman (2009). "Cellular symmetry breaking during *Caenorhabditis elegans* development." Cold Spring Harb Perspect Biol **1**(4): a003400.
- Mylonas, E. and D. I. Svergun (2007). "Accuracy of molecular mass determination of proteins in solution by small-angle X-ray scattering." Journal of Applied Crystallography **40**(s1): s245-s249.
- Nakamura, M., X. Z. Zhou, et al. (2001). "Critical role for the EB1 and APC interaction in the regulation of microtubule polymerization." Curr Biol **11**(13): 1062-7.
- Nathke, I. (2005). "Relationship between the role of the adenomatous polyposis coli protein in colon cancer and its contribution to cytoskeletal regulation." Biochem Soc Trans **33**(Pt 4): 694-7.
- Nathke, I. S. (2004). "The adenomatous polyposis coli protein: the Achilles heel of the gut epithelium." Annu Rev Cell Dev Biol **20**: 337-66.
- Neumuller, R. A. and J. A. Knoblich (2009). "Dividing cellular asymmetry: asymmetric cell division and its implications for stem cells and cancer." Genes Dev **23**(23): 2675-99.
- O'Toole, E. T., M. Winey, et al. (1999). "High-voltage electron tomography of spindle pole bodies and early mitotic spindles in the yeast *Saccharomyces cerevisiae*." Mol Biol Cell **10**(6): 2017-31.
- Palmer, R. E., D. S. Sullivan, et al. (1992). "Role of astral microtubules and actin in spindle orientation and migration in the budding yeast, *Saccharomyces cerevisiae*." J Cell Biol **119**(3): 583-93.
- Parsons, A. B., R. L. Brost, et al. (2004). "Integration of chemical-genetic and genetic interaction data links bioactive compounds to cellular target pathways." Nat Biotechnol **22**(1): 62-9.
- Pearson, C. G. and K. Bloom (2004). "Dynamic microtubules lead the way for spindle positioning." Nat Rev Mol Cell Biol **5**(6): 481-92.
- Pease, J. C. and J. S. Tirnauer (2011). "Mitotic spindle misorientation in cancer--out of alignment and into the fire." J Cell Sci **124**(Pt 7): 1007-16.

REFERENCES

- Pereira, G., T. U. Tanaka, et al. (2001). "Modes of spindle pole body inheritance and segregation of the Bfa1p-Bub2p checkpoint protein complex." EMBO J **20**(22): 6359-70.
- Pettersen, E. F., T. D. Goddard, et al. (2004). "UCSF Chimera--a visualization system for exploratory research and analysis." J Comput Chem **25**(13): 1605-12.
- Piatti, S., M. Venturetti, et al. (2006). "The spindle position checkpoint in budding yeast: the motherly care of MEN." Cell Div **1**(1): 2.
- Powell, S. M., N. Zilz, et al. (1992). "APC mutations occur early during colorectal tumorigenesis." Nature **359**(6392): 235-7.
- Pruyne, D. and A. Bretscher (2000). "Polarization of cell growth in yeast. I. Establishment and maintenance of polarity states." J Cell Sci **113** (Pt 3): 365-75.
- Quinlan, R. A., C. I. Pogson, et al. (1980). "The influence of the microtubule inhibitor, methyl benzimidazol-2-yl-carbamate (MBC) on nuclear division and the cell cycle in *Saccharomyces cerevisiae*." J Cell Sci **46**: 341-52.
- Rappaport, R. (1997). "Cleavage furrow establishment by the moving mitotic apparatus." Dev Growth Differ **39**(2): 221-6.
- Rhyu, M. S. and J. A. Knoblich (1995). "Spindle orientation and asymmetric cell fate." Cell **82**(4): 523-6.
- Rost, B. (1999). "Twilight zone of protein sequence alignments." Protein Eng **12**(2): 85-94.
- Sambrook, J. and D. W. Russell (2001). Molecular cloning : a laboratory manual. Cold Spring Harbor, N.Y., Cold Spring Harbor Laboratory Press.
- Sandblad, L., K. E. Busch, et al. (2006). "The *Schizosaccharomyces pombe* EB1 homolog Mal3p binds and stabilizes the microtubule lattice seam." Cell **127**(7): 1415-24.
- Schrodinger, LLC (2010). The PyMOL Molecular Graphics System, Version 1.3r1.
- Schuyler, S. C. and D. Pellman (2001). "Search, capture and signal: games microtubules and centrosomes play." J Cell Sci **114**(Pt 2): 247-55.
- Schwartz, K., K. Richards, et al. (1997). "BIM1 encodes a microtubule-binding protein in yeast." Mol Biol Cell **8**(12): 2677-91.
- Segal, M., K. Bloom, et al. (2000). "Bud6 directs sequential microtubule interactions with the bud tip and bud neck during spindle morphogenesis in *Saccharomyces cerevisiae*." Mol Biol Cell **11**(11): 3689-702.
- Segal, M., D. J. Clarke, et al. (2000). "Coordinated spindle assembly and orientation requires Clb5p-dependent kinase in budding yeast." J Cell Biol **148**(3): 441-52.
- Shang, C., T. R. Hazbun, et al. (2003). "Kinetochore protein interactions and their regulation by the Aurora kinase Ipl1p." Mol Biol Cell **14**(8): 3342-55.
- Sheldrick, G. M. (2008). "A short history of SHELX." Acta Crystallogr A **64**(Pt 1): 112-22.

REFERENCES

- Siller, K. H. and C. Q. Doe (2009). "Spindle orientation during asymmetric cell division." Nat Cell Biol **11**(4): 365-74.
- Slep, K. C., S. L. Rogers, et al. (2005). "Structural determinants for EB1-mediated recruitment of APC and spectraplakins to the microtubule plus end." J Cell Biol **168**(4): 587-98.
- Slep, K. C. and R. D. Vale (2007). "Structural basis of microtubule plus end tracking by XMAP215, CLIP-170, and EB1." Mol Cell **27**(6): 976-91.
- Soding, J., A. Biegert, et al. (2005). "The HHpred interactive server for protein homology detection and structure prediction." Nucleic Acids Res **33**(Web Server issue): W244-8.
- Sousa, R. (1995). "Use of glycerol, polyols and other protein structure stabilizing agents in protein crystallization." Acta Crystallogr D Biol Crystallogr **51**(Pt 3): 271-7.
- Stearns, T., M. A. Hoyt, et al. (1990). "Yeast mutants sensitive to antimicrotubule drugs define three genes that affect microtubule function." Genetics **124**(2): 251-62.
- Su, L. K., M. Burrell, et al. (1995). "APC binds to the novel protein EB1." Cancer Res **55**(14): 2972-7.
- Sun, L., J. Gao, et al. (2008). "EB1 promotes Aurora-B kinase activity through blocking its inactivation by protein phosphatase 2A." Proc Natl Acad Sci U S A **105**(20): 7153-8.
- Svergun, D., C. Barberato, et al. (1995). "CRY SOL - a Program to Evaluate X-ray Solution Scattering of Biological Macromolecules from Atomic Coordinates." Journal of Applied Crystallography **28**(6): 768-773.
- Svergun, D. I., M. V. Petoukhov, et al. (2001). "Determination of domain structure of proteins from X-ray solution scattering." Biophys J **80**(6): 2946-53.
- Svergun, D. I. B., C.; Koch, M.H.J. (1995). "CRY SOL - a program to evaluate X-ray solution scattering of biological macromolecules from atomic coordinates." J. Appl. Crystallogr. **28**: 768-773.
- Tirnauer, J. S. and B. E. Bierer (2000). "EB1 proteins regulate microtubule dynamics, cell polarity, and chromosome stability." J Cell Biol **149**(4): 761-6.
- Tirnauer, J. S., E. O'Toole, et al. (1999). "Yeast Bim1p promotes the G1-specific dynamics of microtubules." J Cell Biol **145**(5): 993-1007.
- Toyoshima, F. and E. Nishida (2007). "Spindle orientation in animal cell mitosis: roles of integrin in the control of spindle axis." J Cell Physiol **213**(2): 407-11.
- Trzepacz, C., A. M. Lowy, et al. (1997). "Phosphorylation of the tumor suppressor adenomatous polyposis coli (APC) by the cyclin-dependent kinase p34." J Biol Chem **272**(35): 21681-4.
- Vagin, A. and A. Teplyakov (2010). "Molecular replacement with MOLREP." Acta Crystallogr D Biol Crystallogr **66**(Pt 1): 22-5.
- Waterhouse, A. M., J. B. Procter, et al. (2009). "Jalview Version 2--a multiple sequence alignment editor and analysis workbench." Bioinformatics **25**(9): 1189-91.

REFERENCES

- Wen, Y., C. H. Eng, et al. (2004). "EB1 and APC bind to mDia to stabilize microtubules downstream of Rho and promote cell migration." *Nat Cell Biol* **6**(9): 820-30.
- Wernimont, A. and A. Edwards (2009). "In situ proteolysis to generate crystals for structure determination: an update." *PLoS One* **4**(4): e5094.
- Wiese, C. and Y. Zheng (2000). "A new function for the gamma-tubulin ring complex as a microtubule minus-end cap." *Nat Cell Biol* **2**(6): 358-64.
- Wilkins, M. R., E. Gasteiger, et al. (1999). "Protein identification and analysis tools in the ExPASy server." *Methods Mol Biol* **112**: 531-52.
- Wilkinson, K. A. and J. M. Henley (2010). "Mechanisms, regulation and consequences of protein SUMOylation." *Biochem J* **428**(2): 133-45.
- Wolyniak, M. J., K. Blake-Hodek, et al. (2006). "The regulation of microtubule dynamics in *Saccharomyces cerevisiae* by three interacting plus-end tracking proteins." *Mol Biol Cell* **17**(6): 2789-98.
- Yamashita, Y. M. and M. T. Fuller (2008). "Asymmetric centrosome behavior and the mechanisms of stem cell division." *J Cell Biol* **180**(2): 261-6.
- Yamashita, Y. M., D. L. Jones, et al. (2003). "Orientation of asymmetric stem cell division by the APC tumor suppressor and centrosome." *Science* **301**(5639): 1547-50.
- Ye, P., B. D. Peyser, et al. (2005). "Gene function prediction from congruent synthetic lethal interactions in yeast." *Mol Syst Biol* **1**: 2005 0026.
- Yin, H., D. Pruyne, et al. (2000). "Myosin V orientates the mitotic spindle in yeast." *Nature* **406**(6799): 1013-5.
- Yu, F., C. T. Kuo, et al. (2006). "Drosophila neuroblast asymmetric cell division: recent advances and implications for stem cell biology." *Neuron* **51**(1): 13-20.
- Zimniak, T., K. Stengl, et al. (2009). "Phosphoregulation of the budding yeast EB1 homologue Bim1p by Aurora/Ipl1p." *J Cell Biol* **186**(3): 379-91.

7 Appendix

7.1 Abbreviations

%	per cent	s	seconds
°C	degree celcius	SAD	single anomalous diffraction
Å	angström	SAXS	Small angle X-ray scattering
$A_{260/280/600}$	absorption at 260/280/600 nm	SDS	Sodium Dodecyl Sulfate
μ	micro	SeMet	Selenomethionine
Conc.	concentration	TCA	Trichloroacetic acid
C-term	C-terminus	TLS	Twin Lattice Symmetry
Da	Dalton	Tris	tris(hydroxymethyl)aminomethane
DAPI	4',6-diamidino-2-phenylindole	WT	wild type
DLS	Dynamic light scattering	σ	sigma
DNA	Deoxyribonucleic acid		
<i>E.coli</i>	<i>Escherichia coli</i>		
EDTA	ethylenediaminetetraacetic acid		
FL	Full-length		
g	gram		
GST	Glutathion-S-Transferase		
h	Hours, human		
His	Histidine		
I	Intensity		
k	kilo		
l	litre		
M	molar		
MES	2-(<i>N</i> -morpholino)ethanesulfonic acid		
min	minute		
MBP	Maltose binding protein		
MW	Molecular weight		
n	nano		
NaCl	Sodium Chloride		
NCS	Non Crystallographic Symmetry		
PAGE	polyacrylamide gel electrophoresis		
PEG	Polyethylene glycol		
Pt	Platine		
PVFD	polyvinylidene fluoride		
RMSD	root-mean-square deviation		
rpm	Rounds per minute		
RT	Room temperature		

7.2 Proteins identified by co-immunoprecipitations of Kar9p

Mass-spectrometry of co-immunoprecipitations (co-IP) of Kar9p

Tables show mass spectrometry results after CoIP. Co-IPs were performed with wild-type yeast and yeast strains harbouring mutations in the phosphorylation sites of Kar9p.

left column: name of associated protein, middle column: number of measured peptides, right column: sequence coverage of peptide sequence in relation to protein sequence, cut off was 20% sequence coverage, bold: proteins known to be associated with Kar9p, italic: possible new interaction partners

Co-immunoprecipitations from YDH001 (WT)

Protein	Number of peptides	Sequence coverage
<i>Tpm1p</i>	23	86%
Actin	18	73%
<i>Nap1p</i>	14	64%
Myo2p	53	62%
Bim1p	1	3%

Co-immunoprecipitations from YDH003 (S197A)

Protein	Number of peptides	Sequence coverage
<i>Tpm1p</i>	15	72%
Actin	15	35%
Myo2p	51	30%
<i>Nap1p</i>	5	16%
Bim1p	1	3%

Co-immunoprecipitations from YDH004 (S496A)

Protein	Number of peptides	Sequence coverage
Actin	16	45%
Myo2p	45	37%
<i>Tpm2p</i>	4	36%
<i>Nap1p</i>	7	27%
Bim1p	1	3%

Co-immunoprecipitations from YDH005 (S197A + S496A)

Protein	Number of peptides	Sequence coverage
<i>Tpm1p</i>	17	74%
Actin	19	55%
Myo2p	74	52%
<i>Nap1p</i>	8	27%
Bim1p	2	7%

7.3 Supplemental Figures and Tables

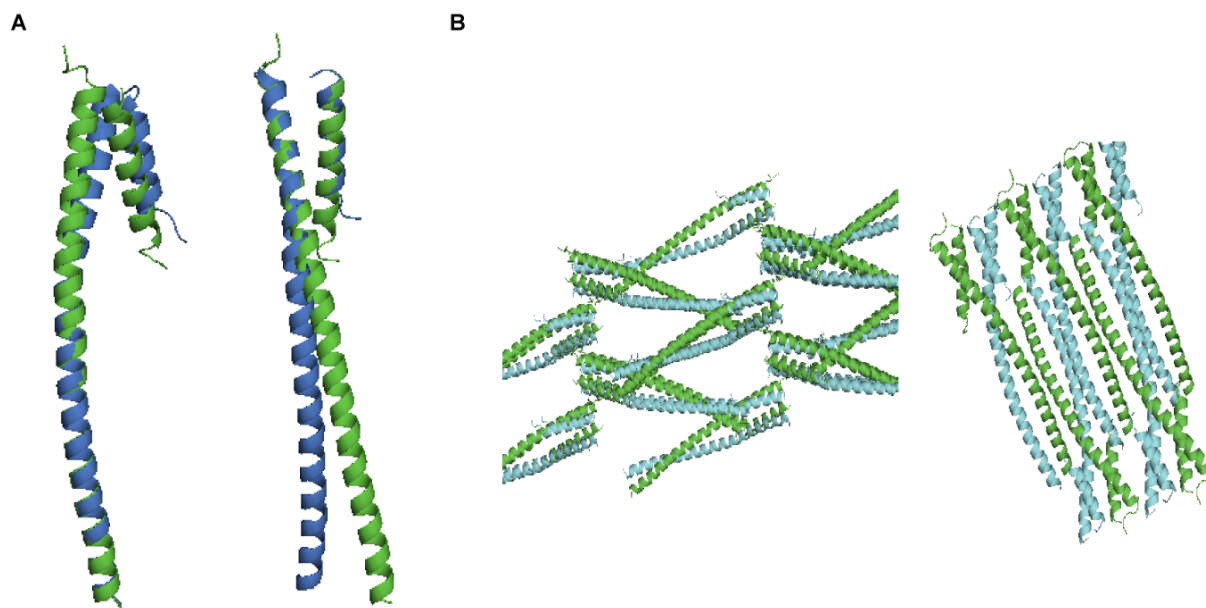


Figure 29 Monomers A and B of Bim1p (C-term) are not related by a noncrystallographic symmetry axis. (A) Alignment of the two monomers A and B. The structure of the two monomers is not identical after superimposition. The monomers can be either aligned from residue 1-41 or from residue 41-106. Residues 43-46 contain a highly conserved “FYF”-motif that might influence the difference in the structure. These residues are involved in the binding to Kar9p and also in forming intramolecular contacts. (B) Crystal packing in Bim1p (C-term) crystals. The protein-protein crystal-packing contacts do not seem to influence the structural difference between the two monomers.

Crystallographic contacts of Bim1p				
Type of interface	Number of interface residues	Buried surface interface (\AA^2)	$\Delta^{\dagger}G$ (kcal/mol)	$\Delta^{\dagger}G$ P value
coiled-coil	47	1987	-45.8	0.051
dimer-dimer	10	434	-8.7	0.227
dimer-dimer	10	350	-6.7	0.407
dimer-dimer	8	314	-4.8	0.412

$\Delta^{\dagger}G$ indicates the calculated solvation free energy gain upon formation of the interface. A corresponding P-value above 0.5 indicates a lower-than-average hydrophobicity and thus an interface likely to occur only in crystal packing. A P-value below 0.5 indicates a higher-than-expected hydrophobicity, indicating a potential protein-interaction surface in solution. Among the four interfaces with the largest buried surface interfaces ($>300 \text{\AA}^2$) only the calculated values of the coiled-coil interaction are consistent with a physiologic dimer. Calculations have been performed with the EBI-PISA server (http://www.ebi.ac.uk/msd-srv/prot_int/cgi-bin/piserver).

Table 5 Data obtained from the PDBe PISA server

APPENDIX

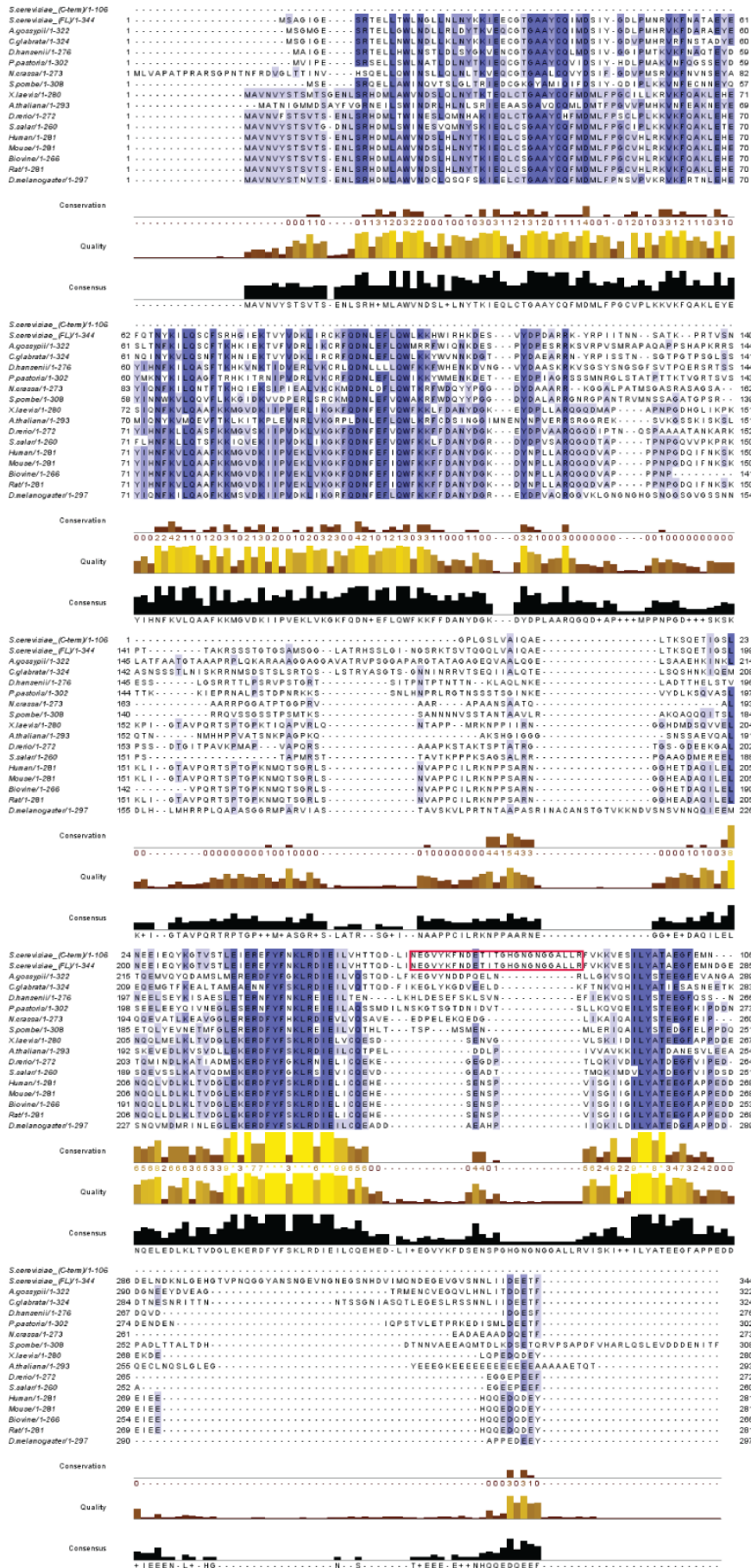


Figure 30 Sequence alignment of EB1-family members from different eukaryotes

Publications

Parts of this work will be published or are in process of publication:

Hüls D, Storchova Z, Niessing D. “Two Kar9p-binding domains in Bim1p and posttranslational modifications regulate assembly of the spindle-orientation complex in yeast” (submitted)

Hüls D, Niessing D. “Preliminary results on purification and crystallization of Kar9p” (in preparation)

Other publications:

Heuck A, Fetka I, Brewer DN, Hüls D, Munson M, Jansen RP, Niessing D.”The structure of the Myo4p globular tail and its function in ASH1 mRNA localization.” JCB 2010 May 3; 189(3):497-510

Acknowledgements

This thesis would not have been possible without the support of many people.

First of all I would like to thank Dierk Niessing for giving me the opportunity to work in his laboratory at the Gene Center. I am very grateful to him for believing in me and for helping me to see things in a more positive way.

I want to thank the members of my thesis advisory committee, Klaus Förstemann, Dirk Kostrewa and Zuzana Storchova without whose knowledge and assistance this thesis would not have been possible. Especially, I would like to thank Zuzana Storchova for her accordance to collaborate with us on my project.

I am grateful to Klaus Förstemann and Dietmar Martin for being the first and second examiner of my thesis.

I want to thank all the present and former members of the Niessing lab for the nice atmosphere. In particular I want to thank: Sigrun, for keeping the lab running and the discussions about other important things in life. Stephane, for teaching me a lot about crystallography. Marisa, for showing me how to deal with SAXS data. Alex, for sharing the bench with me and for being always open for discussions. Roland, for many discussions about science and life beyond science. Additionally, I would like to thank my practical students Andreas, Martina and Yildiz for their help in the lab.

I am grateful to the supervisor of my diploma thesis, Elmar Schiebel and his lab members, who introduced me into the work with yeast. Without this knowledge I would not have been able to do all the yeast work on my own.

Many thanks to all the beamline staffs at the ESRF and the crystallization facility at the MPI, and of course to all the people who gave me a lift to the ESRF.

Special thanks go to Marc Waldenberger, who was always there for me and managed to cheer me up. You are a very special part of my life and words alone cannot express my appreciation for you.

Finally, I would like to thank my parents and my family for their constant support and love. Thank you for giving me the freedom and opportunities to become what I am. Especially, I want to thank my brother Volker for his advice during my thesis and assistance on editing my thesis writing.